EFFECT OF COBALT DOPING ON THE PHOTOCATALYTIC ACTIVITY OF ZINC OXIDE THIN FILMS UNDER UV LIGHT IRRADIATION

PRAPHAN KENTHAO

A THESIS SUBMITTED IN PARTIAL FULFILLMENT OF THE REQUIREMENTS

FOR THE DEGREE OF MASTER OF SCIENCE

MAJOR IN CHEMISTRY

FACULTY OF SCIENCE

UBON RATCHATHANI UNIVERSITY

YEAR 2012

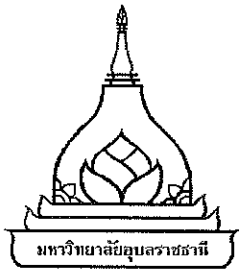

THESIS APPROVAL

UBON RATCHATHANI UNIVERSITY

MASTER OF SCIENCE

MAJOR IN CHEMISTRY FACULTY OF SCIENCE

TITLE EFFECT OF COBALT DOPING ON THE PHOTOCATALYTIC ACTIVITY OF ZINC OXIDE THIN FILMS UNDER UV LIGHT IRRADIATION

NAME MR. PRAPHAN KENTHAO

THIS THESIS HAS BEEN ACCEPTED BY

..... CHAIR

(ASST.PROF.DR.SUWAT PABCHANDA)

..... COMMITTEE

(DR.PANIDA PROMPINIT)

..... COMMITTEE

(DR.PRANORM SAEJUENG)

..... COMMITTEE

(DR.KITTIYA WONGKHAN)

..... DEAN

(ASST.PROF.DR.JANPEN INTARAPRASERT)

APPROVAL BY UBON RATCHATHANI UNIVERSITY

.....

(ASSOC.PROF.DR.UTITH INPRASIT)

VICE PRESIDENT FOR ACADEMIC AFFAIRS

FOR THE PRESIDENT OF UBON RATCHATHANI UNIVERSITY

ACADEMIC YEAR 2012

ACKNOWLEDGMENTS

The author would like to express gratitude to the people who contribute to this thesis. First of all, I would like to express my admiration and sincere appreciation to my thesis advisor: Asst. Prof. Dr. Suwat Pabchanda, who provided valuable guidance and encouragement throughout this work. I would also like to thank Dr. Panida Prompinit for being an external committee and her suggestions.

Special gratitude is felt for Dr. Pranorm Saejueng and Dr. Kittiya Wongkhan for their valuable recommendations in this work and for serving on the thesis committee.

I would like to thank Department of Chemistry and Department of Physics, Faculty of Science, Ubon Ratchathani University for UV-Vis spectrophotometer, FT-IR spectrometer, PL spectrometer, AFM and XRD diffraction measurements.

Thank so much to Center of Excellence for Innovation in Chemistry (PERCH-CIC), Office of the Higher Education Commission, Ministry of Education and Ubon Ratchathani University for the financial support.

Most of all, I feel appreciate and grateful to my beloved family and friends for their kindness and encouragement during this study.

(Mr.Praphan Kenthao)

Researcher

บทคัดย่อ

ชื่อเรื่อง : ผลของการเจือโคบอลต์ต่อกิจกรรมการเร่งปฏิกิริยาเชิงแสงของฟิล์มบางสังกะสีออกไซด์ภายใต้การฉายแสงยูวี

โดย : ประพันธ์ เดนท้าว

ชื่อปริญญา : วิทยาศาสตรมหาบัณฑิต

สาขาวิชา : เคมี

ประธานกรรมการที่ปรึกษา : ผู้ช่วยศาสตราจารย์ ดร. สุวัฒน์ ผาบจันดา

ศัพท์สำคัญ : สังกะสีออกไซด์ ฟิล์มบาง การเจือโคบอลต์ เทคนิคการเคลือบจุ่ม

วัตถุประสงค์ของงานวิจัยนี้คือศึกษาผลของสารเจือโคบอลต์และความเข้มข้นของสารเจือต่อคุณสมบัติทางโครงสร้าง หมู่ฟังก์ชัน ลักษณะพื้นผิว สมบัติทางแสง และความว่องไวต่อการเร่งปฏิกิริยาเชิงแสงของฟิล์มบางสังกะสีออกไซด์ที่เคลือบบนฐานรองกระจกสไลด์โดยเทคนิคเคลือบจุ่ม เตรียมสารละลายในการจุ่มโดยใช้ 0.7 โมลาร์ ซิงค์อะซิเตตไดไฮเดรตในตัวทำละลายผสมของเอธานอล ไดเอธานอลเอมีน และน้ำปราศจากไอออน ในอัตราส่วนโดยโมลาร์ของไดเอธานอลเอมีนต่อซิงค์อะซิเตต และน้ำปราศจากไอออนต่อซิงค์อะซิเตตเท่ากับ 1 : 1 และ 2 : 1 ตามลำดับ ในงานนี้ใช้โคบอลต์อะซิเตตเตตระไฮเดรต เป็นสารเจือซึ่งปรับเปลี่ยนความเข้มข้นจากร้อยละ 0 ถึง 10 โดยโมล บ่มฟิล์มบางที่ได้ที่อุณหภูมิ 500 องศาเซลเซียส นาน 1 ชั่วโมง

ตรวจสอบคุณสมบัติของฟิล์มบางที่ได้โดยเทคนิคการเลี้ยวเบนรังสีเอกซ์ ฟูเรียร์ทรานสฟอร์มอินฟราเรดสเปกโทรสโกปี กล้องจุลทรรศน์แรงอะตอม โฟโตลูมิเนสเซนซ์สเปกโทรสโกปี และอัลตราไวโอเลต-วิสิเบิลสเปกโทรสโกปี การตรวจวัดความว่องไวต่อการเร่งปฏิกิริยาเชิงแสงของฟิล์มบางศึกษาด้วยการย่อยสลายสีย้อมมาลาไคท์กรีนทั้งภายใต้สภาวะแสงอัลตราไวโอเลตและในที่มืด ผลการเลี้ยวเบนรังสีเอกซ์ชี้บ่งว่าทุกตัวอย่างเป็นพหุผลึกด้วยโครงสร้างแบบเฮกซะโกนอลเวิร์ธไซต์ ทั้งความเป็นผลึกและขนาดผลึกของฟิล์มลดลงเมื่อความเข้มข้นของสารเจือเพิ่มสูงขึ้น จากผลฟูเรียร์ทรานสฟอร์มอินฟราเรด ไอออนสังกะสีในโครงร่างผลึกสังกะสีออกไซด์ถูกแทนที่ด้วยไอออนโคบอลต์ ส่งผลให้พีคการสั่นของฟิล์มบางสังกะสีออกไซด์เลื่อนไปยังเลขคลื่นต่ำลง จากผลกล้องจุลทรรศน์แรงอะตอม ขนาดเกรนและลักษณะพื้นผิวของฟิล์มบางที่เตรียมได้มีแนวโน้มลดลงเมื่อปริมาณโคบอลต์เพิ่มขึ้นโดยเปรียบเทียบกับสังกะสีออกไซด์

อย่างไรก็ตามทั้งขนาดผลึกและความขรุขระของพื้นผิวที่ร้อยละ 7 และ 10 โดยโมล มีค่าเพิ่มขึ้นเล็กน้อยเมื่อเปรียบเทียบกับฟิล์มบางสังกะสีออกไซด์เจือโคบอลต์ร้อยละ 5 โดยโมล จากการวิเคราะห์โฟโตลูมิเนสเซนซ์ชี้บ่งว่าความเข้มโฟโตลูมิเนสเซนซ์ของฟิล์มบางสังกะสีออกไซด์เจือโคบอลต์ต่ำกว่าสังกะสีออกไซด์ ยิ่งไปกว่านั้นพลังงานแถบช่องว่างของฟิล์มบางเพิ่มสูงขึ้นเล็กน้อย ส่วนความโปร่งใสของฟิล์มบางลดลงเมื่อการเจือโคบอลต์เพิ่มขึ้น

ความว่องไวต่อการเร่งปฏิกิริยาเชิงแสงของฟิล์มสังกะสีออกไซด์เจือโคบอลต์ตรวจวัดด้วยการฉายแสงยูวีในสีย้อมมาลาไคท์กรีน พบว่าค่าคงที่อัตราของฟิล์มบางสังกะสีออกไซด์เจือโคบอลต์ (ร้อยละ 0 3 5 7 และ 10 โดยโมล) และการย่อยสลายเชิงแสงของมาลาไคท์กรีนเท่ากับ 0.0150 0.0078 0.0069 0.0071 0.0109 และ 0.0006 ต่อนาที ตามลำดับ จากการทดลองแสดงให้เห็นว่าประสิทธิภาพการย่อยสลายเชิงแสงของฟิล์มสังกะสีออกไซด์สูงกว่าฟิล์มสังกะสีออกไซด์เจือโคบอลต์อย่างมีนัยสำคัญ

ABSTRACT

TITLE : EFFECT OF COBALT DOPING ON PHOTOCATALYTIC ACTIVITY OF ZINC OXIDE THIN FILMS UNDER UV LIGHT IRRADIATION

BY : PRAPHAN KENTHAO

DEGREE : MASTER OF SCIENCE

MAJOR : CHEMISTRY

CHAIR : ASST. PROF. SUWAT PABCHANDA, Ph.D.

KEYWORDS : ZINC OXIDE / THIN FILM / COBALT DOPING / DIP-COATING TECHNIQUE

The purpose of this research was to investigate the effect of cobalt dopant and their concentrations on the structure, functional group, surface morphology, optical properties and photocataltytic activity of ZnO films deposited on slide glass plates by dip-coating technique. Dipping solutions were prepared by 0.7 M $Zn(CH_3COO)_2 \cdot 2H_2O$ in the mixed solvent of C_2H_5OH, DEA and DI-water. The molar ratio of DEA/zinc acetate and DI-water/zinc acetate were 1:1 and 2:1, respectively. In this work, $Co(CH_3COO)_2 \cdot 4H_2O$ was selected as doping additive, which was varied from 0 to 10 mol%. The obtained thin films were annealed at 500°C for 1 hr.

The obtained thin films were characterized by X-ray diffraction, Fourier transform infrared spectroscopy, Atomic force microscopy, Photoluminescence spectroscopy, and Ultraviolet-Visible spectroscopy. The photocatalytic activity was investigated by the decomposition of Malachite green (MG) dye over the film both under UV-light and darkness conditions. The X-ray diffraction results indicated that the samples have polycrystallite nature with hexagonal wurtzite structure. Both crystallinity and crystallite sizes of film decreased with increasing of doping concentrations. From fourier transform infrared results, zinc ions were replaced by cobalt ions in ZnO lattice, resulting to shift in vibration peak of ZnO film to lower wavenumber. From atomic force microscopy results, the grain sizes and surface roughness of prepared thin films tended to decrease with increasing cobalt content compared with ZnO. However, the slight increase in both crystallite size and surface roughness were found at

7 and 10 mol% doping level as compared with cobalt-doped ZnO thin films (5 mol%). The photoluminescence analysis indicated that the photoluminescence intensity of ZnO films with cobalt-doping was lower than that of ZnO. Moreover, the band gap energy of the thin films slightly increased, whereas the transparency of films decreased with high cobalt-doping level.

The photocatalytic activities of cobalt-doped ZnO films were evaluated using MG dye irradiated with UV light. It was found that the rate constant of cobalt-doped ZnO thin films (0, 3, 5, 7 and 10 mol%) and self photolysis of MG dye were 0.0150, 0.0078, 0.0069, 0.0071, 0.0109 and 0.0006 min^{-1}, respectively. The experiment demonstrated that the photo-degradation efficiency of undoped ZnO films was significantly higher than that of cobalt-doped ZnO films.

CONTENTS

CONTENTS (CONTINUED)

CONTENTS (CONTINUED)

LIST OF TABLES

LIST OF FIGURES

LIST OF FIGURES (CONTINUED)

LIST OF FIGURES (CONTINUED)

LIST OF FIGURES (CONTINUED)

LIST OF ABBREVIATIONS

Abbreviations	Full word
XRD	X-ray diffraction spectroscopy
FT-IR	Fourier transform infrared spectroscopy
AFM	Atomic force microscopy
UV-Vis	Ultraviolet–Visible spectroscopy
PL	Photoluminescence spectroscopy
SEM	Scanning electron microscopy
FWHM	Full width at half maxima
JCPDS	Joint committee on powder diffraction standards
CB	Conduction band
VB	Valence band
MG	Malachite green
LMG	Leucomalachite green
ZnO	Zinc oxide
TiO_2	Titanium dioxide
SnO_2	Tin oxide
NBE	Near band edge
DLE	Deep-level emission
HOMO	Highest occupied molecular orbital
LUMO	Lowest unoccupied molecular orbital
ZnO:Co	Cobalt-doped zinc oxide
W-H	Williamson-Hall
BLB	Black light blue
rpm	Rounds per minute
RMS	Root-mean-square
E_g	Band gap energy
min	Minute

LIST OF ABBREVIATIONS (CONTINUED)

Abbreviations	Full word
hV	Photon energy
eV	Electron volt
g	Gram
^{o}C	Degree celsius
K	Kelvin (temperature)
mol%	Percentage by mole
at%	Percentage by atom
wt%	Percentage by weight
mL	Milliliter
cm	Centimeter
pm	Picometer
ppm	Part per million
No.	Number
θ	Bragg's angle
ε	Lattice strain
%T	Percentage transmittance
Ω	Ohm
M	Molar
Å	Angstrom
cm^3	Cubic centimeter
E^{o}	Non-selective oxidant
h^+	Hole
e^-	Electron
nm	Nanometer
hr	Hour
V	Cell volume

LIST OF ABBREVIATIONS (CONTINUED)

Abbreviations	Full word
λ	Wavelength
D	Degradation percentage
η	Refractive index
R_q	Roughness
k	Reaction rate constant
C_0	Initial concentration
C	Final concentration
λ_{ex}	Excitation wavelength
λ_{em}	Emission wavelength

CHAPTER 1

INTRODUCTION

This chapter provided an introduction and importance of this thesis in the field of wastewater treatment. Then a semiconductor type chosen as a photocatalyst for dye decolorization and the selected technique used for preparation of photocatalysts were described. Finally, the objectives and scope of the thesis were explained.

1.1 Introductions

The elimination of toxic chemicals from wastewater is currently one of the most important subjects in pollution control. Dyes have been used in large quantities and produced great amount of colored wastewater which were released into environment with nasty consequences to human health [1]. Among the various dyes, triphenylmethane dyes make up an important category in many industrial processes.

Malachite green (MG) is a triphenylmethane (*N*-methylated diaminotriphenylmethane) dye, which has been widely used in the dying of cotton, textile, tannery, food, paper and pulp, printing, cosmetics, plastic, pharmaceuticals and dye houses [2-3]. However, there has been much concern regarding to toxicity of MG dye and its metabilte, leucomalachite green (LMG), since they has been reported to cause carcinogenesis, mutagenesis, chromosomal fractures, teratogenecity and respiratory toxicity [2, 4].

In the aquaculture industry, malachite green has been used as an effective compound to control external fungal and protozoan infection of fish, but it has never been authorized as a veterinary drug in fish food because of its toxicity as mentioned above [2]. However, it has been widely used in many countries, due to its effectiveness and relatively low cost. So, wastewater discharged from the processes used MG is usually polluted by dye. Therefore, various attempts have been made to remove malachite green from wastewater, including of adsorption [5], anaerobic [6], ozonation [7], electro-fenton [8], cation-exchange [9], sonochemical [10] and photocatalytic degradation method [11-16].

In recent years, the most environmentally friendly pollution-treatment method is the elimination of low-concentration organic pollutants in water by oxidation through molecular oxygen and sunlight [17-18]. For this purpose, photocatalysts with a high activity should be developed in order to perform the more effectively photocatalytic reactions for elimination of organic waste. The photocatalysis with zinc oxide (ZnO) represents a perspective field, because of its high chemical stability, no toxicity, low cost and good efficiency comparing to titanium dioxide (TiO_2) and tin oxide (SnO_2) in the photocatalytic degradation of some dyes in aqueous solution [19-20]. As a well known, ZnO have been found to decompose aqueous solution of reactive dyes [21], phenol [22], chlorophenol [23], methyl orange [24], methylene blue [25], and other organic environmental pollutants [26-27].

ZnO is a versatile semiconductor material which possesses a direct band gap of 3.37 eV at room temperature [28-30]. Generally, undoped ZnO typically exhibits n-type semiconductor caused by a deviation from stoichiometry due to native defect like oxygen vacancies or zinc interstitials [31]. Although many ZnO nanostructures such as, nanorods [32-33], nanotubes [34], nanowires [35] and nanobelts [36] have been prepared, ZnO thin films were investigated most deeply and extensively because of the difference in their deposition techniques and preparation conditions. ZnO thin films have different structures including dense thin films, porous thin films and nanostructured thin films [37]. The nanostructured ZnO thin films attract much attention due to some special features like larger surface area, gas adsorption and stronger photocatalytic performance [37].

In the wastewater treatment field, the use of conventional powder catalyst had major disadvantages of stirring during the reaction and the need for separation of powder catalyst after the reaction [38-39]. The preparation of thin films catalyst makes it possible to overcome these disadvantages and extend for the industrial applications [40]. Thus in this study, ZnO photocatalyst was prepared in thin film form. In addition, the structural, optical and surface properties of ZnO thin films were changed by extrinsic impurities. Therefore ZnO thin films has been doped to enhance the properties with various elements such as lithium (Li) [41], aluminium (Al) [42], nitrogen (N) [43], indium (In) [44], copper (Cu) [45], silver (Ag) [46] and cobalt (Co) [47]. However, there were not many reports on the systematic study on the effect of cobalt doping to the photodegradation property of ZnO thin films. For the above reasons,

this thesis investigated the cobalt-doped ZnO thin films and their photocatalytic activities to decolorizing organic dye.

The last several years, ZnO thin films were prepared using different host substances, such as $Zn(CH_3COO)_2$ [48], $Zn(CH_3COO)_2 \cdot 2H_2O$ [45, 49-59] and $Zn(NO_3)_2 \cdot 6H_2O$ [60]. $Zn(CH_3COO)_2 \cdot 2H_2O$ was widely used as a precursor via sol-gel route, because of its low cost, and easy fabrication of thin film. For these reasons, $Zn(CH_3COO)_2 \cdot 2H_2O$ was used as a precursor for thin films preparation in this thesis [61].

ZnO thin films can be prepared by various techniques such as chemical vapour deposition (CVD) [62-63], sputtering [64-65], spray pyrolysis [66-67], sol-gel spin coating [68-69] and sol-gel dip-coating techniques [18, 52, 70-73]. A sol-gel dip-coating is the most convenient method because of its excellent homogeneity, easy controlling film thickness, ability to coat large areas and low-cost processing [74-76]. In the present work, the sol-gel dip-coating was chosen to prepare the cobalt-doped ZnO films.

In the present thesis, undoped and cobalt-doped ZnO (3, 5, 7 and 10 mol%) thin films were grown on micro-slide glass substrates by dip-coating technique. The photocatalytic activities of the thin films were investigated by the degradation of malachite green (5.0 mg/L) in aqueous solutions under ultraviolet-light irradiation. The crystalline structure, bonding structure, surface morphology, photoluminescence and optical properties of films were characterized by X-ray diffraction (XRD), fourier transform infrared spectroscopy (FT-IR), atomic force microscopy (AFM), photoluminesecence (PL) and ultraviolet-visible spectroscopy (UV-Vis), respectively.

1.2 Objectives and scope of this thesis

The objectives of this thesis can be expressed as follows:

(1) To prepare undoped ZnO and cobalt-doped ZnO (3, 5, 7 and 10 mol%) thin films by dip-coating method using zinc acetate dihydrate ($Zn(CH_3COO)_2 \cdot 2H_2O$) and cobalt acetate tetrahydrate ($Co(CH_3COO)_2 \cdot 4H_2O$) as a host and dopant, respectively.

(2) To investigate the effect of cobalt-doping on the structure, surface morphology, optical properties and photocatalytic decolorization of malachite green of the films by XRD, FT-IR, AFM, PL and UV-Vis spectroscopic analysis methods.

The scopes of this work were,

(1) To prepare cobalt-doped ZnO thin films on micro-slide glass substrates by dip-coating method at the concentration of cobalt (II) in dipping solution as 0, 3, 5, 7 and 10 mol% with respect to zinc.

(2) To characterize the crystalline structure, bonding structure, surface morphology, photoluminescence and optical properties of the films by XRD, FT-IR, AFM, PL and UV-Vis spectroscopic analysis methods, respectively.

(3) To compare the photocatalytic activities of pure ZnO and cobalt-doped ZnO thin films by degradation of 5.00 mg/L malachite green 25.00 mL under UV-light irradiation and in darkness for 180 minutes.

CHAPTER 2

LITERATURE REVIEWS AND THEORETICALS

The purpose of this chapter is to summarize previous work on preparation, characterization and photocatalytic applications in ZnO and cobalt-doped ZnO films. A brief theory introduction is necessary to permit the reader to understand the sol-gel chemistry, dip-coating, rate law and photocatalysis.

2.1 Literature reviews

2.1.1 Zinc oxide

Zinc oxide crystallizes in two main forms, hexagonal wurtzite and cubic zincblende [77]. The wurtzite structure is the most stable at ambient conditions and thus most common. So, the structure consists of four oxygen ions around each zinc ions. A hexagonal packing of the large oxygen ions with half the tetrahedral interstices filled with zinc ions have been required in order to achieve a maximum cation separation. The lattice constants a = 0.325 nm and c = 0.521 nm; their ratio c/a ~ 1.60 is close to the ideal value for hexagonal cell c/a = 1.633 [78]. Meanwhile, the zincblende form, cubic lattice structure, can be stabilized by growing ZnO on substrates [79-81].

XRD patterns of wurtzite and zincblende structures of ZnO exhibited as shown in Figure 2.1 [82]. For the wurtzite structure (see Figure 2.1a), obvious main peaks can be observed at $2\theta = 32^{\circ}$, 35° and 37°, corresponding to (1 0 0), (0 0 2) and (1 0 1) reflections of ZnO structure, respectively. Meanwhile, the main XRD peaks of zincblende form (see Figure 2.1d) can be observed at $2\theta = 34^{\circ}$, 39° and 57°, corresponding to (1 1 1), (2 2 0) and (3 1 1) planes of ZnO structure, respectively.

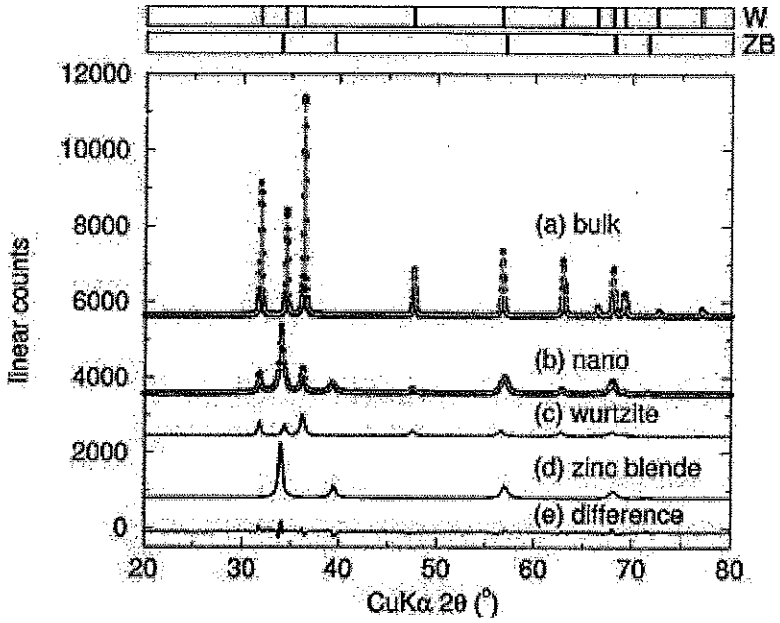

Figure 2.1 XRD data (filled circles) and Rietveld fits (gray lines) for bulk (a) wurtzite ZnO, and (b) nanophase ZnO (wurtzite and zinc blende) obtained from the bulk sample. (c) and (d) are contributions to the Rietveld fit of the nanophase ZnO from wurtzite and zinc blende respectively. (e) is the difference profile for the nanophase ZnO. Vertical lines at the top of the plot indicate expected peak positions [82].

Several properties of ZnO films depend critically on the physical and chemical parameters such as deposition techniques, precursor solution, annealing temperature and metal dopants. Therefore it was reasonable to understand those parameters for ability to control the properties of the thin films.

ZnO thin films have been prepared by various vacuum deposition techniques and solution-based deposition processes. Solution-based deposition processes offer a simple, low cost, and large area thin-film coating alternative to vacuum deposition techniques. An example of solution-based deposition technique includes dip-coating and spin-coating. The dip-coating method not only enables easy fabrication of a large area thin film at a low cost, but also easy controlling over the film composition and uniformity of thickness. Several properties of polycrystalline ZnO thin films prepared by the sol–gel process depend on the different host substances [45, 48-60, 83-86], sol concentration [48, 54, 87-88], heat-treatment conditions [89-94].

ZnO thin films can be prepared using different host substances, such as zinc acetate ($Zn(CH_3COO)_2$) [48], zinc acetate dihydrate ($Zn(CH_3COO)_2 \cdot 2H_2O$) [45, 49-59], zinc nitrate ($Zn(NO_3)_2 \cdot 6H_2O$) [60] and zinc chloride ($ZnCl_2$) [83]. From the previous work, N. Lehraki et al. [84] reported that the films deposited with zinc acetate had a smooth surface, dense network and higher transparency in comparison to films prepared with zinc nitrate and zinc chloride as precursors, while films deposited with zinc chloride have a better crystallinity and low optical transmittance. In contrast, E. Arca et al. [85] found that using zinc chloride precursor led to rough discontinued layers, while films deposited with zinc nitrate shown a more rapid and random crystallization than the films grown by zinc acetate. However, H. Bahadur et al. [86] reported that a smoother surface topography was obtained for the films grown by zinc acetate than for the films grown by zinc nitrate. Therefore, the best results have been achieved by employing zinc acetate as precursor that resulted in smooth and good quality layer of thin films.

The effect of zinc acetate concentration on the properties of ZnO thin films were studied in the previous works [48, 54, 87, 95]. For spin-coating [48, 54], 0.7 M of zinc acetate dihydrate was used for preparation of ZnO thin films. The results revealed that these thin films have polycrystallite wurtzite structures and high c-axis preferred orientation. For dip-coating, the porous texture of ZnO thin films were adjusted in preparing the sol: $Zn(CH_3COO)_2$ concentration was 0.2–1.2 mol/L; PEG content was 0–2.0 g in 50 mL sol; and water bath temperature was 20–70°C. ZnO porous thin film could be made due to the better phase separation according to the following conditions: $Zn(CH_3COO)_2$ concentration was 0.6 mol/L and PEG content was 0.7 g in 50 mL solvent. The sol should be pretreated in water bath at 70°C before dipping, and then sintered at 500°C for 1 hr. For sol–gel drain coating technique [95], different sols of concentration 0.03, 0.05, 0.08, and 0.1 M were prepared by adding required amount of zinc acetate dihydrate [$Zn(CH_3COO)_2 \cdot 2H_2O$] to dehydrated isopropyl alcohol. Diethanolamine (DEA) was added to the solution as a sol stabilizer followed by a thorough mixing process with a magnetic stirrer. The results showed that with increase in sol concentration, the value of full width at half maximum (FWHM) of (0 0 2) peak decreased while the strain first increased and then decreased. The sol with higher concentration resulted in the increase in the grain size. The studies on the optical properties indicated that the band gap value increased from 3.27 to 3.30 eV when the sol concentration changed from 0.03 to 0.10 M.

The heat treatment appears to be one of the most important factors governing the ZnO film property. From previous works [89-94], it was found that the ZnO films on glass substrates were annealed at temperature range of 300°C to 550°C. At lower annealing temperature, the poor crystal quality and amorphous structure of thin films were obtained. Annealing temperature of 500°C promoted the enhancement of crystallinity. At the same time, the grain size of thin films increased with higher annealing temperatures that may be due to the merging activity of the ZnO particles to form denser film at higher annealing temperature [94]. However, if the annealing temperature was higher than 500°C, the glass substrates were in a worst shape or shrinkage due to the heating that closed to the glass transition temperature (Tg) [96].

2.1.2 Cobalt-doped zinc oxide

As well known, cobalt-doped ZnO was still n-type extrinsic semiconductor [97]. Many research groups had been reported that the crystal structure of ZnO did not change with a small amount of a cobalt dopant [47, 98-100]. The structure model of cobalt-doped ZnO was shown in Figure 2.2.

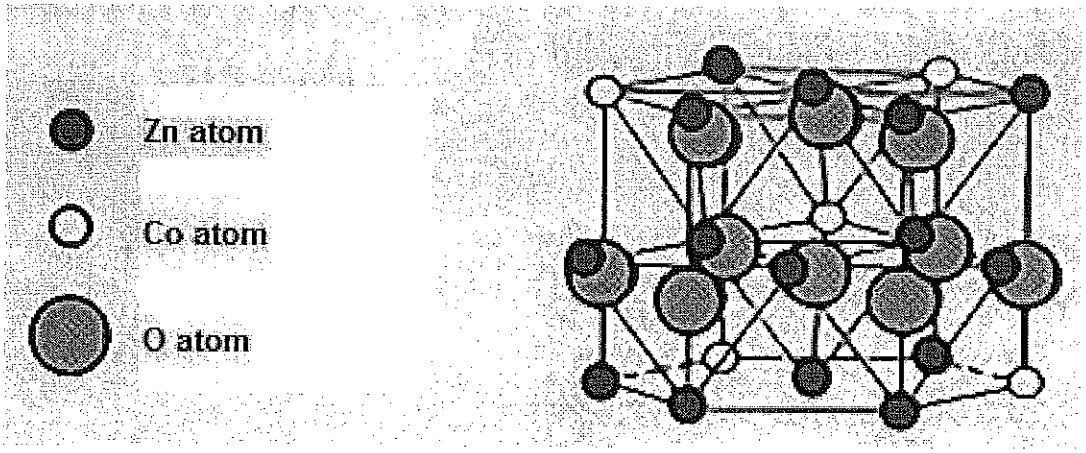

Figure 2.2 The structure model of cobalt-doped ZnO [47].

Various deposition techniques have been used for the fabrication of cobalt-doped ZnO thin films such as sputtering [47], spin-coating [56-58], [101-103], spray pyrolysis [59, 104] electrodeposition [60] and plused laser deposition [105-106]. However, most of these fabrication techniques require highly sophisticated instruments. Sol–gel dip coating is a simple and low cost technique and it is suitable for preparing quality films for a large surface

device applications. Therefore, the sol–gel process is used to fabricate the cobalt-doped ZnO films in the present work [107].

The influence of cobalt doping on the properties of ZnO thin films have been investigated [57-58, 60, 101-104, 106-107]. For example, nanostructured $Zn_{1-x}Co_xO$ ($0 \le x \le 0.10$) thin films were fabricated by sol–gel spin coating technique [57]. Structural characterization indicated that Co^{2+} ions systematically substituted for Zn^{2+} ions in the film without changing the wurtzite structure. For $x \ge 0.035$, CoO (cubic) was detected as the secondary phase. Increase in cobalt content in the range $0 \le x \le 0.10$ led to quenching of near-band edge and blue emissions, and decrease in band gap energy (E_g) from 3.36 eV to 3.26 eV. Increasing the cobalt content deteriorated the crystallization of ZnO [103]. For cobalt-doped ZnO prepared by spray pyrolysis, the particle size and roughness of the films were found to decrease with the increase in cobalt doping percentage [104]. For dip-coating, three-dimensional (3D) atomic force microscopy images of the cobalt-doped ZnO films deposited on p-type silicon substrate suggested that the structure of 5% and 15% cobalt-doped ZnO films were distributed almost homogenously on silicon surface. The roughness values of the films with 5% and 15% cobalt dopants were 317.53 nm and 255.10 nm, respectively [107].

The effect substrate temperature on the properties of undoped and cobalt-doped ZnO films prepared by ultrasonic spray pyrolysis were investigated [59]. The deposition was performed with different glass substrate temperatures at 300, 350 and 400°C. It was found that both pure and cobalt-doped ZnO films were (0 0 2) preferentially oriented. An increase in the substrate temperature and the presence of dopant resulted in the increased crystallinity of the thin films.

Cobalt-doped ZnO thin films can also be prepared by solution-based deposition using different dopant substances, such as cobalt acetate tetrahydrate ($Co(CH_3COO)_2 \cdot 4H_2O$) [56, 58, 103], cobalt chloride ($CoCl_2$) [57, 59, 102, 104] and cobalt nitrate hexahydrate ($Co(NO_3)_2 \cdot 6H_2O$) [60, 101]. Films were prepared using sol-gel spin coating method and the sol was prepared using conventional cobalt acetate tetrahydrate ($Co(CH_3COO)_2 \cdot 4H_2O$) [56, 58]. Cobalt chloride ($CoCl_2$) were added to obtain sols for spin coating [57] and spray pyrolysis [59], where zinc acetate dihydrate ($Zn(CH_3COO)_2 \cdot 2H_2O$) was taken as the host substance. For spin coating method, $Zn_{1-x}Co_xO$ thin films up to $x = 0.05$, the change in microstructure and

evolution of secondary phase have been found which was attributed to the use of cobalt chloride as dopant substance [57], while the films prepared with cobalt acetate tetrahydrate were single phase at the same doping concentration [56].

2.1.3 Photocatalysis of zinc oxide and cobalt-doped zinc oxide for dye degradation

In the last few years, there have been an increase interest in applications of the semiconductor materials for photocatalytic oxidation to oxidize poisonous pollutants. A number of organic matters can be decomposed into smaller and low toxicity compounds. Because this kind of reaction needs only light, catalyst and air, the processing cost is lower and become a kind of new promising method of liquid waste processing [108]. ZnO is an excellent photocatalytic oxidation material. It has been widely used to treat wastewater, such as pharmacy wastewater, printing and dyeing wastes, papermaking wastewater, and so on. The catalytic activity of nano-ZnO is much better than bulk materials. It can also absorb the light in wider spectrum. Its catalytic activity is mostly affected by the dosage of the catalyst, the original concentration of reactants, illumination time, intensity of illumination and atmosphere (oxygen) flow [25].

To compare the photocatalytic activity of ZnO, thin films prepared on glass substrates by the sol–gel method using both dip coating and spin-coating were investigated [11]. Two different procedures were applied for preparation of the films: (i) polymeric one (zinc acetate and ethylcellulose) and (ii) one with complexing agent monoethanolamine (zinc acetate and 2-methoxyethanol). The as-obtained ZnO films were studied with respect to the photoinitiated bleaching of malachite green (MG) under UV illumination in aqueous solutions. It indicated that the films obtained by procedure (ii) have a better photocatalytic activity than those deposited by procedure (i). It was proven that the films also have activities in darkness but were lower than the activities under UV-light.

Recently, zinc oxide thin films were deposited on aluminum foil and glass substrates by two different chemical methods: (i) polymer modified spray pyrolysis and (ii) sol–gel dip-coating from zinc acetate complex solution [109]. The films obtained by procedure (i) possess a porous structure, while the films obtained by procedure (ii) have ganglia on the surface. The influence of the thermal treatment temperature (350 or 450^{o}C) on the film microstructure and photocatalytic efficiency toward the organic dyes malachite green (MG) and reactive black (RB5) was also investigated. The films obtained by both methods have a better

photocatalytic activity in the degradation of RB5 compared to MG due to the weaker N-N bond in comparison with the C-C bond between the central carbon atom and *N,N*-dimethylaminobenzyl in MG.

For cobalt-doped ZnO nanoparticles, the location of dopant ions and the effect of doping level on the photocatalytic activity have been investigated on cobalt-doped ZnO nanopowders [99]. The photocatalytic activity under simulated sunlight irradiation was characterized by the decomposition of Rhodamine B dye molecules, which revealed the successful reduction of photocatalytic activity by cobalt-doping. It was suggested that cobalt-doping did not appear to create significant physical defects in ZnO crystal. Hence the mechanism of the reduction of the photocatalytic activity by cobalt-doping was considered to be not by creating physical defects but mainly by introducing deep band gap energy levels between the valence and conduction bands that would act as efficient recombination centers for photo-generated excitons. The recombination of electrons and holes inside of the particles will give the charge carriers less chance to generate hydroxyl radicals ($^{\bullet}OH$) and superoxide anion radicals ($O_2^{-\bullet}$) on particle surfaces. For other dye, the Methylene Blue (MB) decomposition rate of the synthesized pure ZnO and cobalt-doped ZnO nanoparticles were studied under the UV region. In the UV region, synthesized pure ZnO and cobalt-doped ZnO decomposed Methylene Blue (MB). However, the MB decomposition rate obtained using pure ZnO was much higher than that by cobalt-doped ZnO nanoparticles [100].

Highly photocatalytically active cobalt-doped ZnO nanorods have been prepared by a facile hydrothermal process [110]. The as-prepared cobalt-doped ZnO nanorods have an extended light absorption range compared with pure ZnO and showed highly efficient photocatalytic activity, only requiring 60 min to decompose ~93% of alizarin red dye under visible light irradiation ($\lambda > 420$ nm). The photophysical mechanism of the visible photocatalytic activity was investigated with the help of surface photovoltage spectroscopy. The results indicated that a strong electronic interaction between the cobalt and ZnO was present, and that the incorporation of cobalt promoted the charge separation and enhanced the charge transfer ability and, at the same time, effectively inhibited the recombination of photogenerated charge carriers in ZnO, resulting in high visible light photocatalytic activity.

Cobalt-doped ZnO films were sputtered using an RF magnetron sputter system. The photo-degradation of methylene blue and the inactivation of bacteria were obviously enhanced under visible light exposure [47].

2.1.4 The postulated photocatalytic degradation of MG and mineralization pathways

To identify reaction by-products accompanying MG degradation, samples subjected to various treatment schemes and times were analyzed by means of GC/MS [111]. The proposed reaction network for the degradation of MG via two parallel and competing pathways were shown in Figure 2.3. The first involves hydroxyl radical attack to the central carbon atom of MG (1) yielding a reactive cationic radical (2) whose bond between the central carbon atom and the *N,N*-dimethylamino phenyl ring is cleaved to give *N,N*-dimethyl-benzenamine (3) and 4-dimethylamino-benzophenone (4). In addition, *N,N*-dimethyl-benzenamine can further be attacked by hydroxyl radicals giving a reactive cationic radical (5) which is demethylated resulting in benzenamine (6). The latter is further oxidized to form nitrobenzene (7). In a similar fashion, 4-dimethylamino-benzophenone is demethylated to 4-amino-benzophenone (9) which is oxidized to 4-nitro-benzophenone (10) and this is eventually converted to benzophenone (11) and NO_3^-. Cleavage of benzophenone yields benzaldehyde (15) and benzene (16). The second pathway involves hydroxyl radical attack to the *N,N*-dimethylamino group of MG giving a reactive cationic radical (12) whose subsequent demethylation and oxidation eventually yield benzenamine and 4-amino-benzophenone.

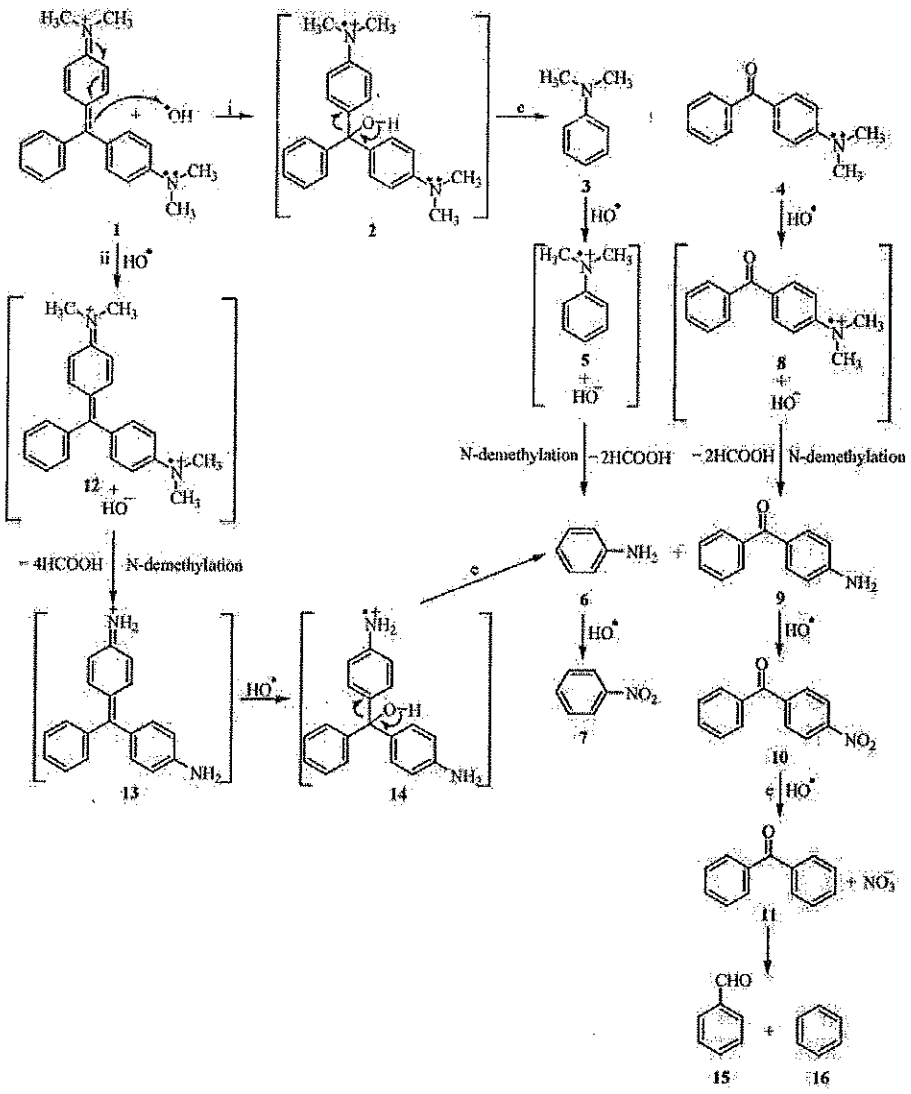

Figure 2.3 Proposed reaction pathways for malachite green degradation over TiO_2 under UV irradiation [111].

2.2 Theoreticals

2.2.1 Sol-gel chemistry

The earliest sol-gel derived material was reported by M. Ebelmen in 1845, at the Manufacture of ceramics in France [112]. Sol-gel process describes, in general, the formation of solid material, mainly inorganic non metallic materials from solutions. This can be a solution of monomeric, oligomeric, polymeric and colloidal precursors. In nature for example, minerals like agate or chalcedony have been formed by a poly-condensation reaction from aqueous siliceous solutions [113]. Before going through the description of sol-gel processes, some terms might be introduced. A colloid is a suspension in which the dispersed phase is so small (1-100 nm) that gravitational forces are negligible and interactions are dominated by short-range forces, such as Van der Waals attraction and surface charges. A sol is a colloidal suspension of solid particles in a liquid. Hydrolysis is a reaction in which metal alkoxide (M-OR) react with water to form metal hydroxide (M-OH). Condensation is a reaction which occurs when two metals hydroxides (M-OH + M-OH) combine to give a metal oxide species (M-O-M). The reaction forms one molecule of water. A gel consists of sponge like, three dimensional solid network hose pores are filled with another substance (usually the original solvent of the sol). When gels are prepared, the pore liquid mainly consists of water and/or alcohol. The resultant wet gels are therefore called aquagel, hydrogel, or alcogels. The pore liquid is replaced by air without decisively altering the network structure or the volume of the gel body, aerogel are obtained (or cryogels when the liquid is freeze-drying). Gel point is the moment at which the network of linked oxide particles spans the container holding the sol. The alcogel can be removed from its original container and can stand on its own [114].

Sol-gel process consists of: (i) preparing a homogeneous solution of easily purified precursors generally in an organic solvent miscible with water or the reagent used in the next step; (ii) converting the solution to the "sol" form by treatment with a suitable reagent, e.g. water which HCl for oxide ceramics; (iii) allowing/inducing the sol to change into a "gel" (or viscous sol) to the finally desired forms or shape such as thin films, fiber, spheres or grains and (v) finally converting (sintering) the shaped gel to the desired ceramic material at temperatures ($\sim 500^{\circ}C$) generally much lower than those required in the conventional procedure of melting oxides together [115]. Usually, alkoxides are used as starting compounds for sol gel process,

that is, organometallic substance of the form M $(OR)_n$ (where M = metal of valence n and R = alkyl group; C_xH_{2x+1}). By two groups of reactions, hydrolysis (equation 2.1) and condensation (equation 2.2), the alkoxides are converted to 3-dimensionally connected networks. The following reactions will take place:

$$M(OR)_n + nH_2O \rightarrow M(OH)_n + nROH \quad (2.1)$$

$$M(OH)_n \rightarrow MO_{\frac{n}{2}} + \left(\frac{n}{2}\right)H_2O \quad (2.2)$$

$$M(OR)_n + \left(\frac{n}{2}\right)H_2O \rightarrow MO_{\frac{n}{2}} + nROH \quad (2.3)$$

These equations are simplified. In fact, the reactions are much more complicated, especially because the hydrolysis occurs in successive steps. In the case of zinc-ethoxide this means:

$$Zn(OC_2H_5)_4 + H_2O \rightarrow ZnOH(OC_2H_5)_3 + C_2H_5OH \quad (2.4)$$

$$ZnOH(OC_2H_5)_3 + H_2O \rightarrow Zn(OH)_2(OC_2H_5)_2 + C_2H_5OH \quad (2.5)$$

$$Zn(OH)_2(OC_2H_5)_2 + H_2O \rightarrow Zn(OH)_3(OC_2H_5) + C_2H_5OH \quad (2.6)$$

$$Zn(OH)_3(OC_2H_5)_2 + H_2O \rightarrow Zn(OH)_4 + C_2H_5OH \quad (2.7)$$

Which the hydrolysis reaction can be summarized as following:

$$Zn(OC_2H_5)_4 + 4H_2O \rightarrow Zn(OH)_4 + 4C_2H_5OH \quad (2.8)$$

Furthermore, the condensation reactions already started before the hydrolysis was completed. This not only reaction such as:

$$(OH)_3ZnOH + OHZn(OH)_3 \rightarrow (HO)_3Zn\text{-}O\text{-}Zn(OH)_3 + H_2O \qquad (2.9)$$

The reactions in the sol gel processes depend on many parameters, for example: compositions and concentrations of alkoxides and solvent used, chemical additives, time schedule of mixing for example aging (for pre-hydrolysis) of components or intermediates that react slowly, conditions of mixing (e.g., mixing efficiency and atmosphere) and temperature.

To get a sol-gel derived coating on a transparent substrate with a high optical quality, the coating process should be carried out in a very clean room, the coating liquid has to be filtered and the substrate has to be cleaned properly. The sol gel method of fabricating thin films offers potential advantages over traditional techniques as shown below: low temperature processing, easy coating to large surface, small thickness, high optical quality and high purity. So, the sol-gel derived coating techniques are summarized below.

2.2.2 Dip-coating

Dip-coating techniques can be described as a process where the substrate to be coated is immersed in a liquid and then withdrawn with a well-defined withdrawal speed under controlled temperature and atmospheric conditions. The schematics of the dip-coating process are shown in Figure 2.4. In the dip-coating process, the atmosphere controls the evaporation of the solvent and subsequent destabilization of the sol by solvent evaporation lead to a gelation process at the formation of a transparent film due to the small particle size in the sols (nanometer range). The gelation process during dip-coating process is shown in Figure 2.5. The resulting film has to be densified by thermal treatment and densification temperature depends on the composition. The coating thickness is defined mainly by the withdrawal speed, the solid content and the viscosity of the liquid. There are six forces acting on the coating during withdrawing [116]:

(1) Viscous drag upward on the liquid by moving substrates

(2) Force on gravity

(3) Resultant force of surface tension in the concavely shaped meniscus

(4) Inertial force of the boundary layer liquid arriving at deposition region

(5) Surface tension gradient

(6) The disjoining or conjoining pressure (important for films less than 1 μm thick)

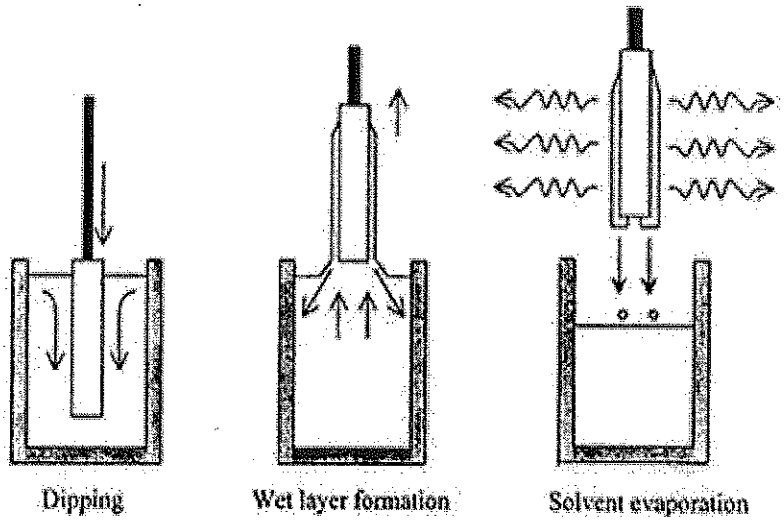

Figure 2.4 Dip-coating process: dipping the substrate in the solution, formation of the wet layer, and gelation of the layer by solvent evaporation.

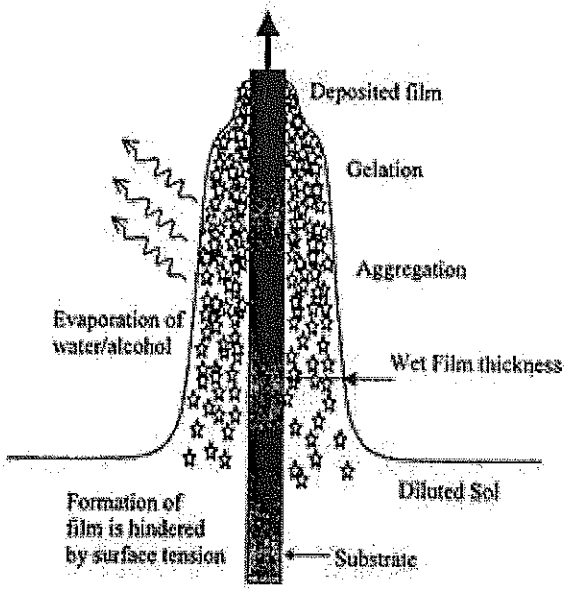

Figure 2.5 Gelation process during dip-coating process obtained by evaporation of the solvent and subsequent destabilization of the sol.

When the viscosity (η) and substrate speed are high enough to lower the curvature of the gravitational meniscus, the deposition films thickness (h) is that which balances the viscous drag ($\alpha\eta U_0/d$) and gravity force (ρgh), the thickness is given by

$$d = C_1\left(\frac{\eta U_0}{\rho g}\right)^{1/2} \tag{2.10}$$

where C_1 is a constant about 0.8 for Newtonian liquids.

When the substrate speed and viscosity are low (often the case for sol-gel deposition), this balance is modulated by the ratio of viscous drag to liquid-vapor surface tension (γ_{LV}) according to the relationship derived by Landau and Levich [117]

$$h_0 = 0.94\frac{\left(\eta U_0\right)^{2/3}}{\gamma_{LV}^{1/6}(\rho g)^{1/2}} \tag{2.11}$$

The interesting part of dip-coating processes in that by choosing an appropriate viscosity the thickness of the coating can be varied with high precision from 20 nm up to 50 nm while maintaining high optical quality. Dip coating processes are used for plate glass and bulbs. Dip- coating processes have also been developed for curved surface like eyeglass lenses, mainly to employ scratch resistant coating for plastic substrates. For bottles, a variation of the dip-coating process has been developed by revolving the bottle during the withdrawal process.

2.2.3 Rate law for a chemical reaction

The rate law or rate equation for a chemical reaction is an equation that links the reaction rate with concentrations or pressures of reactants and constant parameters (normally rate coefficients and partial reaction orders). To determine the rate equation for a particular system one combines the reaction rate with a mass balance for the system. For a generic reaction

$$aA + bB \longrightarrow C \tag{2.12}$$

with no intermediate steps in its reaction mechanism (that is, an elementary reaction), the rate is given by

$$r = k[A]^x [B]^y \tag{2.13}$$

where [A] and [B] express the concentration of the species A and B, respectively (usually in moles per liter (molarity, M)); x and y are the respective stoichiometric coefficients of the slowest step of the reaction mechanism; they only equal the stoichiometric coefficients "a" and "b" if the reaction takes place in a single step without intermediates. k is the rate coefficient or rate constant of the reaction. The value of this coefficient k depends on conditions such as temperature, ionic strength, surface area of the adsorbent or light irradiation. For elementary reactions, the rate equation can be derived from first principles using collision theory. Again, x and y are not always derived from the balanced equation. The rate equation of a reaction with a multi-step mechanism cannot, in general, be deduced from the stoichiometric coefficients of the overall reaction; it must be determined experimentally. The equation may involve fractional exponential coefficients, or it may depend on the concentration of an intermediate species. The rate equation is a differential equation, and it can be integrated to obtain an integrated rate equation that links concentrations of reactants or products with time. If the concentration of one of the reactants remains constant (because it is a catalyst or it is in great excess with respect to the other reactants), its concentration can be grouped with the rate constant, obtaining a pseudo constant: If B is the reactant whose concentration is constant, then

$$r = k[A]\ [B] = k'[A] \tag{2.14}$$

The second-order rate equation has been reduced to a pseudo-first-order rate equation. This makes the treatment to obtain an integrated rate equation much easier.

2.2.3.1 Zero-order reactions

A zero-order reaction has a rate that is independent of the concentration of the reactant(s). Increasing the concentration of the reacting species will not speed up the rate of the reaction i.e. the amount of substance reacted is proportional to the time. Zero-order reactions are typically found when a material that is required for the reaction to proceed, such as a surface or a catalyst, is saturated by the reactants. The rate law for a zero-order reaction is

$$r = k \tag{2.15}$$

where r is the reaction rate and k is the reaction rate coefficient with units of concentration/time. If, and only if, this zero-order reaction 1) occurs in a closed system, 2) there is no net build-up of intermediates, and 3) there are no other reactions occurring, it can be shown by solving a mass balance equation for the system that:

$$r = -\frac{d[A]}{dt} = k \tag{2.16}$$

If this differential equation is integrated it gives an equation often called the integrated zero-order rate law,

$$[A]_t = -kt + [A]_0 \tag{2.17}$$

where $[A]_t$ represents the concentration of the chemical of interest at a particular time, and A_0 represents the initial concentration. A reaction is zero order if concentration data are plotted versus time and the result is a straight line. The slope of this resulting line is the negative of the zero order rate constant k. The half-life of a reaction describes the time needed for half of

the reactant to be depleted (same as the half-life involved in nuclear decay, which is a first-order reaction). For a zero-order reaction the half-life is given by

$$t_{\frac{1}{2}} = \frac{[A]_0}{2k} \tag{2.18}$$

2.2.3.2 First-order reactions

A first-order reaction depends on the concentration of only one reactant (a unimolecular reaction). Other reactants can be present, but each will be zero-order. The rate law for a reaction that is first order with respect to a reactant A is

$$r = -\frac{d[A]}{dt} = k[A] \tag{2.19}$$

Where k is the first order rate constant, which has units of 1/s. The integrated first-order rate law is

$$\ln[A] = -kt + \ln[A]_0 \tag{2.20}$$

A plot of ln [A] vs. time t gives a straight line with a slope of -k. The half-life of a first-order reaction is independent of the starting concentration and is given by

$$t_{\frac{1}{2}} = \frac{\ln(2)}{k} \tag{2.21}$$

2.3.2.3 Second-order reactions

A second-order reaction depends on the concentrations of one second-order reactant, or two first-order reactants. For a second order reaction, its reaction rate is given by:

$$-\frac{d[A]}{dt} = 2k[A]^2 \text{ or} \tag{2.22}$$

$$-\frac{d[A]}{dt} = k[A][B] \text{ or} \tag{2.23}$$

$$-\frac{d[A]}{dt} = 2k[B]^2 \tag{2.24}$$

In several popular kinetics books, the definition of the rate law for second-order reactions is written instead as

$$-\frac{d[A]}{dt} = 2k[A]^2 \tag{2.25}$$

This effectively conflates the 2 inside the constant, k, whose numerical meaning then becomes different. This simplifying convention is followed in the integrated rate laws provided below. It should be noted however that this simplification leads to potentially problematic inconsistencies, i.e. if the reaction rate is described in terms of product formation vs. reactant disappearance. Instead, the option of keeping the 2 in the rate law (rather than absorbing it into a rate constant with an altered meaning) maintains a consistent meaning for k and is considered more correct technically. This more technically consistent convention is almost always used in peer-reviewed literature, tables of rate constants, and simulation software. The integrated second-order rate laws are respectively

$$\frac{1}{A} = \frac{1}{[A]_0} + kt \text{ or} \tag{2.26}$$

$$\frac{[A]}{[B]} = \frac{[A]_0}{[B]_0} e^{([A]_0 - [B]_0)kt} \tag{2.27}$$

$[A]_0$ and $[B]_0$ must be different to obtain that integrated equation. The half-life equation for a second-order reaction dependent on one second-order reactant is

$$t_{\frac{1}{2}} = \frac{1}{k[A]_0} \tag{2.28}$$

2.2.3.4 Pseudo-first-order

Measuring a second-order reaction rate with reactants A and B can be problematic: The concentrations of the two reactants must be followed simultaneously, which is more difficult; or measure one of them and calculate the other as a difference, which is less precise. A common solution for that problem is the pseudo-first-order approximation. If either [A] or [B] remains constant as the reaction proceeds, then the reaction can be considered pseudo-first-order because, in fact, it depends on the concentration of only one reactant. If, for example, [B] remains constant, then:

$$r = k[A][B] = k'[A] \tag{2.29}$$

where $k' = k[B]_0$ (k' or k_{obs} with units s^{-1}) and an expression is obtained identical to the first order expression above. One way to obtain a pseudo-first-order reaction is to use a large excess of one of the reactants ([B] >> [A]) would work for the previous example) so that, as the reaction progresses, only a small amount of the reactant is consumed, and its concentration can be considered to stay constant. By collecting k' for many reactions with different (but excess) concentrations of [B], a plot of k' versus [B] gives k (the regular second order rate constant) as the slope.

2.2.3.5 Summary for reaction orders 0, 1, 2 and n

Elementary reaction steps with order 3 (called ternary reactions) are rare and unlikely to occur. However, overall reactions composed of several elementary steps can, of course, be of any (including non-integer) order.

Table 2.1 Summary for reaction orders 0, 1, 2 and n

	Zero-Order	**First-Order**	**Second-Order**	**nth-Order**
Rate Law	$-\frac{d[A]}{dt} = k$	$-\frac{d[A]}{dt} = k[A]$	$-\frac{d[A]}{dt} = k[A]^2$	$-\frac{d[A]}{dt} = k[A]^n$
Integrated Rate Law	$[A]=[A]_0 - kt$	$[A] = [A]_0 e^{-kt}$	$\frac{1}{[A]} = \frac{1}{[A]_0} + kt$	$\frac{1}{[A]^{n-1}} = \frac{1}{[A]_0^{n-1}} + (n-1)kt$ [Except first order]
Units of Rate Constant (k)	$\frac{M}{s}$	$\frac{1}{s}$	$\frac{1}{M \cdot s}$	$\frac{1}{M^{n-1} \cdot s}$
Linear Plot to determine k	[A] vs. t	ln([A]) vs. t	$\frac{1}{[A]}$ vs. t	$\frac{1}{[A]^{n-1}}$ vs. t [Except first order]
Half-life	$t_{\frac{1}{2}} = \frac{[A]_0}{2k}$	$t_{\frac{1}{2}} = \frac{\ln 2}{k}$	$t_{\frac{1}{2}} = \frac{1}{k[A]_0}$	$t_{\frac{1}{2}} = \frac{2^{n-1}-1}{(n-1)k[A]_0^{n-1}}$ [Except first order]

where M stands for concentration in molarity ($mol \cdot L^{-1}$), t for time, and k for the reaction rate constant. The half-life of a first-order reaction is often expressed as $t_{1/2} = 0.693/k$ (as $\ln 2 = 0.693$).

2.2.4 Photocatalysis

In chemistry, photocatalysis is the acceleration of a photoreaction in the presence of a catalyst. In catalysed photolysis, light is absorbed by an adsorbed substrate. In photogenerated catalysis, the photocatalytic activity (PCA) depends on the ability of the catalyst to create electron–hole pairs, which generate free radicals (e.g. hydroxyl radicals: $^{\bullet}OH$) able to undergo secondary reactions. Its practical application was made possible by the discovery of water electrolysis by means of titanium dioxide. The commercially used process is called the advanced oxidation process (AOP). Generally the defining factor is the production and use of the hydroxyl radical.

2.2.4.1 Homogeneous photocatalysis

In homogeneous photocatalysis, the reactants and the photocatalysts exist in the same phase. The most commonly used homogeneous photocatalysts include, ozone and transition metal oxide. The reactive species is the $^{\bullet}OH$ which is used for different purposes. The mechanism of hydroxyl radical production by ozone can follow two paths.

$$O_3 + h\nu \longrightarrow O_2 + O(1D) \quad (2.30)$$

$$O(1D) + H_2O \longrightarrow {}^{\bullet}OH + {}^{\bullet}OH \quad (2.31)$$

$$O(1D) + H_2O \longrightarrow H_2O_2 \quad (2.32)$$

$$H_2O_2 + h\nu \longrightarrow {}^{\bullet}OH + {}^{\bullet}OH \quad (2.33)$$

2.2.4.2 Heterogeneous photocatalysis

Heterogeneous catalysis has the catalyst in a different phase from the reactants. Heterogeneous photocatalysis is a discipline which includes a large variety of reactions: mild or total oxidations, dehydrogenation, hydrogen transfer, $^{18}O_2$–$^{16}O_2$ and deuterium-alkane isotopic exchange, metal deposition, water detoxification, gaseous pollutant removal. Most common heterogeneous photocatalyts are semiconductors, which have unique characteristics. Unlike the metals which have a continuum of electronic states, semiconductors possess a void energy region where no energy levels are available to promote recombination of an electron and hole produced by photoactivation in the solid. The void region, which extends

from the top of the filled valence band to the bottom of the vacant conduction band, is called the band gap. When light falls on these semiconductors, the electron present in the valence band jumps to the conduction band, a result of which is the generation of a positive hole. The recombination of the electron and the hole must be prevented as much as possible if a photocatalyzed reaction is to be favored. The ultimate goal of the process is to have a reaction between the activated electrons with an oxidant to produce a reduced product, and also a reaction between the generated holes with a reductant to produce an oxidized product. Due to the generation of positive holes and electrons, oxidation-reduction reactions take place at the surface of semiconductors. In the oxidative reaction, the positive holes react with the moisture present on the surface and produce a hydroxyl radical. Oxidative reactions due to photocatalytic effect:

$$UV + MO \longrightarrow MO\,(h^+ + e^-) \qquad (2.34)$$

Here MO stands for metal oxide.

$$h^+ + H_2O \longrightarrow H^+ + {}^{\bullet}OH \qquad (2.35)$$

$$2\,h^+ + 2\,H_2O \longrightarrow 2\,H^+ + H_2O_2 \qquad (2.36)$$

$$H_2O_2 \longrightarrow {}^{\bullet}HO + {}^{\bullet}OH \qquad (2.37)$$

The reductive reaction due to photocatalytic effect:

$$e^- + O_2 \longrightarrow O_2^{-\bullet} \qquad (2.38)$$

$$O_2^{-\bullet} + HO_2^{\bullet} + H^+ \longrightarrow H_2O_2 + O_2 \qquad (2.39)$$

$$HOOH \longrightarrow {}^{\bullet}HO + {}^{\bullet}OH \qquad (2.40)$$

Ultimately, the hydroxyl radicals are generated in both the reactions. These hydroxyl radicals are very oxidative in nature and non selective with redox potential of (E_0 = +3.06 V).

2.2.5 Heterogeneous photocatalytic degradation of dyes in solution [118]

Photocatalytic degradation is a part of advanced oxidation process which has proven to be a promising technology for degrading organic compound. The technique is more effective as compared to other advanced oxidation processes because semiconductors are inexpensive and can easily mineralize various organic compounds [119].

The photocatalytic discoloration of a dye is believed to take place according to the following mechanism. When a catalyst is exposed to UV radiation, electrons are promoted from the valence band to the conduction band. As a result of this, an electron–hole pair is produced [120]

$$\text{Catalyst} + h\nu \rightarrow e^-_{cb} + h^+_{vb} \qquad (2.41)$$

where, e^-_{cb} and h^+_{vb} are the electrons in the conduction band and the electron vacancy in the valence band, respectively. Both these entities can migrate to the catalyst surface, where they can enter in a redox reaction with other species present on the surface. In most cases h^+_{vb} can react easily with surface bound H_2O to produce $^{\bullet}OH$ radicals, whereas, e^-_{cb} can react with O_2 to produce superoxide radical anion of oxygen

$$H_2O + h^+_{vb} \rightarrow {}^{\bullet}OH + H^+ \qquad (2.42)$$

$$O_2 + e^-_{cb} \rightarrow O_2^{-\bullet} \qquad (2.43)$$

This reaction prevents the combination of the electron and the hole which are produced in the first step. The $^{\bullet}OH$ and $O_2^{-\bullet}$ produced in the above manner can then react with the dye to form other species and is thus responsible for the discoloration of the dye.

$$O_2^{-\bullet} + H_2O \rightarrow H_2O_2 \qquad (2.44)$$

$$H_2O_2 \rightarrow 2\,(^{\bullet}OH) \qquad (2.45)$$

$$^{\bullet}OH + \text{dye} \rightarrow \text{dye}_{ox} \qquad (2.46)$$

$$e^-_{cb} + \text{dye} \rightarrow \text{dye}_{red} \qquad (2.47)$$

Direct and Indirect photocatalytic pathways are the two suggested mechanisms for a given photocatalytic reaction. These are discussed below.

2.2.5.1 Direct photocatalytic pathway

Two different approaches have been suggested for this type of mechanism:

(i) Heterogeneous photocatalysis—the Langmuir–Hinshelwood process

The Langmuir–Hinshelwood process is applied to heterogeneous photocatalysis and can be explained on the basis of production of electrons and holes by the photoexcitation of the catalyst. The hole is then trapped by the adsorbed dye molecule on the catalyst surface to form a reactive radical state which can decay as a result of recombination with an electron. The catalyst is regenerated as a result.

(ii) The Eley–Rideal process

In this process, the free carriers are initially photo-fragmented followed by subsequent trapping of the holes by surface defects. The surface active centers (S) can then react with the dye (chemisorption) to form an adduct species such $(S\text{–dye})^+$ which can further decompose to produce products or can recombine with electrons. The reaction scheme is outlined below:

Photogeneration of free carriers: $\text{Catalyst} + h\nu \rightarrow e^-_{cb} + h^+_{vb}$ (2.48)

Hole trapping by surface defects: $S + h^+_{vb} \rightarrow S^+$ (2.49)

Physical decay of active centers: $S + e^-_{cb} \rightarrow S$ (2.50)

Chemisorption: $S^+ + \text{dye}^+ \rightarrow (S\text{—dye})^+$ (2.51)

$(S\text{—dye})^+ \rightarrow S + \text{products}$ (2.52)

2.2.5.2 Indirect photocatalytic mechanism

In this process, electron–hole pairs are photogenerated on the surface of the catalyst. The hole is then trapped by the water molecules leading to the formation of $^{\bullet}OH$ radicals and H^+ and the electrons allow the formation of H_2O_2 which further decomposes in more $^{\bullet}OH$ radicals by means of its reaction with the oxygen supplied in the medium.

Finally, the radicals formed during this mechanism are responsible for the oxidation of the organic molecule producing intermediates and end products. The stepwise mechanism is illustrated below:

$$\text{Catalyst} + h\nu \rightarrow e^-_{cb} + h^+_{vb} \quad (2.53)$$

$$h^+_{vb} + H_2O_{(ads)} \rightarrow {}^{\bullet}OH_{(ads)} + H^+_{(ads)} \quad (2.54)$$

$$O_{2\,(ads)} + e^-_{cb} \rightarrow O_2^{-\bullet}{}_{(ads)} \quad (2.55)$$

$$O_2^{-\bullet}{}_{(ads)} + H^+_{(ads)} \rightarrow HO_2^{\bullet}{}_{(ads)} \quad (2.56)$$

$$HO_2^{\bullet}{}_{(ads)} + HO_2^{\bullet}{}_{(ads)} \rightarrow H_2O_{2\,(ads)} + O_{2\,(ads)} \quad (2.57)$$

$$H_2O_{2\,(ads)} \rightarrow {}^{\bullet}OH_{(ads)} + {}^{\bullet}OH_{(ads)} \quad (2.58)$$

$${}^{\bullet}OH_{(ads)} + dye_{(ads)} \rightarrow \text{products} \quad (2.59)$$

CHAPTER 3

EXPERIMENTAL DETAIL

This chapter reported the chemicals used for preparation of thin films. Moreover the experimental procedure was clearly described with a step-by-step and various characterization methods for sample analysis were discussed.

3.1 Chemicals and instruments

The chemicals and instruments used in this study were shown in the table 3.1 and 3.2.

Table 3.1 Chemicals used in the experiment.

Chemicals	Formula	Assay (%)	Manufacturer
Zin (II) acetate dihydrate	$Zn(CH_3COO)_2 \cdot 2H_2O$	99.0 %	Sigma Aldrich
Cobalt (II) acetate tetrahydrate	$Co(CH_3COO)_2 \cdot 4H_2O$	97.0 %	Sigma Aldrich
Diethanolamine	$HN(CH_2CH_2OH)_2$	99.0 %	Carlo Erba
Malachite oxalate green	$(C_{52}H_{54}N_4O_{12})$	93.0%	Panreac
Ethyl alcohol	CH_3CH_2OH	99.9 %	AnalaR
Hydrochloric acid	HCl	37.0 %	J. T. Baker
Nitric acid	HNO_3	69.0 %	J. T. Baker

Table 3.2 Instruments

Instruments	Model	Company
X-ray Diffractometer (XRD)	Philips X 'pert MPD	Philips
Fourier transform infrared spectrometer (FT-IR)	Spectrum X1	Perkin Elmer
Atomic force microscope (AFM)	XE 100	Park System
Fluorescence spectrophotometer	LS—55	Perkin Elmer
UV-Vis spectrophotometer	Lambda 25	Perkin Elmer

3.2 Experimental procedures

The pure and cobalt doped zinc oxide (ZnO:Co) thin films were deposited on micro-slide glass substrate by home-made dip-coating experimental set-up. The Zn^{2+} solution was prepared by dissolving a 35 mmol of zinc acetate dihydrate ($Zn(CH_3COO)_2 \cdot 2H_2O$) into 50.00 mL of absolute ethanol under vigorous stirring at room temperature for 30 min in a closed vessel. The solution was cleared by adding diethanolamine (DEA) and deionized water (DI water). The molar ratio of DEA/zinc acetate and DI water/zinc acetate were 1:1 and 2:1, respectively [87, 121]. The clear solution was further heated to 50°C and stirred for 5.5 hr. For doped thin films, cobalt (II) acetate tetrahydrate ($Co(CH_3COO)_2 \cdot 4H_2O$) at 3, 5, 7 and 10 mol% was added into the mixture solution. The final solution was aged at room temperature for 24 hr before dip-coating.

For thin film preparation, the cleaned glass substrate was dipped into the solution and subsequently withdrawing it up at constant speed of 6.0 cm/min [87, 122]. After each deposition the film was dried at room temperature, pre-heated at 100°C and treated at 500°C for 15 min per each step [87, 122]. Coating and heat-treated process was repeated for 10 times. Finally, the obtained thin films were annealed at 500°C for 1 hr [87, 122]. The preparation of thin films can be shown as the following diagram:

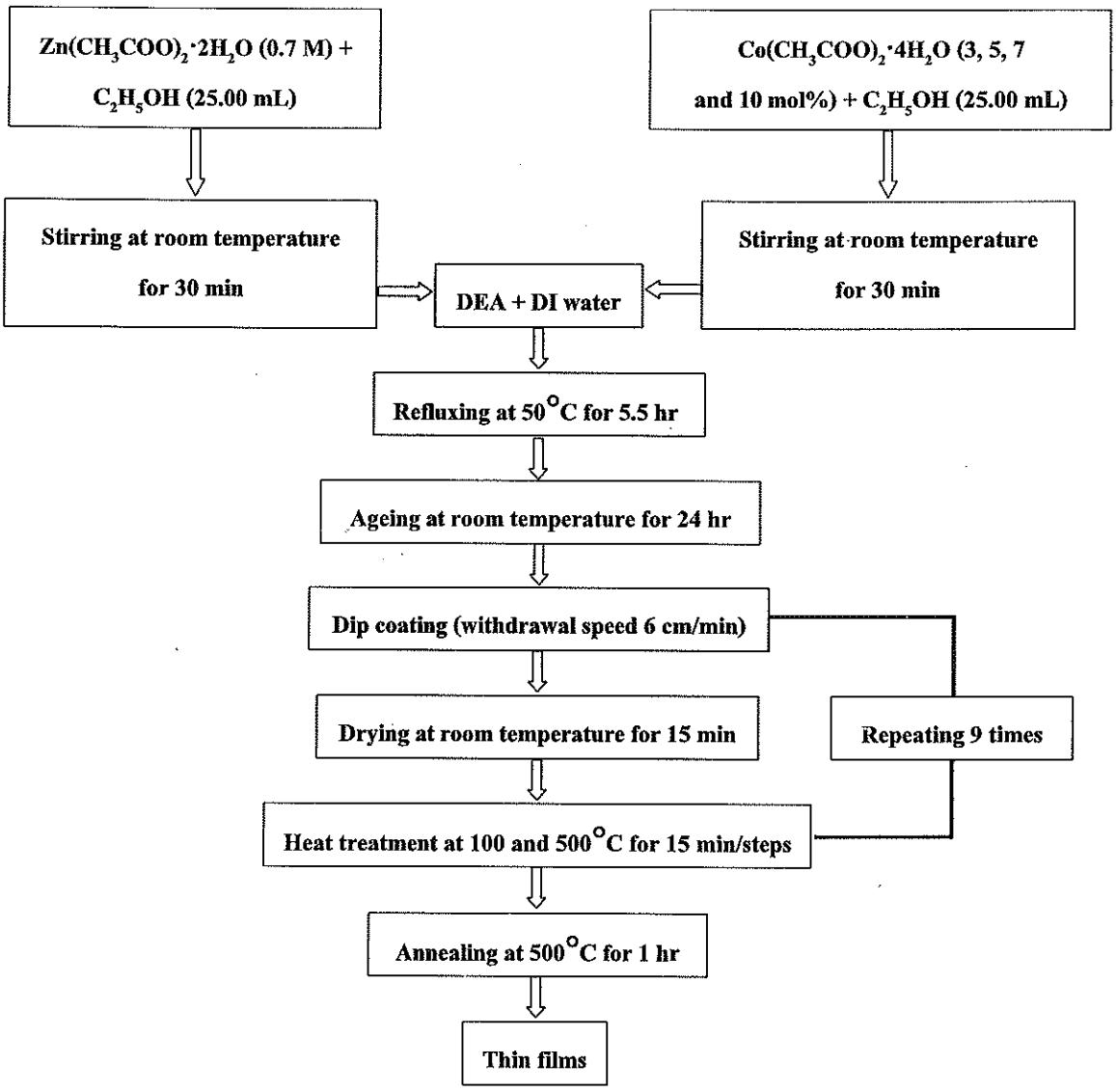

Figure 3.1 Diagram for preparation of cobalt-doped ZnO thin films.

3.3 Sample Characterizations

3.3.1 X-ray diffractometry (XRD)

The X-ray diffraction studies were carried out using X-ray diffractometer (Philips X'pert MPD) to investigate the structure of the deposited films using CuK_α radiation with a wavelength 0.154059 nm. The scanning range of 2θ was restricted to the range 20° to 60° with scan rate of 0.02° θ/min. The lattice parameter constants "a" and "c" and cell volume (V) of hexagonal wurtzite structure of ZnO can be calculated using the relations (3.1), (3.2) and (3.3) given below [123-124]:

$$a = \sqrt{\frac{1}{3}}\frac{\lambda}{\sin\theta} \tag{3.1}$$

$$c = \frac{\lambda}{\sin\theta} \tag{3.2}$$

$$V = \frac{\sqrt{3}a^2C}{2} \tag{3.3}$$

The strain (ε) and average crystallite size (D) of the films was calculated using Williamson-Hall (W-H) method:

$$\beta_{hkl}\cos\theta = \frac{K\lambda}{D} + 4\varepsilon\sin\theta \tag{3.4}$$

Where β is the full width at haft maximum (FWHM) of XRD peaks

θ is the Bragg angle [125]

K is the constant value (0.94)

λ is the X-ray wavelength (0.154059 nm)

D is the average crystallite size (nm)

ε is the strain

The above equation is W-H equation. The strain of the films was estimated from the slope of the fit curve which drawn with $4\sin\theta$ along the axis and $\beta_{hkl}\cos\theta$ along the y-axis. The crystallite size was estimated from the y-intercept [126-127].

3.3.2 Fourier transform infrared spectroscopy (FT-IR)

The FT-IR gives information about functional groups present in a compound along with the molecular geometry and inter or intra molecular interactions. The ZnO powder (99.0% purity, CARLO ERBA) and powder scratched from deposited ZnO thin film and cobalt-doped ZnO thin films with 3, 5, 7 and 10 mol% were characterized by fourier transform infrared (FT-IR) spectroscopy using Perkin Elmer FT-IR spectrometer model spectrum RX1. The FT-IR spectra were measured from samples prepared by KBr pallet technique (KBr : sample ratio, 300 : 1) in the wavenumber ranges of 4000-400 cm^{-1}.

3.3.3 Atomic force microscopy (AFM)

The surfaces morphology of cobalt-doped ZnO thin films (0, 3, 5, 7 and 10 mol%) were scanned using a atomic force microscopy (AFM) instrument (XE-100, Park Systems) on a non-contact mode. The cantilever is made from silicon nitride (Si_3N_4). Important measurement information was shown in table 3.3.

Table 3.3 The operated information used in AFM method.

Factor	Value
X scan size	1 μm
Y scan size	1 μm
Z servo grain	1
Scan rate	0.5 Hz
Set point	10.16 nm
Amplitude	20.26 nm

3.3.4 UV-Vis spectroscopy

The transparency of cobalt-doped ZnO thin films (0 and 3, 5, 7 and 10 mol%) were measured by UV-Vis spectroscopy method, using lambda 25 UV-Vis double beam

spectrometer (Perkin Elmer) in the wavelength range of 300 to 1,100 nm. The thickness of films (t) was determined by using the optical transmission spectra (%T) and the following equation:

$$t = \frac{\lambda_1 \lambda_2}{2\eta(\lambda_1 - \lambda_2)} \tag{3.5}$$

where t is the film thickness (nm)

λ_1, λ_2 are the two consecutive in transmission spectra

η is the refractive index of ZnO ($\sim$ 1.60) [128]

The direct optical band gap (Eg) of the films were obtained by extrapolating the linear portion of the plot $(\alpha h\nu)^2$ versus photon energy ($h\nu$) in electron volt (eV), according to the equation as below:

$$\alpha h\nu = A(h\nu - Eg)^n \tag{3.6}$$

where $h\nu$ is the photon energy

Eg is the band gap (eV)

A is the edge parameter

n is the direct gap of material [129].

3.3.5 Photoluminescence (PL) spectroscopy

Photoluminescence spectra of the films were carried out at room temperature using Perkin-Elmer spectrometer (Model LS-55) equipped with a 450 W xenon flash lamp as the excitation source, and the exciting wavelength was chosen at 325 nm. A glass substrate was taken as a reference, the excitation and emission spectra were recorded for the films deposited on the substrates. Before recording the emission spectra, the films were scanned for excitation bands, by fixing the monochromator at 393 nm. Once the optimum excitation wavelength were found, the films emission spectra were recorded in the wavelength range 200–800 nm which the data was

collected at the scanning interval of 0.5 nm. Meanwhile, the excitation and emission slit width were used at 10 and 2.5 nm, respectively.

3.3.6 Photocatalytic degradation

Photocatalytic performance of the film was examined using the degradation of Malachite Green (MG) dye in DI water. The coated glass plates were immersed into 25.00 mL aqueous MG solution (5.0 mg/L) in 50.00 mL beaker. The beaker was immediately located in the Solar Box ready for UV irradiation. The coated plate and dye solution were irradiated in the vertical direction with continuously stirring. The distance between the UV lamp and plate/dye solution system was kept within 15.00 cm. The light source of illumination was UV lamp (Philips TL-D 20 Watt T8 Black Light Blue Fluorescent 18in (BLB) lamps, F20T8/BLB, emitting approximately 350-400 nm). All photocatalytic tests were performed with 5.0 mg/L MG at constant stirring rate (500 rpm) and air was continuously pumped into the system (3.0 L/hr) at room temperature for 180 min. The apparent rate constant of photocatalysis (k) was calculated from the experimental data using the equation [130]:

$$\ln\frac{C}{C_0} = -kt \tag{3.7}$$

where C is the final concentration (mg/ L) of MG after irradiation

C_0 is the initial concentration (mg/ L) of MG prior to irradiation

t is the irradiation time (min)

k is the apparent reaction rate constant (min^{-1})

The same equation was used for calculation of the rate constant of the dye adsorption on the films surface under darkness. The degradation efficiency of the MG was calculated using the equation:

$$\text{Degradation}(\%) = \frac{C_0 - C}{C_0} \times 100 \tag{3.8}$$

CHAPTER 4

RESULTS AND DISCUSSIONS

The prepared thin films were characterized by several techniques; X-ray diffraction (XRD), atomic force microscopy (AFM), fourier transform infrared spectroscopy (FT-IR), photoluminescence spectroscopy (PL) and UV-Visible spectroscopy. An attempt has been made to correlate of the structural and optical properties of these films with the cobalt (II) dopant and their concentrations. The structural and optical properties of films were characterized and discussed in the following sections, including their photocatalytic activities for degradation of Malachite green in water both under UV-light illumination and in darkness.

4.1 Structural properties

The crystal structure of pure and cobalt-doped ZnO thin films were investigated by X-ray diffraction (XRD) technique as shown in Figure 4.1. ZnO thin films were detected at 2θ of 31.75°, 34.42°, 36.23°, 47.52° and 56.56°, similar to report by Lupan et al. [131], that the diffraction peaks were found at 2θ of 31.79°, 34.42°, 36.25°, 47.51° and 56.62° for ZnO nanorods. These peak positions of the pure and cobalt-doped ZnO thin films were found to be in good agreement with the files of Joint Committee of Powder Diffraction Standards (JCPDS Card No. 36-1451) in a hexagonal wurtzite structure of ZnO, corresponding to the following lattice planes: (1 0 0), (0 0 2), (1 0 1), (1 0 2) and (1 1 0), respectively. It was also found that the orientation planes of (1 0 0), (0 0 2) and (1 0 1) had higher intensity than (1 0 2) and (1 1 0) planes, and the strongest diffraction peak for all the films was (1 0 1) preferred orientation (see Figure 4.1 (a-e)). These results were similar to those of ZnO films [93] and ZnO nanorods [132].

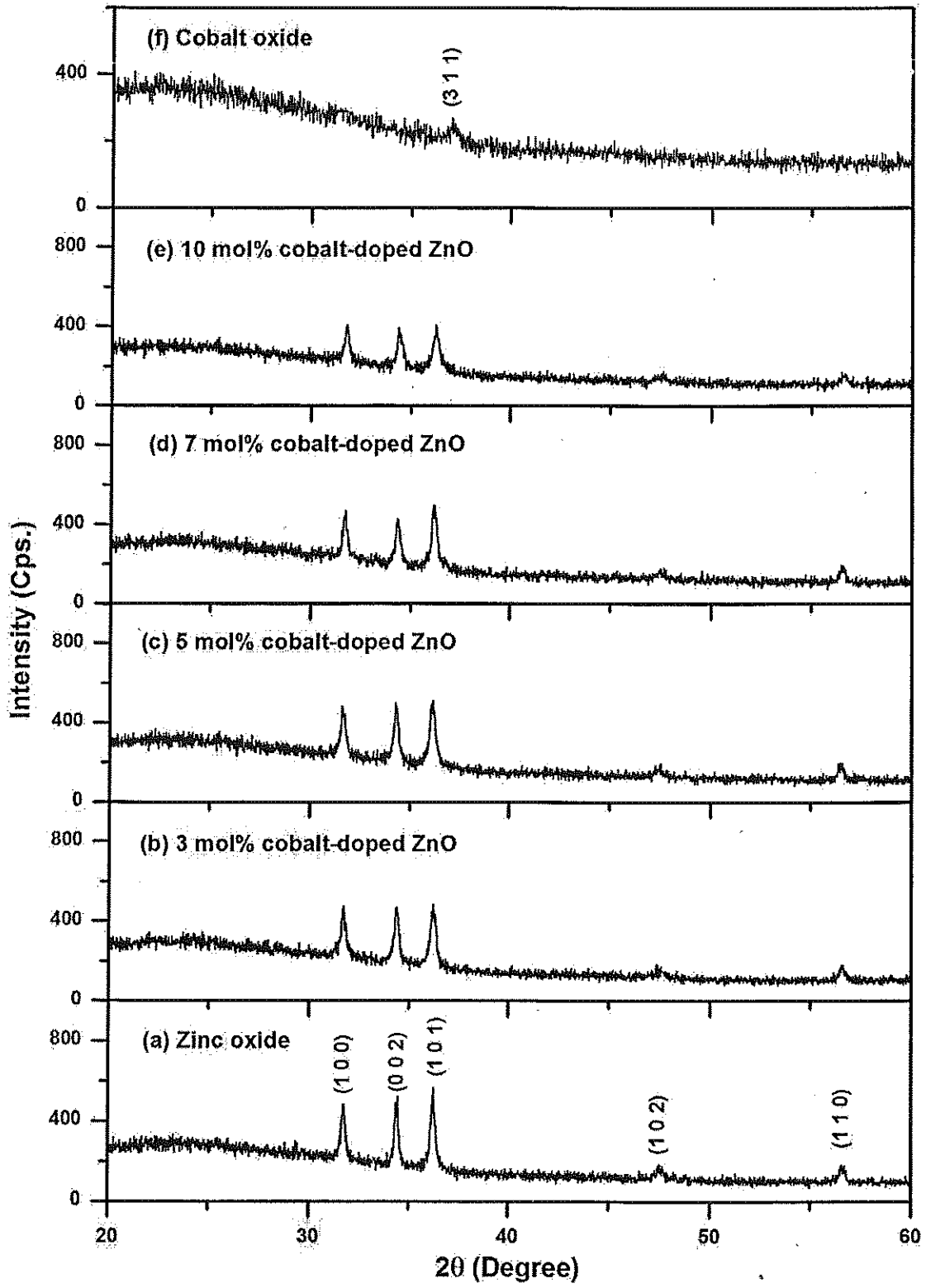

Figure 4.1 XRD patterns of cobalt-doped ZnO thin films with different cobalt contents.

No impurity was observed in the cobalt-doped ZnO film, and doping level in the range of 3 to 10 mol% did not affect the crystal structure of ZnO, in agreement with previously published results of ZnO films [47, 56-60, 101-106] and nanoparticles [29, 49, 98-100, 110, 133-140]. Previous work on cobalt-doped ZnO films [47] have shown that doping cobalt up to 20 at% did not change the wurtzite structure of ZnO. However, for ZnO nanoparticles prepared by a one-step solution route [137], doping cobalt of 10 mol% resulted in $Co(OH)_2$ impurity in cobalt-doped ZnO powder. On the other hand, in this work no diffraction peaks corresponding to $Co(OH)_2$ or other impurities were detected within the limits of experimental error for all doping concentration up to 10 mol% (Figure 4.1b-e).

Since, a change in 2θ presents inverse relation to the crystal radius of dopant, therefore 2θ values of (1 0 0), (0 0 2) and (1 0 1) planes were plotted as function of cobalt-doping level as shown in Figure 4.2. Considered the preferred orientation (1 0 1) plane, it was found that the percentage change of cobalt-doped ZnO films for 3, 5, 7 and 10 mol% cobalt-doping compared with ZnO were -0.05%, -0.25, -0.10 and + 0.06 %, respectively [57]. This indicated that some of Zn^{2+} in ZnO lattice sites were replaced by Co^{2+} which was good agreement with the Shannon-Prewitt crystal radius (CN = 6) of Zn^{2+}, Co^{2+} and Co^{3+} as 0.0880, 0.0885 and 0.0750 nm, respectively [141].

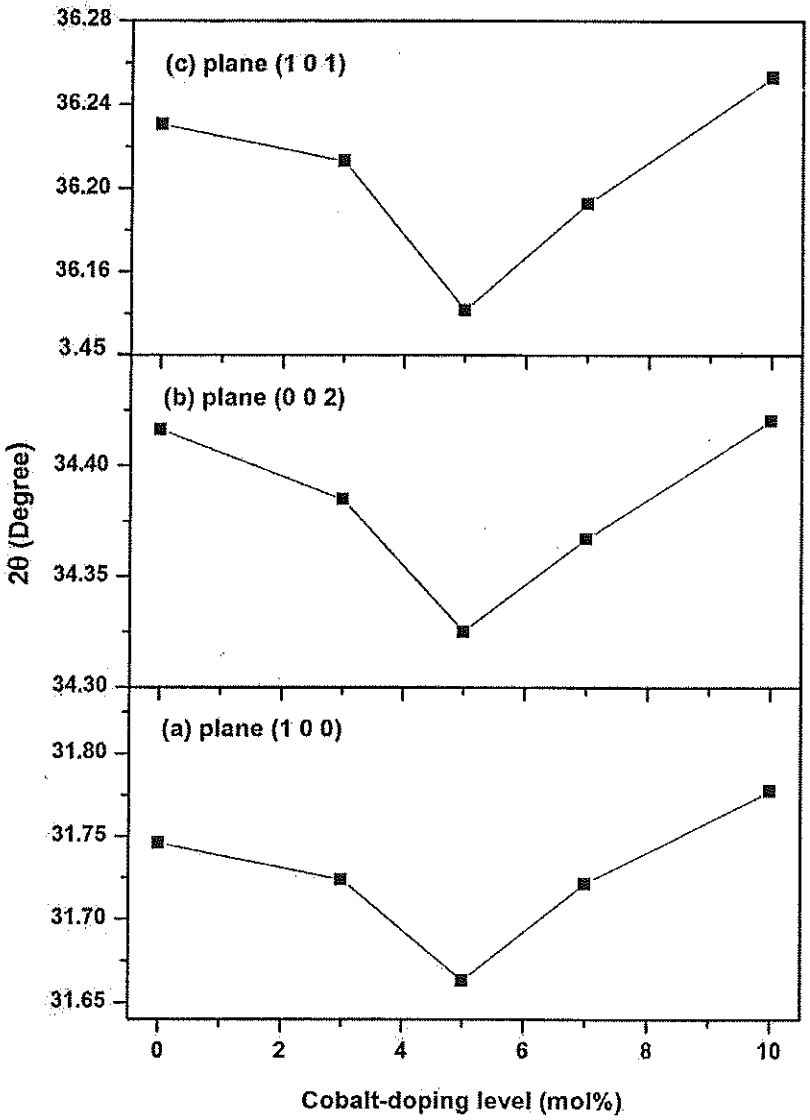

Figure 4.2 2θ (degree) of XRD peaks as a function of cobalt-doping levels (mol% in dipping solution).

The a- and c-lattice constant values for pure ZnO thin films in (1 0 0) and (0 0 2) planes were found to be 0.3255 and 0.5212 nm, respectively which were in good agreement with the lattice constants for ZnO powder reported in JCPDS card no. 36-1451 (a = 0.3249 nm and c = 0.5206 nm). For cobalt-doped ZnO at 3, 5, 7 and 10 mol%, the calculated a-lattice constants of were 0.3256, 0.3259, 0.3260 and 0.3251 nm, and the calculated c-lattice constants were 0.5215, 0.5219, 0.5221 and 0.5209 nm, respectively. The cobalt-doping did not change the a- and c-lattice constants of ZnO because the size of Co^{2+} in octahedral configuration

(0.0885 nm) is close to the value of Zn^{2+} in octahedral coordination (0.0880 nm). It was indicated that Co^{2+} ions systematically substituted Zn^{2+} ions in the samples without changing its crystal structure. These resulted in the similar calculated cell volume of cobalt-doped ZnO films that were 0.0478, 0.0479, 0.0480, 0.0480 and 0.0477 nm^3 for 0, 3, 5, 7 and 10 mol%, respectively. Therefore, it can be concluded that the cobalt-doping did not change both crystalline structure and lattice parameters of ZnO due to a small mismatch in crystal radius between Zn^{2+} and Co^{2+} [47, 56, 100, 138].

The effect of cobalt-doping on crystallinity of ZnO thin films was also investigated. The full width at half maximum (FWHM) values of the peaks from (1 0 0), (0 0 2) and (1 0 1) planes with different cobalt contents were increased with increasing cobalt-doping concentration from 0 to 10 mol% (see Figure 4.3). From Figure 4.3c, the FWHM values of (1 0 1) plane were 0.333°, 0.357°, 0.324° and 0.434°, for zinc oxide doped with cobalt at 3, 5, 7 and 10 mol%, respectively. The FWHM of thin films were slightly increased with increasing in cobalt-doping concentrations compared with ZnO (0.293°). The percentage increase of FWHM values were 13.40%, 21.76%, 10.36% and 48.03% as compared with pure ZnO thin films. The increase in FWHM along with increasing of doping level suggested that dopant incorporation into the ZnO lattice resulted in a reduction of crystallinity [59, 102].

The FWHM values gradually increased in proportion to the cobalt concentration due to the enhanced strain caused by cobalt ions substituting for zinc ions. The strain of the films was calculated using Williamson-Hall (W-H) method as in equation 4.1:

$$\beta_{hkl}\cos\theta = \frac{K\lambda}{D} + 4\varepsilon\sin\theta \qquad (4.1)$$

where β_{hkl} is the FWHM of the rocking curve for a reciprocal lattice point hkl, θ is the Bragg angle for the hkl reflection, K is shape factor (0.9), D is the crystallite size, λ is the X-ray wavelength and ε is the strain.

A plot was drawn with $4\sin\theta$ along the x-axis and $\beta_{hkl}\cos\theta$ along the y-axis for cobalt-doped ZnO films as shown in Figure 4.4. From the linear fit to the data, the strain (ε) was

estimated from the slope of the fit and the average crystallite sizes have been estimated from the y-intercept. The strain values of zinc oxide doped with cobalt at 0, 3, 5, 7 and 10 mol% were 4.8 x 10^{-3}, 6.5 x 10^{-3}, 10.2 x 10^{-3}, 7.4 x 10^{-3} and 8.7 x 10^{-3}. The trend of strain values changed in proportion to the FWHM value indicated that the crystallinity of ZnO film was controlled by cobalt-doping level [59, 102].

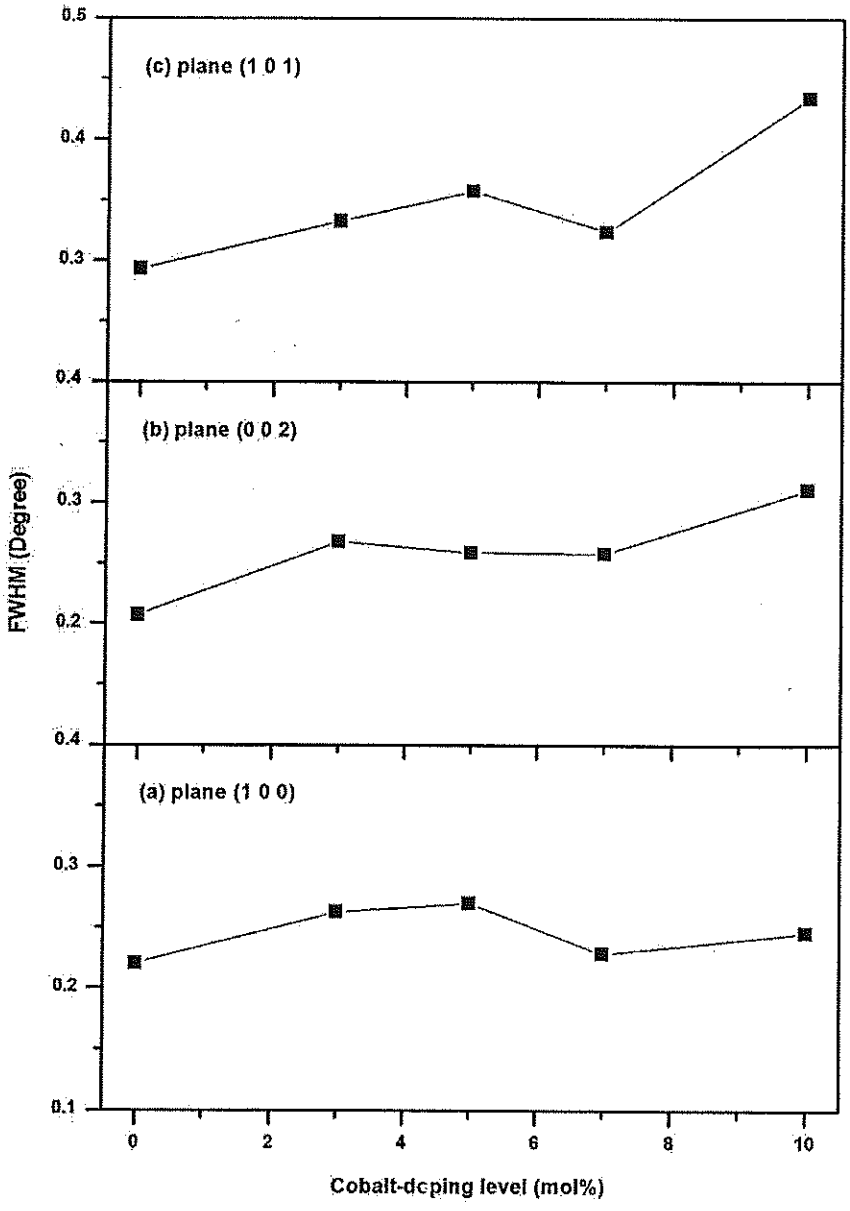

Figure 4.3 FWHM (degrees) of XRD peaks as a function of cobalt-doping levels (mol% in dipping solution).

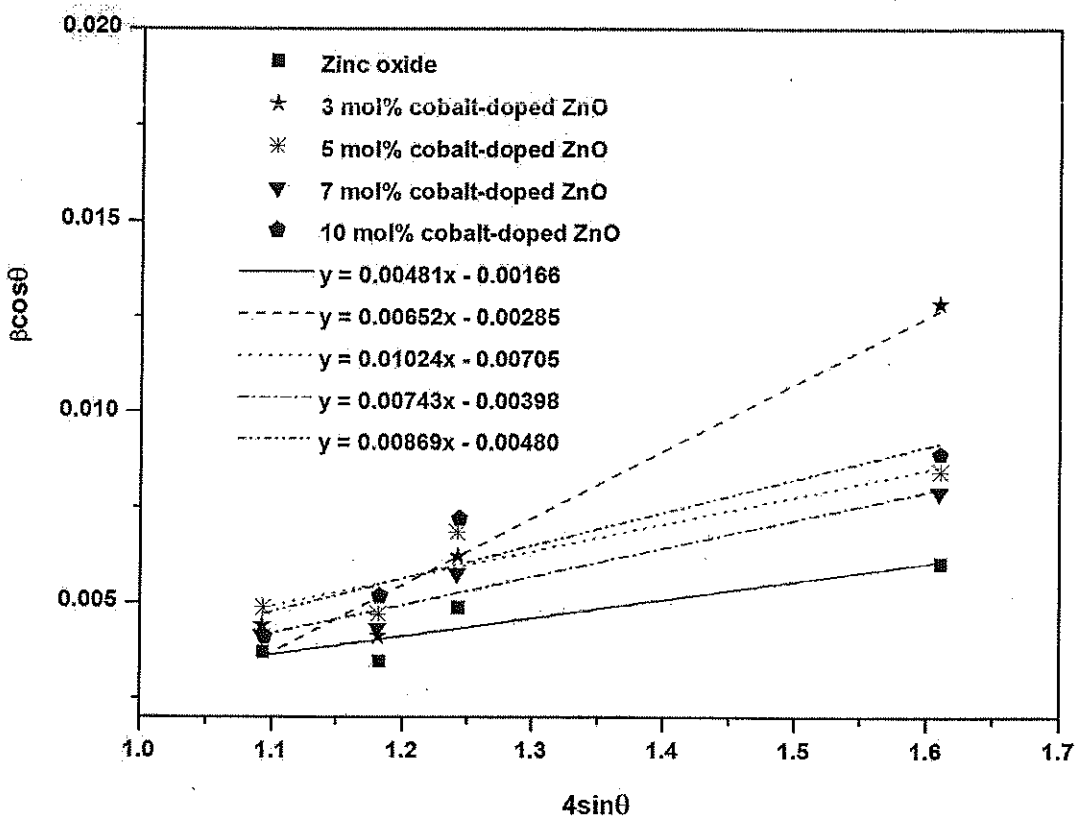

Figure 4.4 Williamson-Hall analysis as a function of cobalt-doping levels (mol% in dipping solution). Strain was extracted from the slope.

The average crystallite size of thin films was estimated using the W-H equations based on the diffraction peaks of (1 0 0), (0 0 2), (1 0 1) and (1 0 2) as shown in Figure 4.4. The crystallite sizes of zinc oxide doped with cobalt at 3, 5, 7 and 10 mol% were 50.81 nm, 20.54 nm, 36.39 nm and 30.17 nm, respectively. The crystallite sizes were tended to decrease with increasing cobalt content compared with ZnO (87.24 nm) as shown in Figure 4.5. An increase in Co^{2+} ions incorporated in ZnO host matrix leaded to crystallite growth suppression, resulting in reduction of crystallite sizes [59, 102]. However, the slightly increased in the crystallite size at 7 and 10 mol% doping level as compared with cobalt-doped ZnO thin films (5 mol%) could be accompanied by a decrease in the lattice strain (see Figure 4.4).

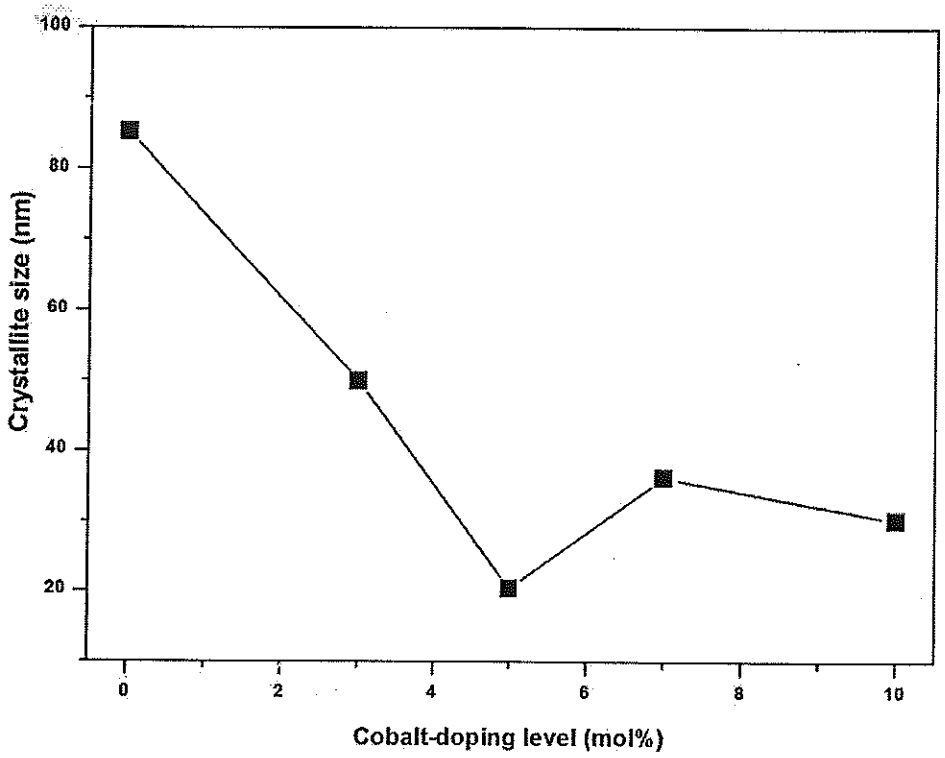

Figure 4.5 Crystallite size (nm) along diffraction planes as a function of cobalt-doping levels (mol% in dipping solution).

Due to the solubility limit of cobalt, M. Li et al. successfully fabricated cobalt-doped ZnO nanoparticles with doping level up to 3 mol% [29]. However, it largely depends on the preparation techniques, for example, H. Yang and S. Nie [135] prepared cobalt-doped ZnO nanopowder with cobalt content from 2 mol% to 10 mol% by novel freeze-drying route. They found that the solubility limit for cobalt-doped ZnO is 10 mol%. As well known, the limit of solubility is the amount of mole of a dopant that a host can hold. The cobalt ions incorporated into ZnO lattice could be induced by the crystal lattice distortion degree (R). This value can be determined by the equation 4.2 [29].

$$R = \frac{2a\sqrt{\frac{2}{3}}}{c} \qquad (4.2)$$

where a and c are lattice constants and can be calculated from the XRD patterns. The crystal lattice distortion degrees of ZnO with different cobalt-doping concentrations were shown in Figure 4.6.

It was found that the crystal lattice distortion degree of doped films did not change when compared to pure ZnO, indicating that the solid solution limit of cobalt ions could be lower than 3 mol%.

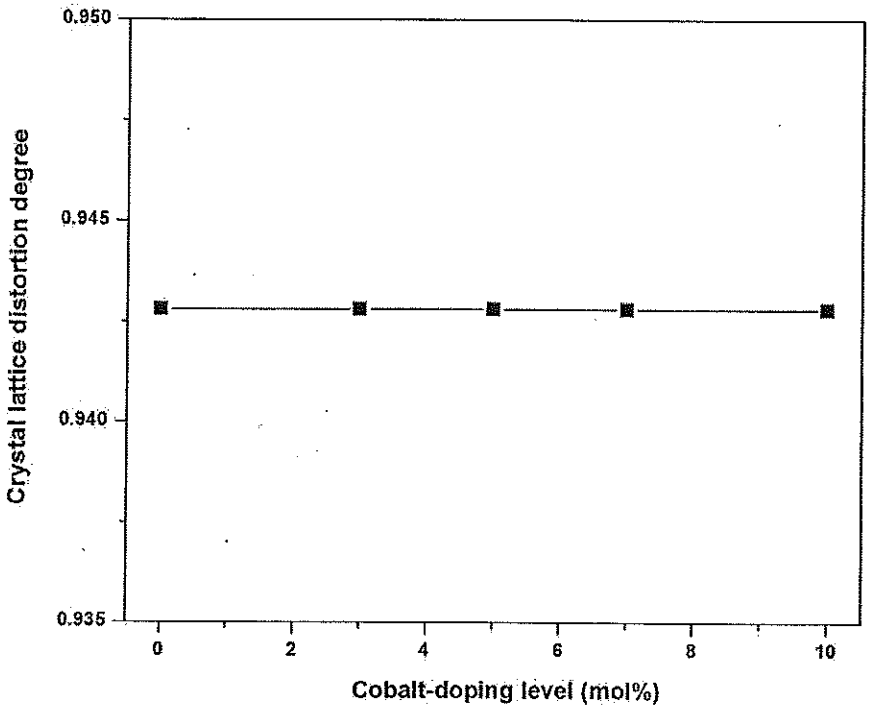

Figure 4.6 Crystal lattice distortion degree of cobalt-doped ZnO thin films with different cobalt-doping levels (mol% in dipping solution).

4.2 Characterization of thin film by FT-IR

Infrared transmission measurements were employed to rule out the formation of secondary phases such as CoO or Co_3O_4 [140]. In this work, the FT-IR transmittance spectra of the powder scratched from the ZnO and cobalt-doped ZnO thin films in the wavenumber range 4000–400 cm^{-1} were illustrated in Figure 4.7. The FT-IR transmittance spectra presented the information about phase composition, and the way of oxygen was bound to the metal ions (M–O structure). The vibration of Zn-O and Co-O were appeared in the range of 700-400 cm^{-1} as a result of condensation reaction. For the standard ZnO powder (99.0% purity from CARLO ERBA), the FT-IR transmission band appeared at 428 cm^{-1} (see Figure 4.7a) which could be attributed to stretching frequency of Zn-O [133, 138]. Meanwhile, the FT-IR transmittance spectra

ZnO film showed peak at 436 cm^{-1} (see Figure 4.7b). The vibration band frequency of ZnO film as compared to the standard ZnO powder was an indication of successful ZnO film preparation in the present work. In the other work, R. Elilarassi and G. Chandarasekaran prepared cobalt-doped ZnO nanoparticle by auto-combustion method and the FT-IR transmission spectra of ZnO nanoparticle presented at 439 cm^{-1} which had been attributed to stretching vibration frequency of Zn-O [140].

For cobalt-doped ZnO films, the FT-IR transmission peaks of doped films at 3, 5, 7 and 10 mol% were 435, 428, 428 and 420 cm^{-1}, respectively. The transmission band of cobalt-doped ZnO thin films slightly shifted to the lower wavenumbers compared with pure ZnO (436 cm^{-1}). The results could be explained that, in cobalt-doped ZnO, cobalt had been supposed to substitute Zn in ZnO lattice resulted in shifting of Zn-O group vibration. The difference in charge and crystal radius of zinc and cobalt changed the vibration of Zn-O and increased the defect in ZnO lattice because of lattice mismatch. In another possible reason, a solubility limit of cobalt atom in ZnO lattice generated the excess of cobalt atoms, which could not replace the zinc atoms in the lattice, but form the interstitial additives. The presence of interstitial additives increased the disorder of lattice markedly, which caused the shifting of Zn-O vibration frequency at high doping levels. In addition, the Co-O vibration was clearly observed at high cobalt-doping concentration (see Figure 4.7e-f). The Co-O vibration band of 7 and 10 mol% cobalt-doped ZnO films were presented around 678 and 677 cm^{-1}, respectively. Whereas, the FT-IR transmittance spectra of the powder scratched from the cobalt oxide thin film (see Figure 4.7g) showed peaks at 570 and 663 cm^{-1}. The variation of vibration band for cobalt-doped ZnO films as compared to the FT-IR transmittance spectra of the ZnO (Figure 4.7b) and cobalt oxide (Figure 4.7g) thin films was a confirmation of the presence of interstitial additives in ZnO lattice above 7 mol% cobalt-doping.

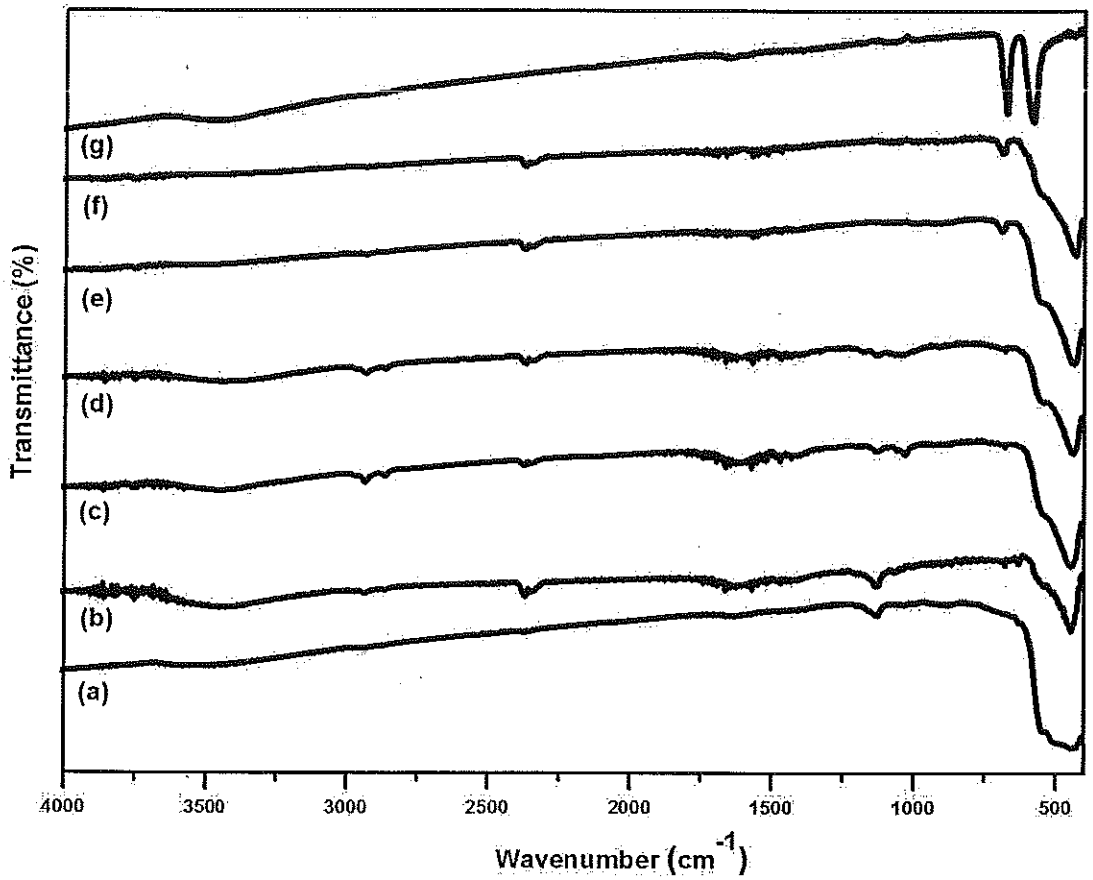

Figure 4.7 FT-IR spectra in the range 4000-400 cm^{-1}: (a) standard ZnO powder, (b) the powder scratched from the ZnO film, (c)-(f) the powder scratched from the cobalt-doped ZnO thin films with different cobalt-doping as 3 mol%, 5 mol%, 7 mol%, 10 mol% and (g) the powder scratched from the cobalt oxide film.

4.3. Surface morphology

The surface morphology of cobalt-doped ZnO (0 to 10 mol%) and cobalt oxide thin films prepared by dip coating method were investigated by atomic force microscopy (AFM) measurement with non-contact mode. The surface roughness of the films was measured in the area of 1 μm x 1 μm. The typical morphological feature of the films was recognized readily by visual inspection of both 2-dimensional and 3-dimensional micrographs as shown in Figure 4.8 and 4.9, respectively.

From the 2D-AFM micrographs (see Figure 4.8), the mean grain size of zinc oxide doped with cobalt at 0, 3, 5, 7, 10 mol% and cobalt oxide thin films were 114 nm, 81 nm, 53 nm,

65 nm, 86 nm and 17 nm, respectively. From Figure 4.10, the grain sizes tended to decrease with increasing cobalt content compared with ZnO (114 nm) [104]. An increase in Co^{2+} ions incorporated in ZnO host matrix promoted the crystallite growth suppression, resulting in reduction of grain sizes. However, the slightly increase in crystallite size at 7 and 10 mol% doping level as compared with cobalt-doped ZnO thin films (5 mol%) could be explained by an increase in the number of grain boundary [142]. In this study, it was indicated that the cobalt-doping level played an important role in the grain size of ZnO.

Surface roughness can be presented as root mean square (RMS) roughness (R_q) which is calculated by equation 4.3 [143]:

$$R_q = \sqrt{\frac{1}{n}\sum_{i=1}^{n} Z_i^2} \tag{4.3}$$

where Z_i is height at point i, and n is number of points in the image.

The roughness values of the thin films were determined from the 3D-micrographs (see Figure 4.9) as shown in Figure 4.11. The data presented that the surface morphology of the cobalt-doped ZnO films was smoother than the undoped ZnO thin film. The surface roughness was found to decrease with the increase in the cobalt doping percentage up to 5 mol%. The similar result was obtained from cobalt-doped ZnO films prepared by spray pyrolysis method [104]. However, for more than 5 mol% cobalt-doped ZnO film, the surface roughness of film increased along with increasing the grain size (Figure 4.10). An increase in the number of grain boundary due to increase in doping concentration leaded to high grain growth promotion and resulted in increasing of surface roughness of films [105, 144].

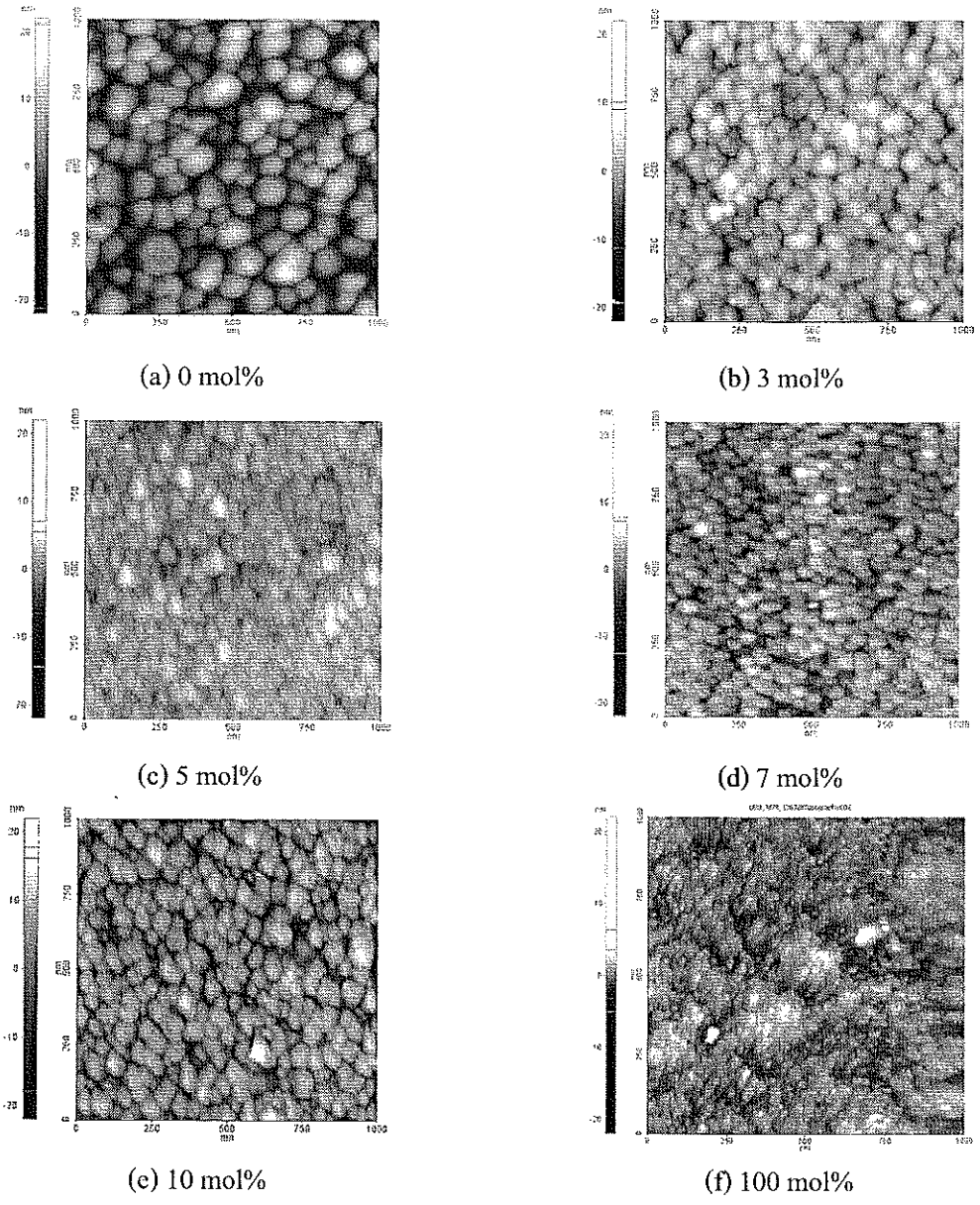

(a) 0 mol%

(b) 3 mol%

(c) 5 mol%

(d) 7 mol%

(e) 10 mol%

(f) 100 mol%

Figure 4.8 2D AFM images of cobalt-doped ZnO thin films with different cobalt doping levels (mol% in dipping solution).

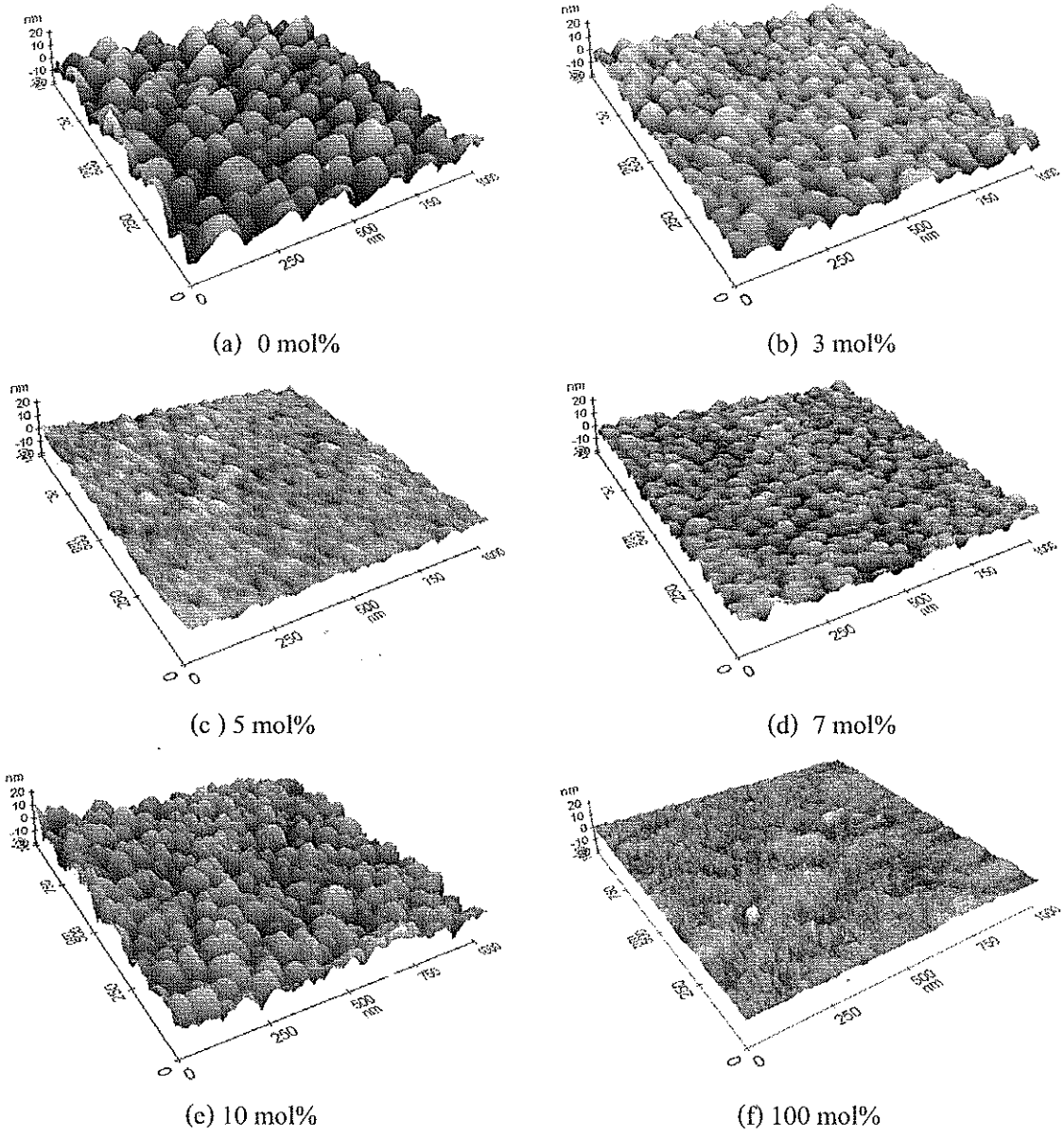

(a) 0 mol%

(b) 3 mol%

(c) 5 mol%

(d) 7 mol%

(e) 10 mol%

(f) 100 mol%

Figure 4.9 3D AFM images of cobalt-doped ZnO thin films with different cobalt doping levels (mol% in dipping solution).

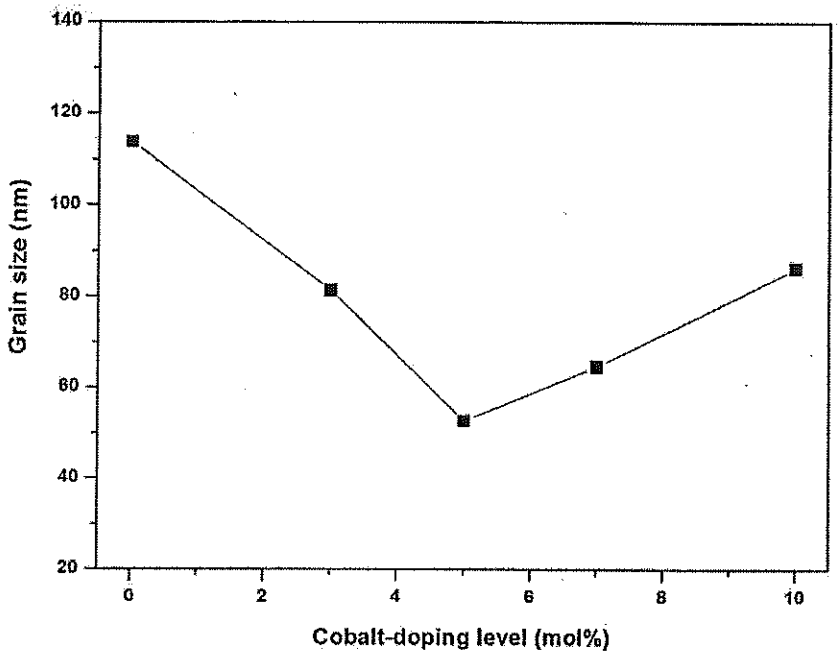

Figure 4.10 Mean grain size of cobalt-doped ZnO thin films as a function of cobalt-doping levels (mol% in dipping solution).

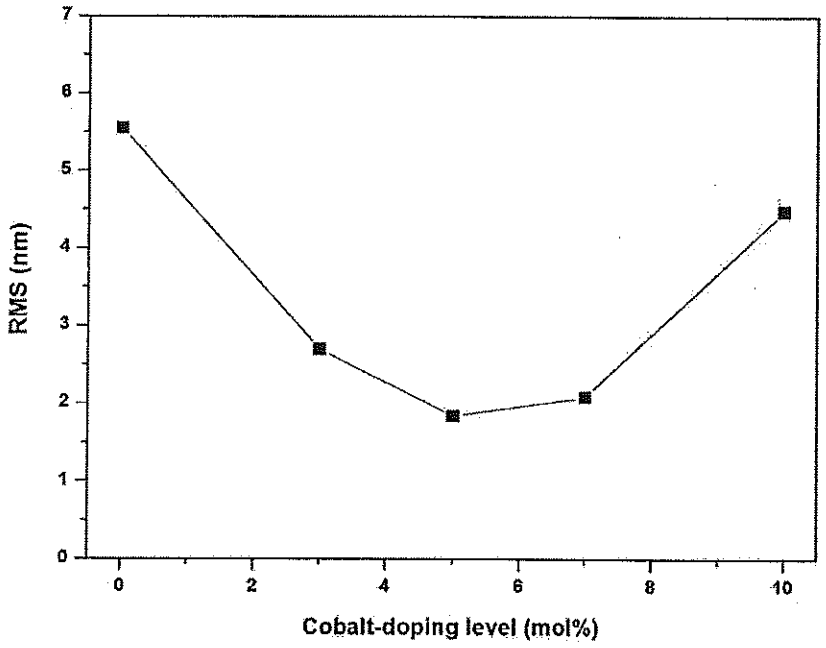

Figure 4.11 Surface roughness of cobalt-doped ZnO thin films as a function of cobalt-doping levels (mol% in dipping solution).

4.4 Optical properties

The optical transmittance spectra of the films were recorded in the wavelength range 300-1,100 nm as shown in Figure 4.12. The average transmittances in visible region (400–800 nm) of pure ZnO, cobalt-doped ZnO (3, 5, 7 and 10 mol%) and cobalt oxide thin films were 95.64 %T, 94.66 %T, 91.19 %T, 90.16 %T, 61.97 %T and 13.58 %T, respectively (see Figure 4.13). The high transmittance of pure ZnO thin film was due to the better crystallinity of thin films, resulting in the low optical scattering which was corresponding to FWHM value from XRD analysis method. It was also found that the average transmittance decreased with increase in cobalt-doping which correlated along with decreasing of crystallinity in the XRD analysis. The similar result was obtained from cobalt-doped ZnO films prepared by spray pyrolysis method [104].

The average thickness of the pure and cobalt-doped ZnO (3, 5, 7 and 10 mol%) thin films were 567 nm, 552 nm, 564 nm, 535 nm and 571 nm, respectively. As seen from Figure 4.14, the film thickness did not significantly change by cobalt-doping up to 10 mol%. Therefore, the transparency of ZnO film did not depend on the film thickness.

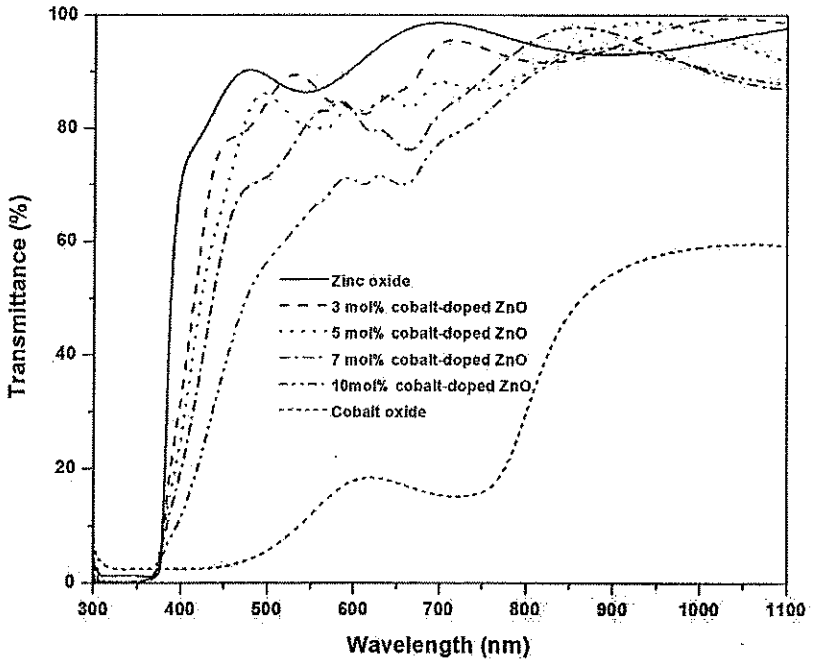

Figure 4.12 The optical transparency of cobalt-doped ZnO thin films with different cobalt-doping levels (mol% in dipping solution).

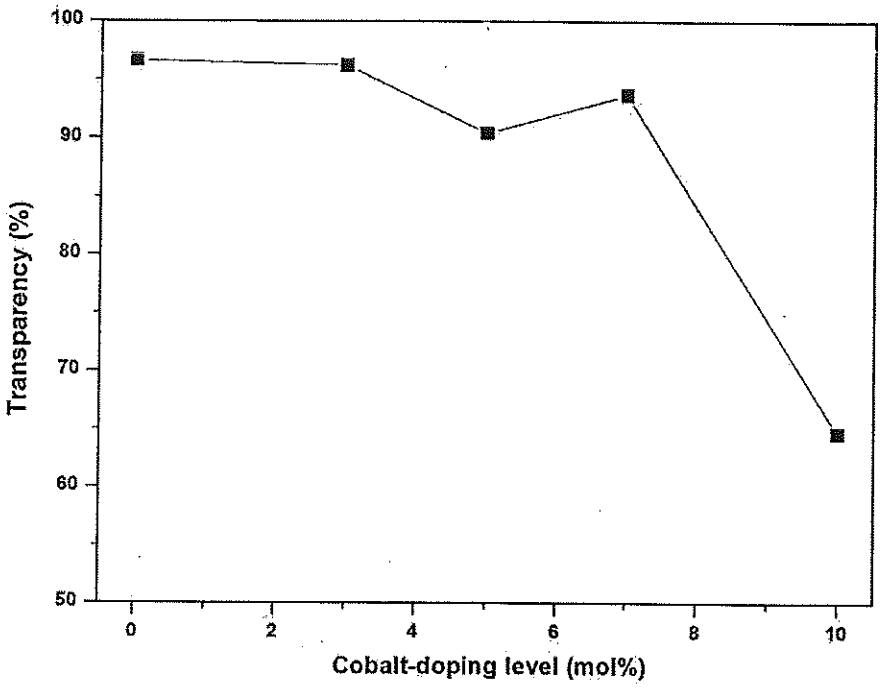

Figure 4.13 Transparency of cobalt-doped ZnO thin films with different cobalt-doping levels (mol% in dipping solution).

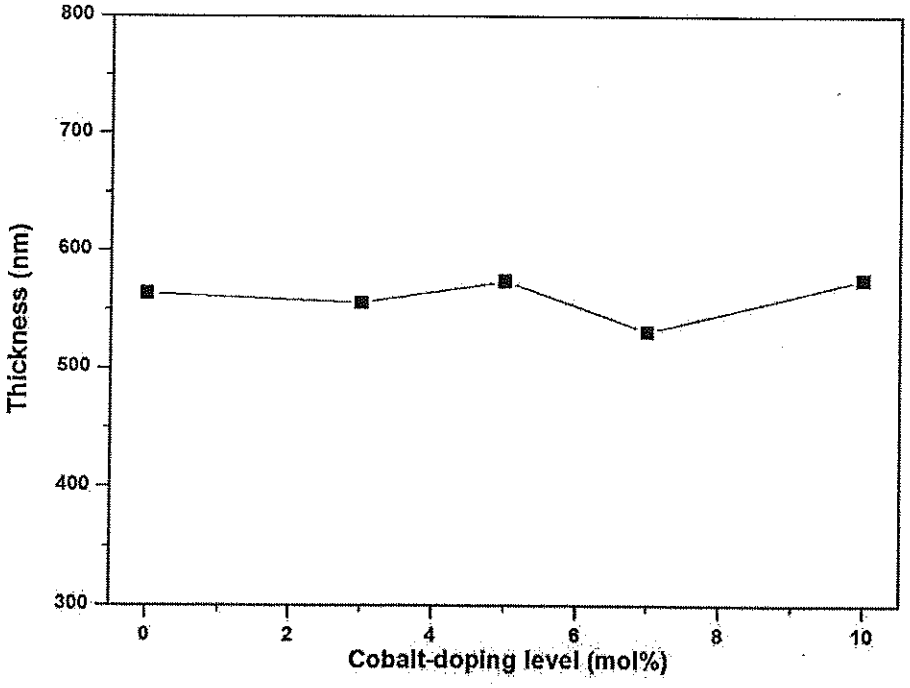

Figure 4.14 Thickness of doped ZnO thin films with different cobalt-doping levels (mol% in dipping solution).

The band gap of the films were estimated by extrapolation of the linear portion of an $(\alpha h\nu)^2$ versus $(h\nu)$ plot as given in Figure 4.15. The mean direct optical band gap of pure ZnO, cobalt-doped ZnO (3, 5, 7 and 10 mol%) and cobalt oxide thin films were 3.21 eV, 3.27 eV, 3.28 eV, 3.26 eV, 3.25 eV and 2.10 eV, respectively. It indicated that the band gap of cobalt-doped ZnO thin films slightly increased with increase in cobalt-doping up to 5 mol% and then decreased as shown in Figure 4.16 [145].

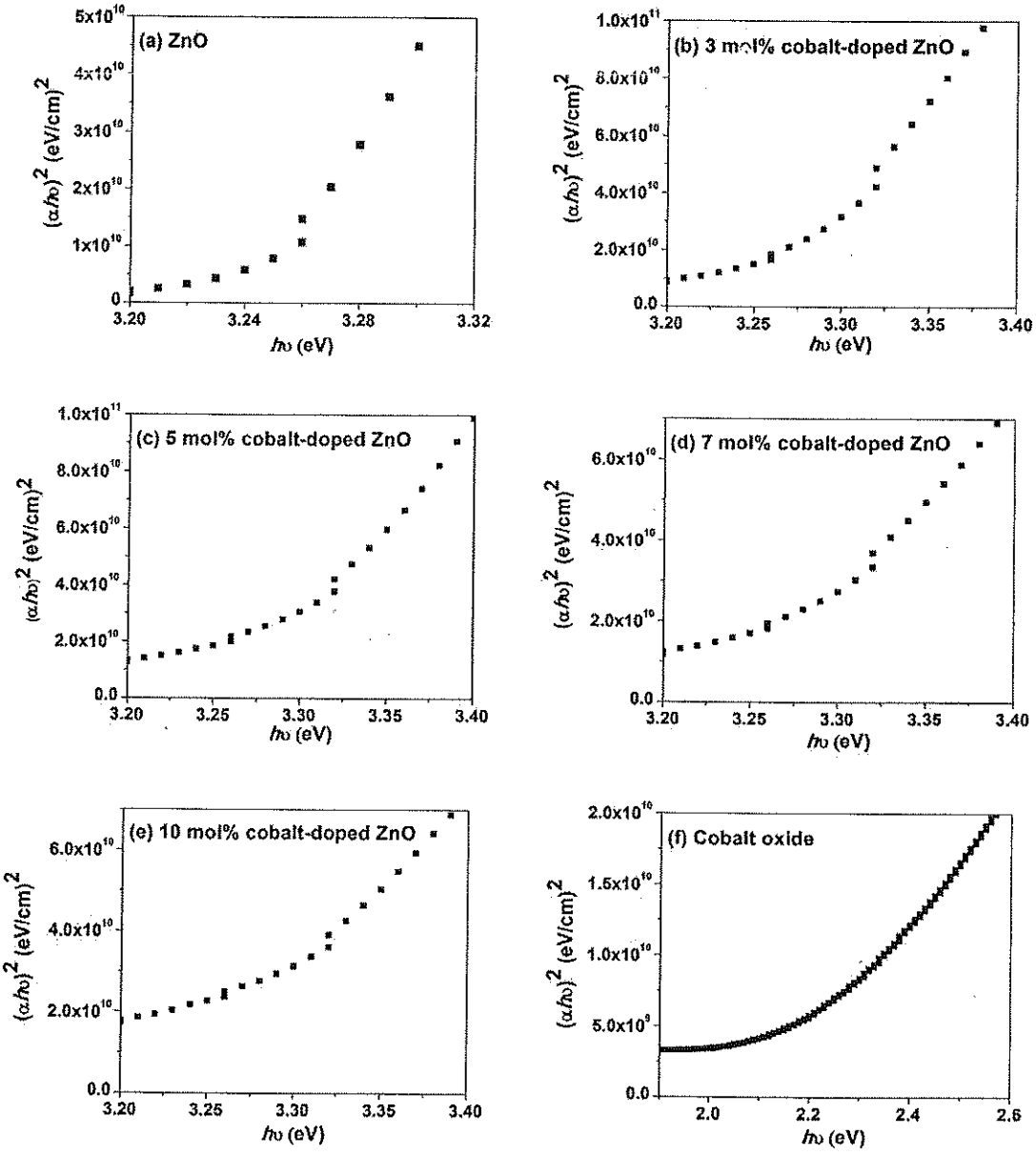

Figure 4.15 Plot of $(\alpha h\nu)^2$ versus photon energy ($h\nu$) for cobalt-doped ZnO films with different cobalt-doping levels (mol% in dipping solution).

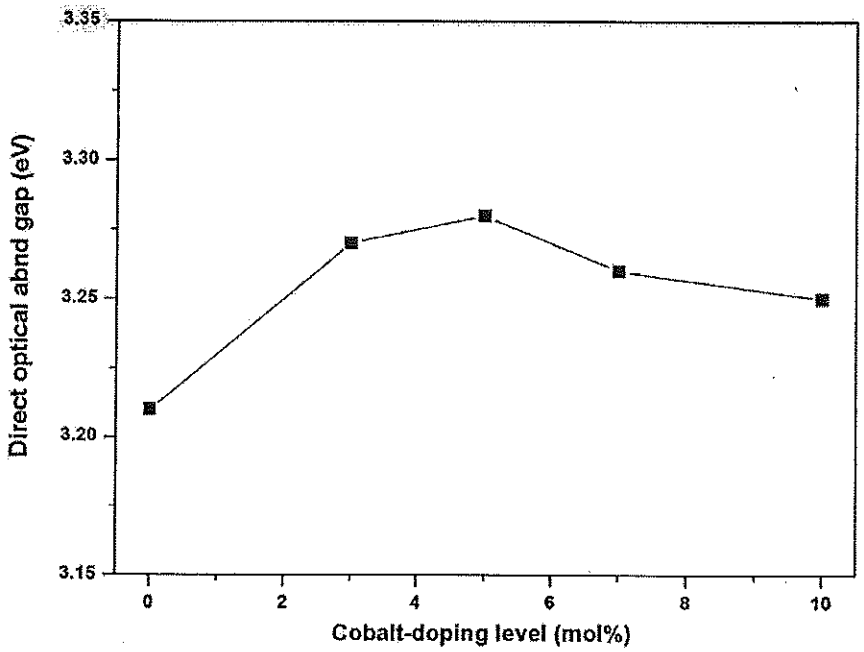

Figure 4.16 Mean direct optical band gaps of cobalt-doped ZnO thin films with different cobalt-doping levels (mol% in dipping solution).

4.5 Photoluminesecence

Photoluminescence (PL) spectroscopy is an important tool to characterize the optical properties of a photocatalyst. PL intensity is directly correlated with the defect density in a fluorescent material. Therefore, it was used to study the luminescence properties of present thin films. First of all, the optimal fluorescence excitation wavelength (in the range of 250 nm to 350 nm) for detection of ZnO thin films was investigated, as shown Figure 4.17. The results showed that excitation wavelength (λ_{ex}) of 325 nm had the highest intensity with emission wavelength (λ_{em}) of 391 nm when compared with other excitation wavelengths. Thus, this excitation wavelength was used for PL intensity detection [29].

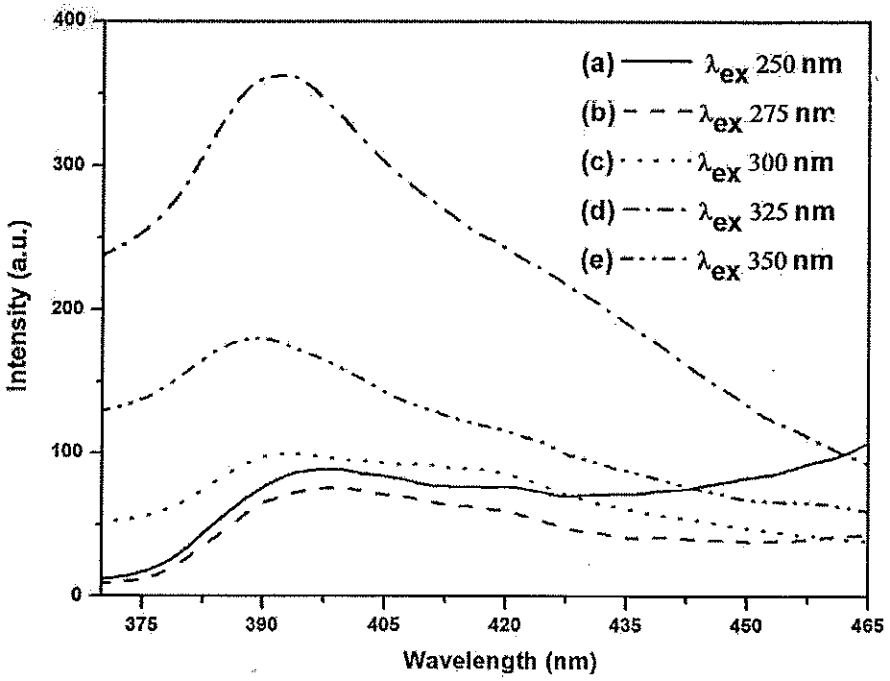

Figure 4.17 Emission spectra of pure ZnO thin films at room temperature with different excitation wavelength.

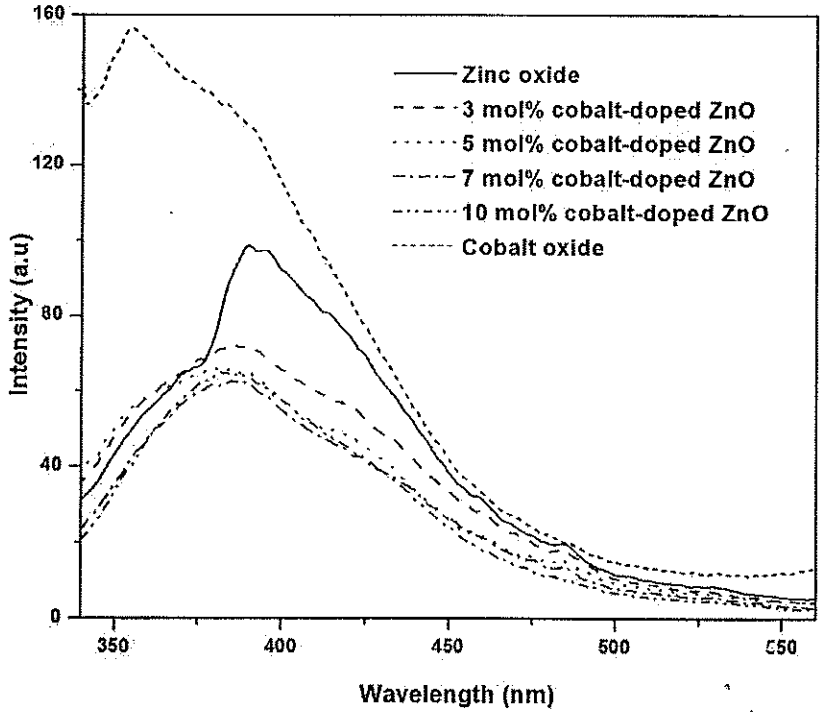

Figure 4.18 Photoluminescence spectra of pure and cobalt-doped ZnO thin films at room temperature with λ_{ex} of 325 nm.

The room temperature PL spectra of pure ZnO, cobalt-doped ZnO (3, 5, 7 and 10 mol%) and cobalt oxide thin films in the wavelength range of 340-600 nm with an excitation wavelength of 325 nm were illustrated in Figure 4.18. As can be seen from the figure that the pure ZnO, cobalt-doped ZnO (3, 5, 7 and 10 mol%) and cobalt oxide thin films exhibited the strong UV emission peaks with a wavelength of about 390 nm, 390 nm, 382 nm, 387 nm, 384 nm and 355 nm, respectively. It can be converted to band gap energy according to the following equation 4.4:

$$Eg = \frac{1239.8}{\lambda} \tag{4.4}$$

where Eg is the band gap energy (eV) and λ is the maximum wavelength (nm) of the emission peak in PL spectra [146].

The band gap energy of the pure ZnO, cobalt-doped ZnO (0, 3, 5, 7 and 10 mol%) and cobalt oxide thin films were found to be 3.18 eV, 3.18 eV, 3.25 eV, 3.21 eV, 3.23 eV and 3.49 eV, respectively. It was noticed that the band gap energy determined from the obtained PL spectra agreed well with the results of UV-Visible absorption measurement (see Figure 4.16). The UV emission must be contributing to the near band edge emission (NBE) of the wide band gap ZnO (3.37 eV) [147]. The position of the UV emission exhibited a blue shift (from 390 nm to 384 nm) as cobalt-doping concentration increased in comparison with the pure ZnO (see Figure 4.18). A slightly blue shift in the cobalt-doped ZnO band edge emission from 390 nm to 384 nm may be related to cobalt ions which take up the energy level located at the bottom of ZnO conduction band and the photogenerated electrons were excited to the ZnO conduction band with higher energy level when cobalt-doped ZnO was irradiated by UV-light. Thus a blue shift happened at the electron and holes recombination, and these results were in good agreement with the observation by many authors [139, 147].

The room temperature PL spectra of pure ZnO, cobalt-doped ZnO (3, 5, 7 and 10 mol%) and cobalt oxide thin films in the wavelength range of 340-600 nm with an excitation wavelength of 325 nm were illustrated in Figure 4.18. As can be seen from the figure that the pure ZnO, cobalt-doped ZnO (3, 5, 7 and 10 mol%) and cobalt oxide thin films exhibited the strong UV emission peaks with a wavelength of about 390 nm, 390 nm, 382 nm, 387 nm, 384 nm and 355 nm, respectively. It can be converted to band gap energy according to the following equation 4.4:

$$Eg = \frac{1239.8}{\lambda} \tag{4.4}$$

where Eg is the band gap energy (eV) and λ is the maximum wavelength (nm) of the emission peak in PL spectra [146].

The band gap energy of the pure ZnO, cobalt-doped ZnO (0, 3, 5, 7 and 10 mol%) and cobalt oxide thin films were found to be 3.18 eV, 3.18 eV, 3.25 eV, 3.21 eV, 3.23 eV and 3.49 eV, respectively. It was noticed that the band gap energy determined from the obtained PL spectra agreed well with the results of UV-Visible absorption measurement (see Figure 4.16). The UV emission must be contributing to the near band edge emission (NBE) of the wide band gap ZnO (3.37 eV) [147]. The position of the UV emission exhibited a blue shift (from 390 nm to 384 nm) as cobalt-doping concentration increased in comparison with the pure ZnO (see Figure 4.18). A slightly blue shift in the cobalt-doped ZnO band edge emission from 390 nm to 384 nm may be related to cobalt ions which take up the energy level located at the bottom of ZnO conduction band and the photogenerated electrons were excited to the ZnO conduction band with higher energy level when cobalt-doped ZnO was irradiated by UV-light. Thus a blue shift happened at the electron and holes recombination, and these results were in good agreement with the observation by many authors [139, 147].

4.6 Characterization of photocatalytic activity

Malachite green was used as a test reactive dye, because its absorption peak is in the visible range and its degradation can be easily monitored by optical absorption spectroscopy. In this work, four sets of experiments were performed in order to prove the photocatalytic activity of ZnO and coblat-doped ZnO films with respect to Malachite green (MG) degradation. First, experiments were carried out on the exposure of MG to films under UV illumination (the photocatalytic condition). Second, experiments were performed at the same conditions, but without UV illumination (the catalytic condition). Third, experiments were done by exposing MG aqueous solution to UV-light without the presence of film in the solution (the photolysis condition). Finally, experiments were measured for the MG aqueous solutions in darkness without the presence of film in the solution (the self degradation condition).

Figure 4.19-Figure 4.20 showed the visible absorption spectra of MG dye solution with different irradiating time using the cobalt-doped ZnO (0, 3, 5, 7 and 10 mol%) and cobalt oxide thin films as catalysts under both UV-light illumination and darkness, respectively. The absorption peaks of dye diminished over time and finally disappeared. This indicated that the dye had been degraded and no new absorption band appeared in the visible region as shown in Figure 4.21. After 180 min UV-light irradiation, it was found that the absorbance intensity (at 616 nm) was reduced from 0.6853 (MG initial concentration) to 0.0354, 0.1492, 0.1773, 0.1768, 0.0966 and 0.5267 for pure ZnO, cobalt-doped ZnO (3, 5, 7 and 10 mol%) and cobalt oxide thin film, respectively. It can be concluded that the pure ZnO films has the highest decolorization efficiency in the MG solution under UV-light illumination.

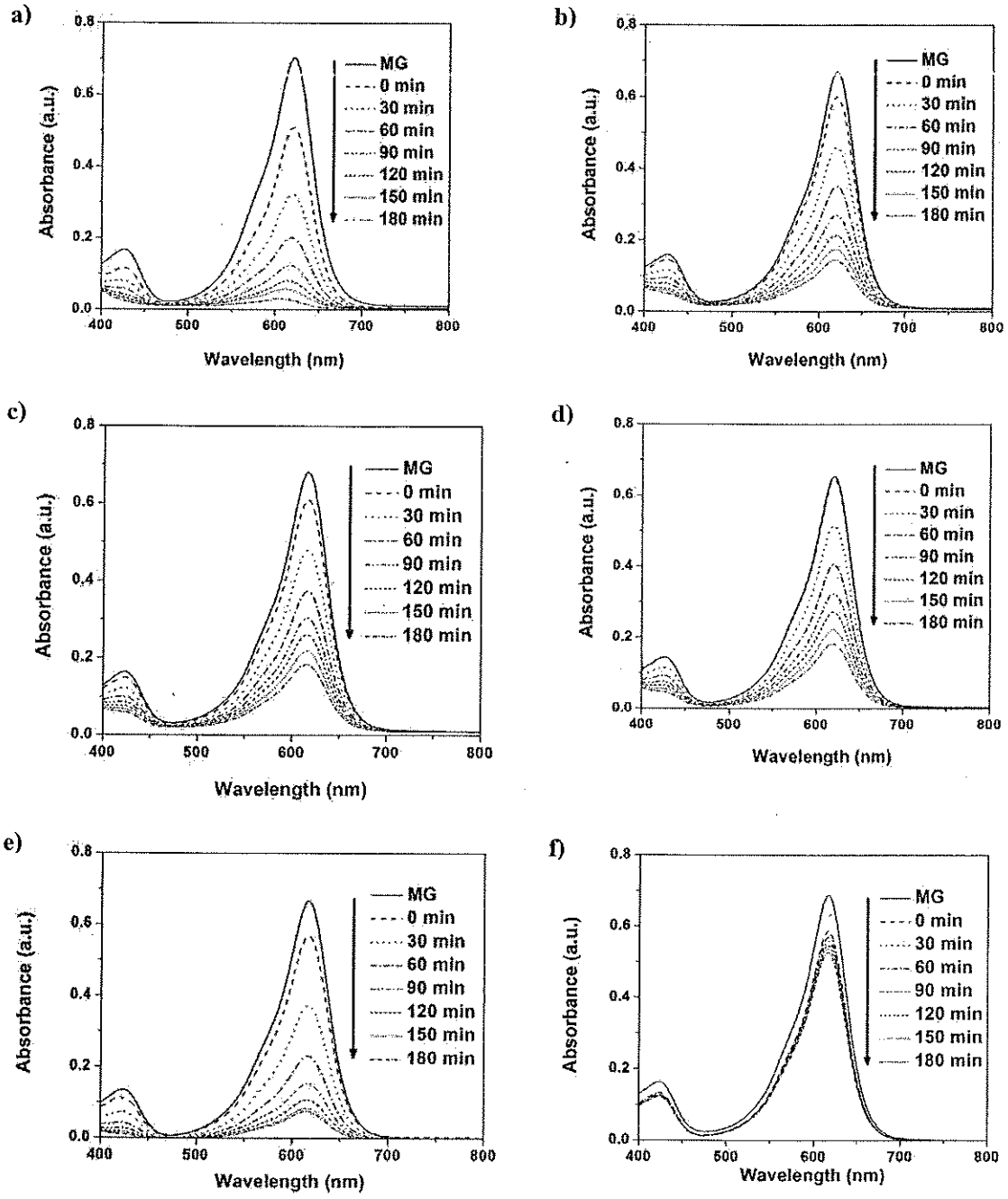

Figure 4.19 Absorption spectra of MG under UV-light illumination time over cobalt-doped ZnO thin films with different cobalt-doping levels (mol% in dipping solution): a) 0 mol%, b) 3 mol%, c) 5 mol%, d) 7 mol%, e) 10 mol% and f) 100 mol%.

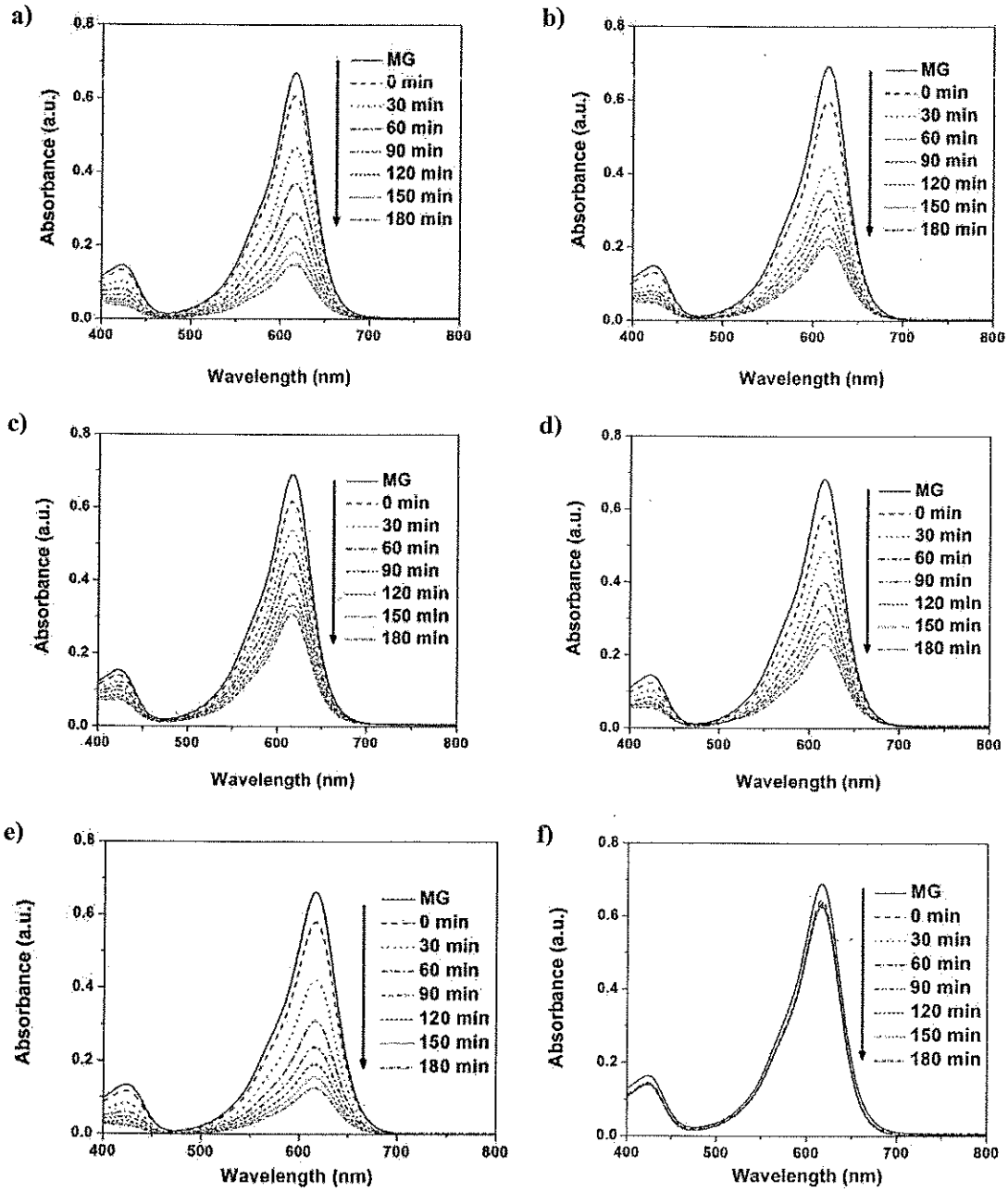

Figure 4.20 Absorption spectra of MG in darkness over cobalt-doped ZnO thin films with different cobalt-doping levels (mol% in dipping solution): a) 0 mol%, b) 3 mol%, c) 5 mol%, d) 7 mol%, e) 10 mol% and f) 100 mol%.

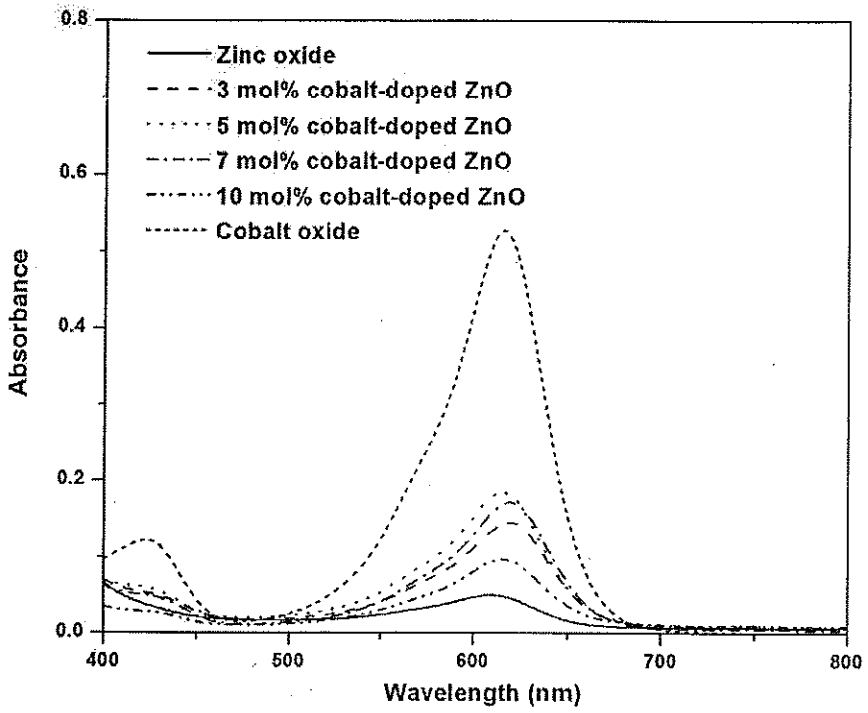

Figure 4.21 Absorption spectra of MG under 180 min UV-light illumination time over cobalt-doped ZnO thin films with different doping levels.

As seen from Figure 4.22, absorption peaks of MG dye exhibited two maxima of absorbance at 423 nm and 616 nm, respectively. The intensity of absorption peak of MG dye at 616 nm was higher than peak at 423 nm. In this work, the absorbance value of absorption peak of MG dye at 616 nm was selected to obtain high sensitivity of detection. A calibration line was plotted by the absorbance at 616 nm versus the MG dye concentration in the standard solution (C; ppm) as shown in Figure 4.23. The calibration plot (correlation coefficient 0.9977) showed the linear dependence of optical absorbance (A) on the dye concentration expressed as in equation 4.5:

$$A = 0.14C - 0.01 \quad (4.5)$$

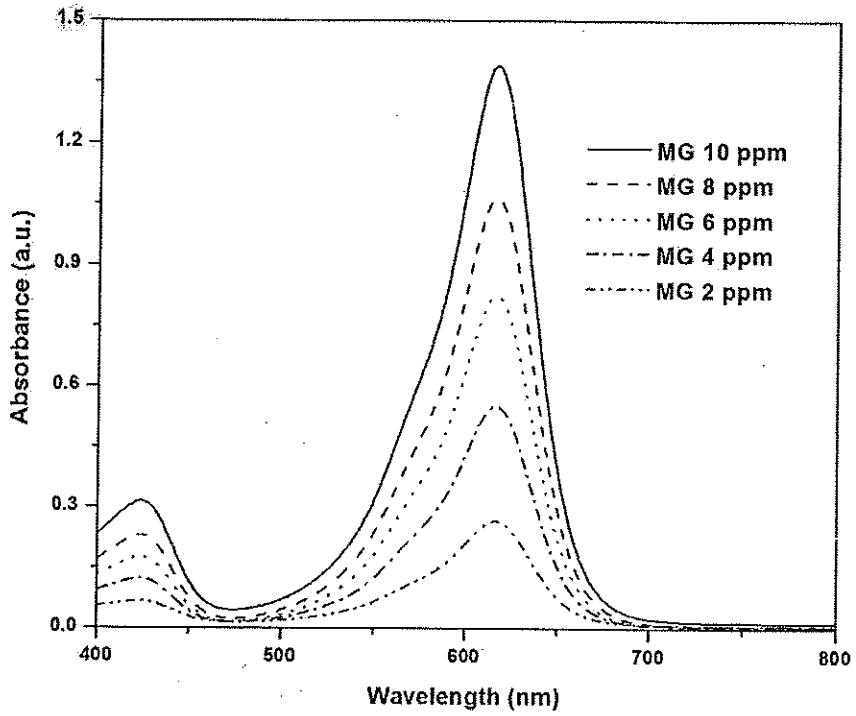

Figure 4.22 Absorption spectra of MG dye standard solution with different concentrations.

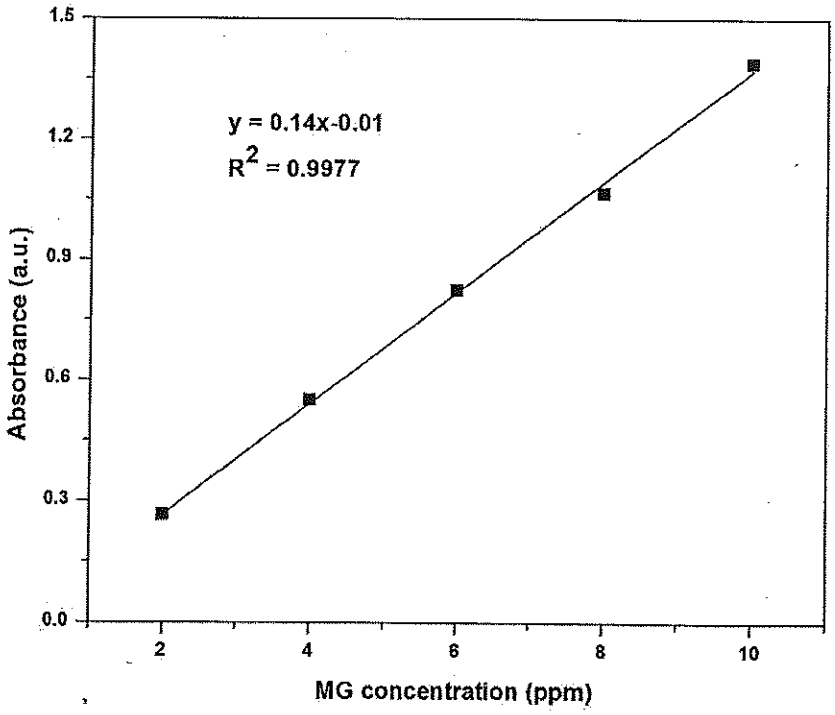

Figure 4.23 The calibration line of the absorbance maxima at wavelength 616 nm versus the dye concentration.

The degradation percentage (D) of MG dye was calculated as shown in equation 4.6 :

$$D=100\times\left[\frac{C_0-C}{C_0}\right] \tag{4.6}$$

where C_0 is the initial concentration (5 mg/L) of MG

C is the concentration of MG after irradiation at selected time interval.

The relationship between the decolorization percentage and time under UV-light irradiation was illustrated in Figure 4.24. It was exhibited that the degradation percentages of cobalt-doped ZnO films with different cobalt-doping level at 0, 3, 5, 7, 10 mol%, cobalt oxide film and self photolysis of MG dye were 93.51%, 73.35%, 70.97%, 72.31%, 85.33%, 9.43% and 8.09% after 180 min, respectively. It was clearly observed that the increment in cobalt concentration gave a lower photocatalytic activity.

In darkness condition (see Figure 4.25), it was found that the degradation percentages of cobalt-doped ZnO films with different cobalt content at 0, 3, 5, 7, 10 mol%, cobalt oxide film and self degradation of MG dye were 71.77%, 61.23%, 51.76%, 58.48%, 79.16%, 2.27% and 1.76% after 180 min, respectively. As seen in Figure 4.24 and 4.25, the pure ZnO thin films had the highest degradation percentage under UV-light illumination, whereas 10 mol% of cobalt-doping had the highest degradation percentage in darkness condition. It was interesting that the films could decolorize the MG dye without UV illumination (Figure 4.25), however the decolorization efficiency was lower than the respective photocatalytic reactions. A decrease in MG concentration in this case was most probably due to the adsorption on the films or due to a sort of chemical activity of the films even in darkness. Moreover, our measurements of the absorbance of ZnO thin films used in the dye decolorization showed that there was no residual dye deposited on the film within the experimental error (see Figure 4.26). The obtained results indicated that a sort of chemical activity of the films even in darkness had more significant influence on the decolorization percentage of MG than the adsorption process.

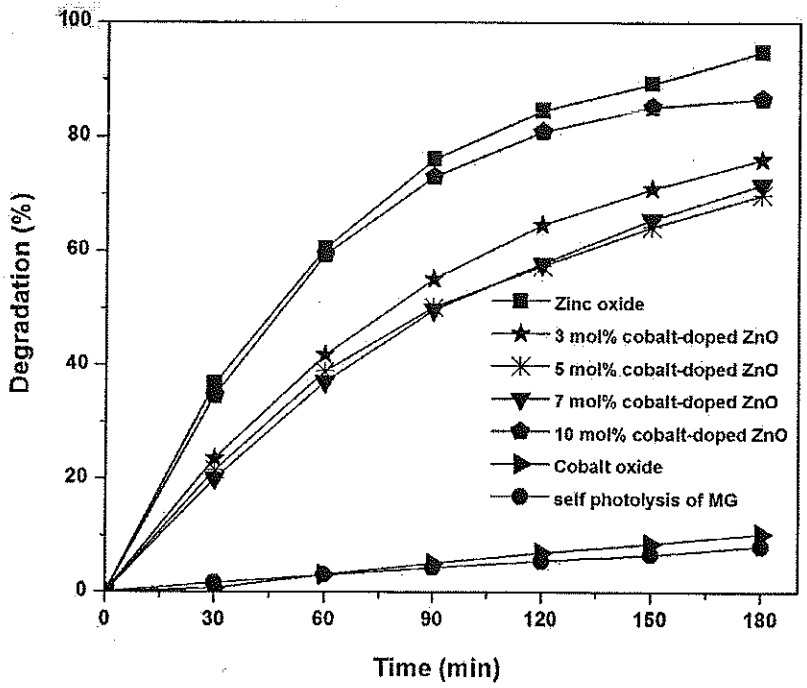

Figure 4.24 The degradation percentages of 5.0 mg/L MG solution as a function of UV-light irradiation times.

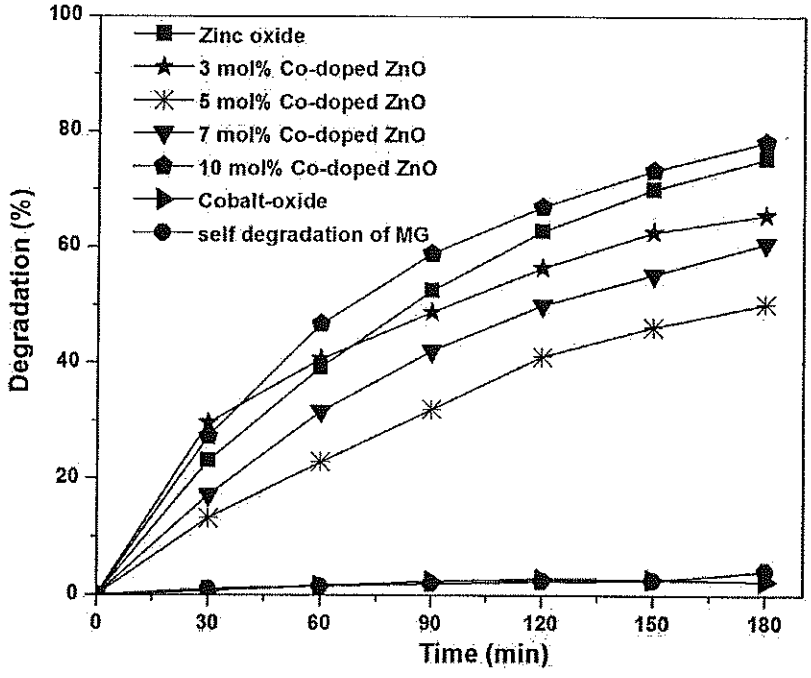

Figure 4.25 The degradation percentages of 5.0 mg/L MG solution as a function of times in darkness.

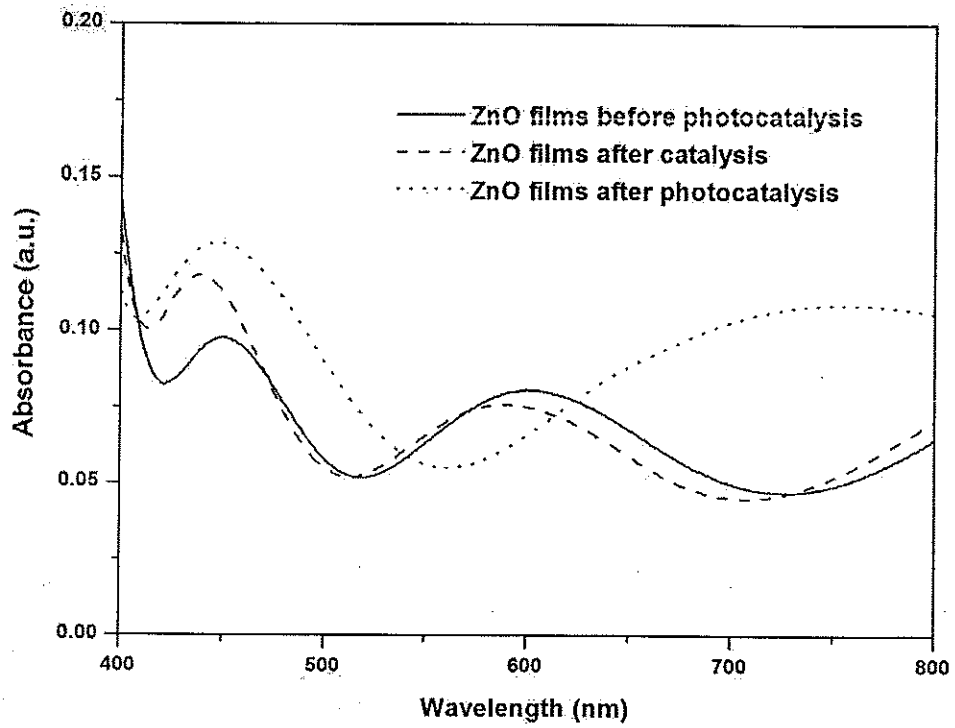

Figure 4.26 Comparison of absorption spectra of films used in the decolorization of MG after 180 minute.

The reaction kinetics was revealed by plotting the natural logarithm of concentration ratio (ln (C_0/C)) versus the irradiation time (t). Straight lines were obtained, indicating that the reaction was the first order. The slopes of these lines corresponded to the rate constant of reaction (k). The photocatalytic and photolytic degradation of MG dye by cobalt-doped ZnO (0, 3, 5, 7 and 10 mol%) and cobalt oxide film were found to be the pseudo-first-order reaction as shown in Figure 4.27. It was clear in Figure 4.27 that the increment in cobalt concentration gave a lower photocatalytic activity compared with ZnO, but this reduction of activity was not proportional to the doping level. The photocatalytic activity decreased for 3 and 5 mol% cobalt concentrations, but for higher concentration (7 and 10 mol%) the degradation rate constants increased. ZnO film had the highest reaction rate under UV-light, giving k = 0.0150 min^{-1}, while the rate constant of cobalt-doped ZnO films at 3, 5, 7, 10 mol% cobalt concentration and cobalt oxide film were 0.0078 min^{-1}, 0.0069 min^{-1}, 0.0071 min^{-1}, 0.0109 min^{-1} and 0.0006 min^{-1}, respectively. Meanwhile, the rate constant of photolytic degradation of MG dye under UV-light irradiation was

0.0006 min^{-1}. Obviously, the degradation of MG dye under UV-light illumination was more sensible to the photocatalytic activity, rather than the photolytic degradation.

The above results were compared with the decolorization of MG over films without UV illumination (in darkness). The degradation of MG dye over films without UV-light followed the pseudo-first-order reaction as shown in Figure 4.28. It was found that the rate constant of catalytic degradation of dyes at different cobalt concentration of 0, 3, 5, 7, 10 mol% and cobalt oxide film were 0.0069 min^{-1}, 0.0053 min^{-1}, 0.0041 min^{-1}, 0.0050 min^{-1}, 0.0089 min^{-1} and 0.0001 min^{-1}, respectively, whereas self degradation of MG was 0.0001 min^{-1}. As seen, the 10 mol% cobalt-doping had the highest rate constant in darkness. The results could be explained with the increase in cobalt content actually increased the number of the active sites on the catalyst surface thus causing an increase in the number of the $^{\bullet}HO$ radicals which can take part in actual decolorization of MG dye solution.

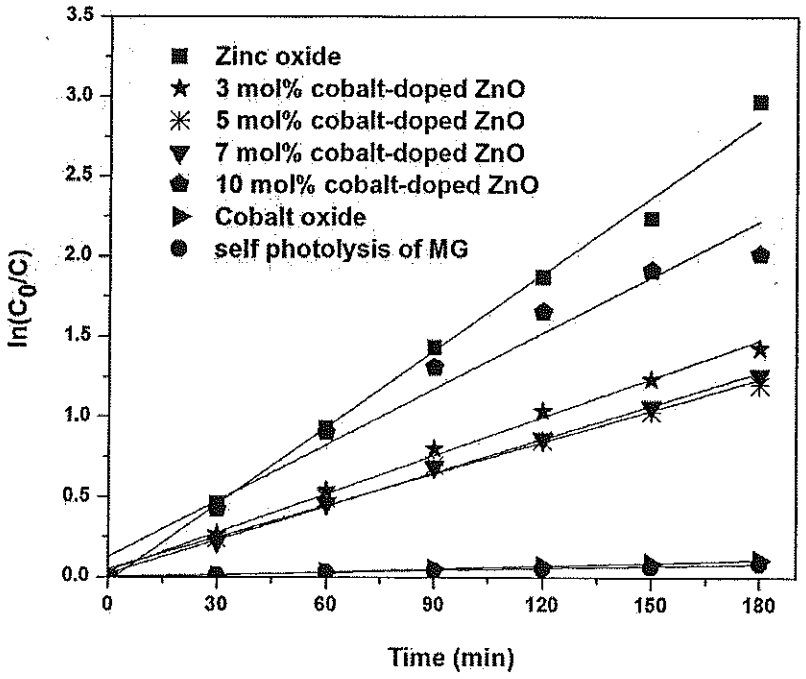

Figure 4.27 Pseudo-first-order reaction kinetics curves for photocatalytic degradation of MG under UV-light irradiation.

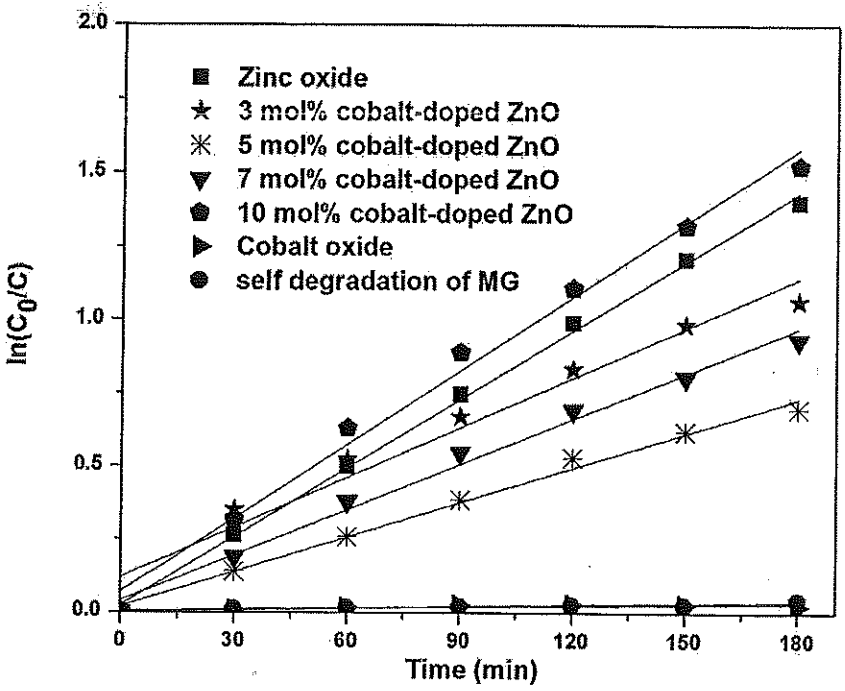

Figure 4.28 Pseudo-first-order reaction kinetics curves for catalytic degradation of MG in darkness.

As the comparison, degradation efficiency of MG dye under both UV-light and darkness in term of the apparent rate constants were shown in Figure 4.29. The photocatalytic efficiency of films was greater than the activity achieved from film in darkness. The results could be explained that UV-light illumination promoted the electrons in the conduction band and the electron vacancy in the valence band of film. Both these entities can migrate to the film surface, where they can enter in a redox reaction with other species present on the surface. The electrons in the conduction band can react with O_2 to produce superoxide radical anion of oxygen ($O_2^{-\bullet}$), whereas the electron vacancy in the valence band can react easily with surface bound H_2O to produce hydroxyl radicals ($^{\bullet}OH$). The $^{\bullet}OH$ and ($O_2^{-\bullet}$) can then react with dye to form other species and is thus responsible for the discoloration of the MG dye.

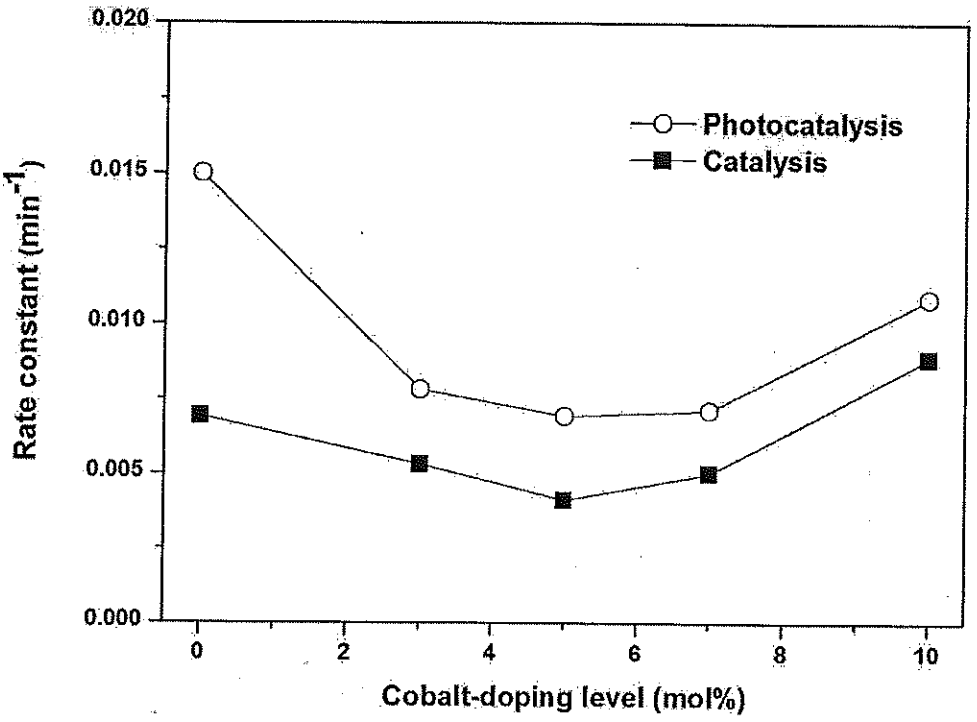

Figure 4.29 Effect of mol% cobalt dopant (mol% in dipping solution) and catalysis condition on the rate constant of cobalt-doped ZnO films.

Dye degradation rate can be influenced by numerous factors such as the band gap energy, PL intensity and RMS roughness as shown in Figure 4.30-4.32. From Figure 4.30, it was found that the band gap energy for both ZnO and cobalt-doped ZnO were the same (about 3.2 eV), so the photocatalytic activity of the present film did not depend on the band gap energy.

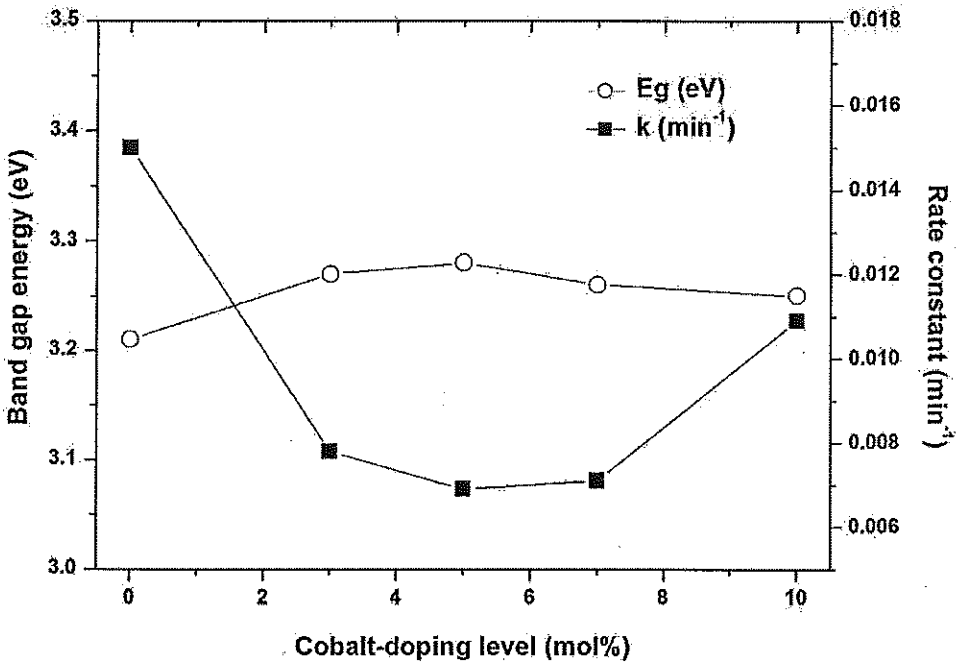

Figure 4. 30 Comparison of the optical band gap and degradation rate constant of doped ZnO thin films with different cobalt-doping levels.

PL spectrum is a useful tool to investigate the recombination rate of electron-hole pairs that greatly affect the photocatalytic activity of photocatalysts. Generally, a low PL intensity indicates an increase in the recombination rate [148]. As well known, during the process of PL, oxygen vacancies and defects could bind photoinduced electrons to form free or binding exactions so that PL signal could easily occur, and the larger the content of oxygen vacancies or defects, the stronger the PL intensity. But, during the process of photocatalytic reactions, oxygen vacancies and defects could become the centers to capture photoinduced electrons so that the recombination of photoinduced electrons and holes could be effectively inhibited. Moreover, oxygen vacancies could promote the adsorption of O_2, and there was strong interaction between the photoinduced electrons bound by oxygen vacancies and adsorbed O_2. This indicates that the binding for photoinduced electrons of oxygen vacancies could make for the capture for photoinduced electrons of adsorbed O_2, and $O_2^{-\bullet}$ free group is produced at the same time. Thus, oxygen vacancies and defects are in favor of photocatalytic reactions in that O_2 is active to promote the oxidation of organic substances [149].

As seen in Figure 4.31, the results was demonstrated that there were certain relationships between PL spectra and photocatalytic activity, namely, the stronger (or sharper) the PL intensity, the larger the content of oxygen vacancies and defects, the higher the photocatalytic activity [134]. Therefore, in this study the doping of cobalt did not enhance the degradation. Similar observation on the close relationship between PL intensity and photocatalytic activity was previous reported by J. Liqiang et al. [150]. Therefore, it is clearly known that the cobalt-doped ZnO had higher recombination of electron and hole as compared with pure ZnO, which reasonably lead to a lower photocatalytic activity.

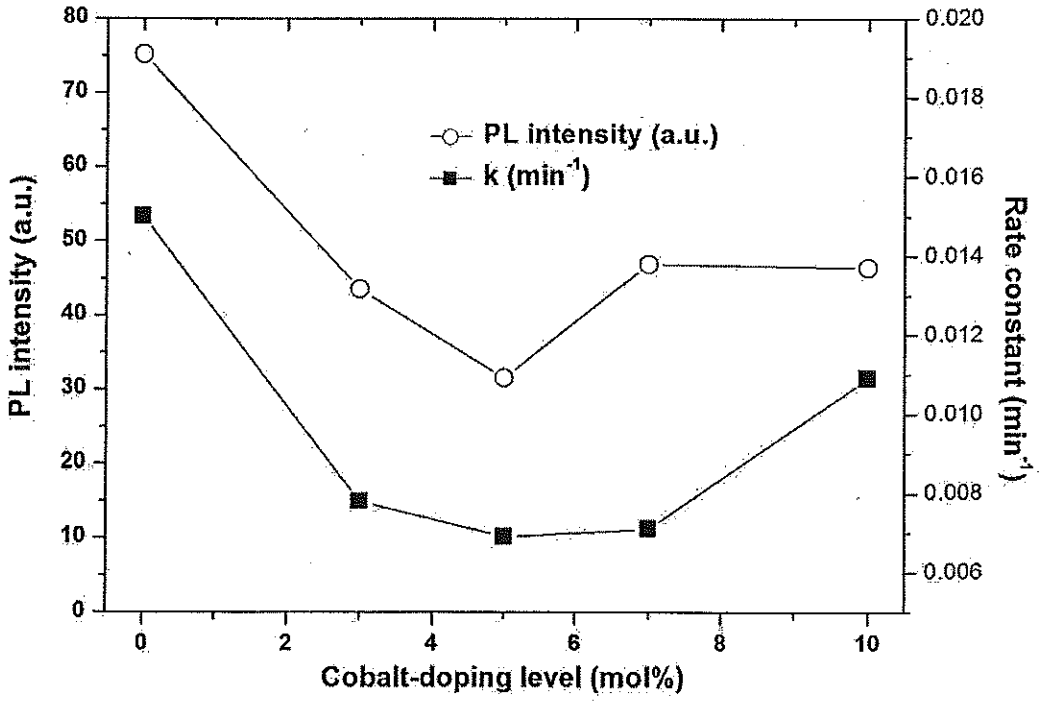

Figure 4.31 Comparison of the PL intensity and degradation rate constant of doped ZnO thin films with different cobalt-doping levels.

It was also known that the roughness of thin film was very important parameter that controled the effective surface area and hence the efficiency of the photocatalytic performance of the film. The surface roughness as reported in term of the root mean square roughness (R_{rms}) was presented in section 4.3. From AFM analysis, it was clearly seen that the ZnO thin film had a larger particle size and more roughness than doped thin films and also showed the highest

photocatalytic activity as shown in Figure 4.32. The results could be explained that rough surface had higher surface area to efficiently absorb light and produced more photocurrent than smooth surface, leading to greater efficiency towards photocatalytic degradation. The cobalt doping leads to a more even surface than the undoped ZnO film. Since the photocatalytic properties were more sensible to the roughness of the film surface, rather than the grain size, therefore the cobalt-doped films which had very fine grains, showed relatively low photocatalytic activities compared to the updoped ZnO film.

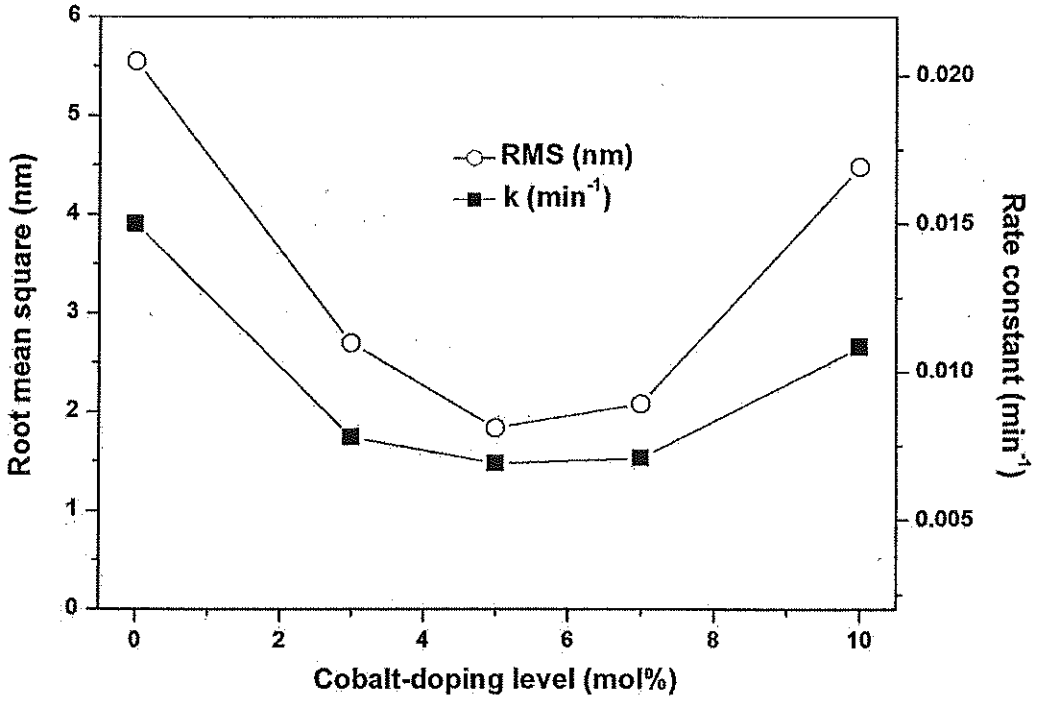

Figure 4.32 Comparison of the surface roughness (RMS) and degradation rate constant of doped ZnO thin films with different cobalt-doping levels.

4.7 Repeatability test on the photocatalytic activity of ZnO thin film

A repeatability test was carried out 4 times using ZnO thin film for MG degradation under UV-light irradiation and the results were shown in Table 4.1. The rate constant of zinc oxide film with repeatability test at 1, 2, 3 and 4 times were 0.0150 min^{-1}, 0.0104 min^{-1}, 0.0101 min^{-1} and 0.0096 min^{-1}, respectively. A decrease in rate constant of MG degradation for the second, third and fourth time were 30.67%, 32.67% and 36.00% compared with the first time, respectively. From AFM analysis (Figure 4.33), the surface roughness of ZnO thin film after the fourth time of photocatalytic activity was 3.70 nm (see Figure 4.33b). It indicated that surface roughness tended to decrease with increase in repeating test compared with ZnO film before photocatalysis (RMS of 5.55 nm). A decrease in photocatalytic activity of ZnO film was probably due to a decrease in surface roughness.

Table 4.1 Repeatability test on the photocatalytic activity of ZnO thin film

Times	Rate constant (min^{-1})	Decrease percentage (%)
1	0.0150	0.00
2	0.0104	-30.67
3	0.0101	-32.67
4	0.0096	-36.00

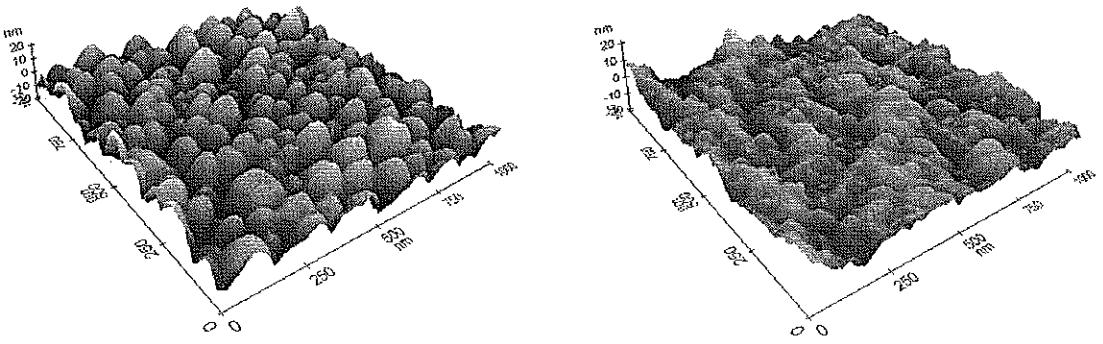

(a) Before photocatalysis (b) After photocatalysis for 4 times

Figure 4.33 3D AFM images of ZnO thin films before and after photocatalysis for 4 times.

4.8 Suggestion for future work

Since there is a variety of oxidation states of cobalt and in the present work only used XRD results to indicate the cobalt ion substituted in the ZnO lattice by a change in the 2θ values, therefore in future work, X-ray absorption spectroscopy will be carried out to characterize the coordination and oxidation states of cobalt in ZnO lattice.

In this work, it was found that the photocatalytic activities of cobalt-doped ZnO films to decompose Malachite green (MG) dye under UV-light irradiation were lower than the undoped ZnO film. In the future work, photocatalytic activities of updoped and cobalt-doped ZnO films for decomposition of MG dye under simulated visible-light will be investigated to study the effect of cobalt dopant.

CHAPTER 5

CONCLUSION

In summary, cobalt-doped zinc oxide thin films have been deposited on the micro-slide glass substrates by using a simple dip-coating method. This method is proved to be a repeatable, low-cost, and high-yield route to fabricate thin films. The thesis data specifically addressed the influence of cobalt concentration on the microstructure and surface morphology which eventually lead to variation in grain size of thin films and the optical properties such as photoluminescence, transmittance and optical band gap of cobalt-doped ZnO thin films. The photocatalytic activity of cobalt-doped ZnO thin films (0, 3, 5, 7 and 10 mol% cobalt in dipping solution) was investigated by malachite green degradation under UV-light illumination and in darkness.

From XRD analysis, all samples retained the original wurtzite structure. No metallic cobalt or other oxide phase impurities were observed within the limit of experimental detection. The results demonstrated that cobalt-doping did not affect the crystal structure of ZnO films with variable concentrations of 3 mol%, 5 mol%, 7 mol%, and 10 mol% of cobalt (II) acetate tetrahydrate ($Co(CH_3COO)_2 \cdot 4H_2O$) in dipping solutions. It was also found that films crystallinity decreased with increasing cobalt doping levels and this may be resulted from the enhanced strain caused by cobalt ions substituting for zinc ions. The decrease in crystallite size up to 5 mol% had been attributed to the presence of Co^{2+} in the ZnO lattice, however with further increase in cobalt content, an increase in crystallite size was attributed to the Co^{2+}/Co^{3+} ions substituting leading to an overall decrease in lattice strain of the films.

The FT-IR transmittance spectra presented the information about phase composition. The powder scratched from the ZnO film showed peak at 436 cm^{-1} which had been attributed to stretching vibration frequency of Zn-O as compared to the standard ZnO powder. Meanwhile, the transmission band of cobalt-doped ZnO thin films slightly shifted to the lower wavenumbers compared with pure ZnO film. In addition to, the Co-O vibration was clearly observed at high

cobalt-doping concentration (above 5 mol%), which was a confirmation of the presence of interstitial additives in ZnO lattice.

AFM analysis showed that an increase in cobalt-doping level up to 5 mol% reduced the grain growth of ZnO films with reduction of both grain size and surface roughness. However, at 7 and 10 mol% doping level, grain size and surface roughness slightly increased as compared with 5 mol% cobalt-doped ZnO thin films. It was concluded that cobalt played an important role in grain size and surface roughness of cobalt-doped ZnO films.

The photoluminescence (PL) analysis showed that the PL intensity of undoped ZnO film was higher than cobalt-doped ZnO films. The higher PL intensity indicates the less recombination of electron-hole pair.

From UV-Visible absorption spectra of cobalt-doped ZnO films, transparency of ZnO film decreased with increasing of cobalt-doping levels due to a decrease in crystallinity and this was in good agreement to the XRD results. Furthermore, the film thickness did not significantly change after cobalt-doping up to 10 mol%. It could be concluded that the thickness did not affect transparency of the cobalt-doped ZnO film. The direct optical band gap of cobalt-doped ZnO thin films slightly increased with increase in cobalt-doping up to 5 mol% and then decreased.

The photocatalytic efficiency for degradation of MG dye over films under UV-light and in darkness were compared in term of the apparent rate constants. The photocatalytic efficiency of ZnO film was greater than the activity achieved with cobalt-doped ZnO films. The results demonstrated that the photocatalytic activities of the films related to their photoluminescence properties. For cobalt-doped ZnO films, the photocatalytic properties were more sensible to a roughness of film surface, rather than grain sizes. Moreover, a sort of chemical activity of the films even in darkness had more significant influence on the decolorization of MG than an adsorption process.

REFERENCES

REFERENCES

[1] Gupta, V.K. and Suhas "Application of low-cost adsorbents for dye removal-a review", Journal of environmental management. 90(8): 2313-42, 2009.

[2] Srivastava, S., Sinha, R. and Roy, D. "Toxicological effects of malachite green", Aquatic Toxicology. 66(3): 319-29, 2004.

[3] Culp, S.J. and Beland, F.A. "Malachite green: A toxicological review", Journal of the American College of Toxicology. 15(3): 219-38, 1996.

[4] Culp, S.J., Blankenship, L.R., Kusewitt, D.F. and et al. "Toxicity and metabolism of malachite green and leucomalachite green during short-term feeding to Fischer 344 rats and B6C3F1 mice", Chemico-Biological Interactions. 122(3): 153-70, 1999.

[5] Nethaji, S., Sivasamy, A., Thennarasu, G. and et al. "Adsorption of Malachite Green dye onto activated carbon derived from Borassus aethiopum flower biomass", Journal of Hazardous Materials. 181(1–3): 271-80, 2010.

[6] Cheng, W., Wang, S.-G., Lu, L. and et al. "Removal of malachite green (MG) from aqueous solutions by native and heat-treated anaerobic granular sludge", Biochemical Engineering Journal. 39(3): 538-46, 2008.

[7] Kusvuran, E., Gulnaz, O., Samil, A. and et al. "Decolorization of malachite green, decolorization kinetics and stoichiometry of ozone-malachite green and removal of antibacterial activity with ozonation processes", Journal of Hazardous Materials. 186(1): 133-43, 2011.

[8] Oturan, M.A., Guivarch, E., Oturan, N. and et al. "Oxidation pathways of malachite green by Fe^{3+}-catalyzed electro-Fenton process", Applied Catalysis B: Environmental. 82(3–4): 244-54, 2008.

[9] Stubbings, G., Tarbin, J., Cooper, A. and et al. "A multi-residue cation-exchange clean up procedure for basic drugs in produce of animal origin", Analytica Chimica Acta. 547(2): 262-8, 2005.

[10] Moumeni, O., Hamdaoui, O. and Pétrier, C. "Sonochemical degradation of malachite green in water", Chemical Engineering and Processing: Process Intensification. 62(0): 47-53, 2012.

REFERENCES (CONTINUED)

[11] Kaneva, N., Stambolova, I., Blaskov, V. and et al. "Photocatalytic activity of nanostructured ZnO films prepared by two different methods for the photoinitiated decolorization of malachite green", Journal of Alloys and Compounds. 500(2): 252-8, 2010.

[12] Solís-Casados, D., Escobar-Alarcón, L., Fernández, M. and et al. "Malachite green degradation in simulated wastewater using Ni_x:TiO_2 thin films", Fuel. (0): 2012.

[13] Zhang, C., He, H., Wang, N. and et al. "Visible-light sensitive $La_{1-x}Ba_xCoO_3$ photocatalyst for malachite green degradation", Ceramics International. (0): 2012.

[14] Chen, C.C., Lu, C.S., Chung, Y.C. and et al. "UV light induced photodegradation of malachite green on TiO_2 nanoparticles", Journal of Hazardous Materials. 141(3): 520-8, 2007.

[15] Fischer, A.R., Werner, P. and Goss, K.U. "Photodegradation of malachite green and malachite green carbinol under irradiation with different wavelength ranges", Chemosphere. 82(2): 210-4, 2011.

[16] Prado, A.G.S. and Costa, L.L. "Photocatalytic decouloration of malachite green dye by application of TiO_2 nanotubes", Journal of Hazardous Materials. 169(1–3): 297-301, 2009.

[17] Rajeshwar, K., Osugi, M.E., Chanmanee, W. and et al. "Heterogeneous photocatalytic treatment of organic dyes in air and aqueous media", Journal of Photochemistry and Photobiology C: Photochemistry Reviews. 9(4): 171-92, 2008.

[18] Jongnavakit, P., Amornpitoksuk, P., Suwanboon, S. and et al. "Surface and photocatalytic properties of ZnO thin film prepared by sol-gel method", Thin Solid Films. 520(17): 5561-7, 2012.

[19] Sakthivel, S., Neppolian, B., Shankar, M.V. and et al. "Solar photocatalytic degradation of azo dye: comparison of photocatalytic efficiency of ZnO and TiO_2", Solar Energy Materials and Solar Cells. 77(1): 65-82, 2003.

[20] Nunes, P., Fortunato, E., Tonello, P. and et al. "Effect of different dopant elements on the properties of ZnO thin films", Vacuum. 64(3–4): 281-5, 2002.

REFERENCES (CONTINUED)

[21] Gouvêa, C.A.K., Wypych, F., Moraes, S.G. and et al. "Semiconductor-assisted photocatalytic degradation of reactive dyes in aqueous solution", Chemosphere. 40(4): 433-40, 2000.

[22] Dindar, B. and Içli, S. "Unusual photoreactivity of zinc oxide irradiated by concentrated sunlight", Journal of Photochemistry and Photobiology A: Chemistry. 140(3): 263-8, 2001.

[23] Lathasree, S., Rao, A.N., SivaSankar, B. and et al. "Heterogeneous photocatalytic mineralisation of phenols in aqueous solutions", Journal of Molecular Catalysis A: Chemical. 223(1–2): 101-5, 2004.

[24] Wang, C., Wang, X., Xu, B.-Q. and et al. "Enhanced photocatalytic performance of nanosized coupled ZnO/SnO_2 photocatalysts for methyl orange degradation", Journal of Photochemistry and Photobiology A: Chemistry. 168(1–2): 47-52, 2004.

[25] Jang, Y.J., Simer, C. and Ohm, T. "Comparison of zinc oxide nanoparticles and its nano-crystalline particles on the photocatalytic degradation of methylene blue", Materials Research Bulletin. 41(1): 67-77, 2006.

[26] Daneshvar, N., Salari, D. and Khataee, A.R. "Photocatalytic degradation of azo dye acid red 14 in water on ZnO as an alternative catalyst to TiO_2", Journal of Photochemistry and Photobiology A: Chemistry. 162(2–3): 317-22, 2004.

[27] Sirtori, C., Altvater, P.K., Freitas, A.M.d. and et al. "Degradation of aqueous solutions of camphor by heterogeneous photocatalysis", Journal of Hazardous Materials. 129(1–3): 110-5, 2006.

[28] Tan, S.T., Chen, B.J., Sun, X.W. and et al. "Blueshift of optical band gap in ZnO thin films grown by metal-organic chemical-vapor deposition", Journal of Applied Physics. 98(1): 013505-5, 2005.

[29] Li, M., Xu, J., Chen, X. and et al. "Structural and optical properties of cobalt doped ZnO nanocrystals", Superlattices and Microstructures. 52(4): 824-33, 2012.

REFERENCES (CONTINUED)

[30] Mote, V.D., Purushotham, Y. and Dole, B.N. "Williamson-Hall analysis in estimation of lattice strain in nanometer-sized ZnO particles", Journal of Theoretical and Applied Physics. 6(1): 1-8, 2012.

[31] Major, S. and Chopra, K.L. "Indium-doped zinc oxide films as transparent electrodes for solar cells", Solar Energy Materials. 17(5): 319-27, 1988.

[32] Wu, L. and Wu, Y. "Synthesis and optical characteristic of ZnO nanorod", Journal of Materials Science. 42(1): 406-8, 2007.

[33] Wu, J.-J. and Tseng, C.-H. "Photocatalytic properties of nc-Au/ZnO nanorod composites", Applied Catalysis B: Environmental. 66(1–2): 51-7, 2006.

[34] Lam, S.-M., Sin, J.-C., Zuhairi Abdullah, A. and et al. "Green hydrothermal synthesis of ZnO nanotubes for photocatalytic degradation of methylparaben", Materials Letters. 93(0): 423-6, 2013.

[35] Pyne, S., Sahoo, G.P., Bhui, D.K. and et al. "Enhanced photocatalytic activity of metal coated ZnO nanowires", Spectrochimica Acta Part A: Molecular and Biomolecular Spectroscopy. 93(0): 100-5, 2012.

[36] Wang, M., Fei, G. and Zhang, L. "Porous-ZnO-Nanobelt Film as Recyclable Photocatalysts with Enhanced Photocatalytic Activity", Nanoscale Research Letters. 5(11): 1800-3, 2010.

[37] Xu, L., Shi, L. and Li, X. "Preparation of nanocone ZnO thin film and its aging effect of photoluminescence", Applied Surface Science. 255(11): 5957-60, 2009.

[38] Sheng, J., Karasawa, J. and Fukami, T. "Thickness dependence of photocatalytic activity of anatase film by magnetron sputtering", Journal of Materials Science Letters. 16(21): 1709-11, 1997.

[39] Rahmani, E., Ahmadpour, A. and Zebarjad, M. "Enhancing the photocatalytic activity of TiO_2 nanocrystalline thin film by doping with SiO_2", Chemical Engineering Journal. 174(2–3): 709-13, 2011.

REFERENCES (CONTINUED)

[40] Iketani, K., Sun, R.-D., Toki, M. and et al. "Sol–gel-derived $V_xTi_{1-x}O_2$ films and their photocatalytic activities under visible light irradiation", Materials Science and Engineering: B. 108(3): 187-93, 2004.

[41] Jeong, S.H., Park, B.N., Lee, S.B. and et al. "Study on the doping effect of Li-doped ZnO film", Thin Solid Films. 516(16): 5586-9, 2008.

[42] Bizarro, M., Sánchez-Arzate, A., Garduño-Wilches, I. and et al. "Synthesis and characterization of ZnO and ZnO:Al by spray pyrolysis with high photocatalytic properties", Catalysis Today. 166(1): 129-34, 2011.

[43] Shinde, S.S., Bhosale, C.H. and Rajpure, K.Y. "Photocatalytic degradation of toluene using sprayed N-doped ZnO thin films in aqueous suspension", Journal of Photochemistry and Photobiology B: Biology. 113(0): 70-7, 2012.

[44] Nolan, M.G., Hamilton, J.A., O'Brien, S. and et al. "The characterisation of aerosol assisted CVD conducting, photocatalytic indium doped zinc oxide films", Journal of Photochemistry and Photobiology A: Chemistry. 219(1): 10-5, 2011.

[45] Jongnavakit, P., Amornpitoksuk, P., Suwanboon, S. and et al. "Preparation and photocatalytic activity of Cu-doped ZnO thin films prepared by the sol–gel method", Applied Surface Science. 258(20): 8192-8, 2012.

[46] Xie, W., Li, Y., Sun, W. and et al. "Surface modification of ZnO with Ag improves its photocatalytic efficiency and photostability", Journal of Photochemistry and Photobiology A: Chemistry. 216(2–3): 149-55, 2010.

[47] Kao, C.-Y., Liao, J.-D., Chang, C.-W. and et al. "Thermal diffusion of Co into sputtered ZnO:Co thin film for enhancing visible-light-induced photo-catalytic activity", Applied Surface Science. 258(5): 1813-8, 2011.

[48] Wang, D., Zhou, J. and Liu, G. "The microstructure and photoluminescence of Cu-doped ZnO nano-crystal thin films prepared by sol–gel method", Journal of Alloys and Compounds. 487(1–2): 545-9, 2009.

REFERENCES (CONTINUED)

[49] Heiba, Z.K. and Arda, L. "XRD, XPS, optical, and Raman investigations of structural changes of nano Co-doped ZnO", Journal of Molecular Structure. 1022(0): 167-71, 2012.

[50] Neogi, S.K., Ghosh, R., Paul, G.K. and et al. "Effects of Co doping on structural, morphological and transport properties of sol–gel AZO thin films", Journal of Alloys and Compounds. 487(1–2): 269-73, 2009.

[51] Musat, V., Teixeira, B., Fortunato, E. and et al. "Al-doped ZnO thin films by sol–gel method", Surface and Coatings Technology. 180–181(0): 659-62, 2004.

[52] Ratana, T., Amornpitoksuk, P. and Suwanboon, S. "The wide band gap of highly oriented nanocrystalline Al doped ZnO thin films from sol–gel dip coating", Journal of Alloys and Compounds. 470(1–2): 408-12, 2009.

[53] Ramesh, J., Pasupathi, G., Mariappan, R. and et al. "Structural and optical properties of Ni doped ZnO thin films using sol–gel dip coating technique", Optik-International Journal for Light and Electron Optics. (0): 2012.

[54] Du, F., Wang, N., Zhang, D. and et al. "Preparation, characterization and infrared emissivity study of Ce-doped ZnO films", Journal of Rare Earths. 28(3): 391-5, 2010.

[55] Girtan, M., Socol, M., Pattier, B. and et al. "On the structural, morphological, optical and electrical properties of sol–gel deposited ZnO:In films", Thin Solid Films. 519(2): 573-7, 2010.

[56] Kumar, S., Kumar, R. and Singh, D.P. "Swift heavy ion induced modifications in cobalt doped ZnO thin films: Structural and optical studies", Applied Surface Science. 255(18): 8014-8, 2009.

[57] Bahadur, N., Srivastava, A.K., Kumar, S. and et al. "Influence of cobalt doping on the crystalline structure, optical and mechanical properties of ZnO thin films", Thin Solid Films. 518(18): 5257-64, 2010.

[58] Kim, K.-C., Kim, E.-k. and Kim, Y.-S. "Growth and physical properties of sol–gel derived Co doped ZnO thin film", Superlattices and Microstructures. 42(1–6): 246-50, 2007.

REFERENCES (CONTINUED)

[59] Benramache, S. and Benhaoua, B. "Influence of substrate temperature and Cobalt concentration on structural and optical properties of ZnO thin films prepared by Ultrasonic spray technique", Superlattices and Microstructures. 52(4): 807-15, 2012.

[60] Wang, A., Zhong, Z., Lu, C. and et al. "Study on field-emission characteristics of electrodeposited Co-doped ZnO thin films", Physica B: Condensed Matter. 406(5): 1049-52, 2011.

[61] Znaidi, L. "Sol–gel-deposited ZnO thin films: A review", Materials Science and Engineering: B. 174(1–3): 18-30, 2010.

[62] Kim, D., Yun, I. and Kim, H. "Fabrication of rough Al doped ZnO films deposited by low pressure chemical vapor deposition for high efficiency thin film solar cells", Current Applied Physics. 10(3, Supplement): S459-S62, 2010.

[63] Zheng, G., Yang, A., Wei, H. and et al. "Effects of annealing treatment on the formation of CO_2 in ZnO thin films grown by metal-organic chemical vapor deposition", Applied Surface Science. 256(8): 2606-10, 2010.

[64] Ki Hyun, Y., Choi, J.-W. and Lee, D.-H. "Characteristics of ZnO thin films deposited onto Al/Si substrates by r.f. magnetron sputtering", Thin Solid Films. 302(1–2): 116-21, 1997.

[65] Minami, T., Oda, J.-i., Nomoto, J.-i. and et al. "Effect of target properties on transparent conducting impurity-doped ZnO thin films deposited by DC magnetron sputtering", Thin Solid Films. 519(1): 385-90, 2010.

[66] Chakraborty, A., Mondal, T., Bera, S.K. and et al. "Effects of aluminum and indium incorporation on the structural and optical properties of ZnO thin films synthesized by spray pyrolysis technique", Materials Chemistry and Physics. 112(1): 162-6, 2008.

[67] Vimalkumar, T.V., Poornima, N., Sudha Kartha, C. and et al. "On tuning the orientation of grains of spray pyrolysed ZnO thin films", Applied Surface Science. 256(20): 6025-8, 2010.

REFERENCES (CONTINUED)

[68] Sahoo, T., Kim, M., Lee, M.-H. and et al. "Nanocrystalline ZnO thin films by spin coating-pyrolysis method", Journal of Alloys and Compounds. 491(1–2): 308-13, 2010.

[69] Farag, A.A.M., CavaŞ, M., Yakuphanoglu, F. and et al. "Photoluminescence and optical properties of nanostructure Ni doped ZnO thin films prepared by sol–gel spin coating technique", Journal of Alloys and Compounds. 509(30): 7900-8, 2011.

[70] Ge, C., Xie, C. and Cai, S. "Preparation and gas-sensing properties of Ce-doped ZnO thin-film sensors by dip-coating", Materials Science and Engineering: B. 137(1–3): 53-8, 2007.

[71] Marotti, R.E., Bojorge, C.D., Broitman, E. and et al. "Characterization of ZnO and ZnO:Al thin films deposited by the sol–gel dip-coating technique", Thin Solid Films. 517(3): 1077-80, 2008.

[72] Casanova, J.R., Heredia, E.A., Bojorge, C.D. and et al. "Structural characterization of supported nanocrystalline ZnO thin films prepared by dip-coating", Applied Surface Science. 257(23): 10045-51, 2011.

[73] Valle, G.G., Hammer, P., Pulcinelli, S.H. and et al. "Transparent and conductive ZnO:Al thin films prepared by sol-gel dip-coating", Journal of the European Ceramic Society. 24(6): 1009-13, 2004.

[74] Geraldo, V., Scalvi, L.V.A., Morais, E.A. and et al. "Ultraviolet excitation of photoconductivity in thin films of sol–gel SnO_2", Journal of the European Ceramic Society. 25(12): 2825-8, 2005.

[75] Zhou, H.-m., Yi, D.-q., Yu, Z.-m. and et al. "Preparation of aluminum doped zinc oxide films and the study of their microstructure, electrical and optical properties", Thin Solid Films. 515(17): 6909-14, 2007.

[76] Yu, Q., Yang, H., Fu, W. and et al. "Transparent conducting yttrium-doped ZnO thin films deposited by sol–gel method", Thin Solid Films. 515(7–8): 3840-3, 2007.

[77] Ashrafi, A. and Jagadish, C. "Review of zincblende ZnO: Stability of metastable ZnO phases", Journal of Applied Physics. 102(7): 071101-12, 2007.

REFERENCES (CONTINUED)

[78] Zhang, Y., Ram, M.K., Stefanakos, E.K. and et al. "Synthesis, Characterization, and Applications of ZnO Nanowires", Journal of Nanomaterials. 2012: 22, 2012.

[79] Kogure, T. and Bando, Y. "Formation of ZnO nanocrystallites on ZnS surfaces by electron beam irradiation", Journal of Electron Microscopy. 47(2): 135-41, 1998.

[80] Ashrafi, A.B.M.A., Ueta, A., Avramescu, A. and et al. "Growth and characterization of hypothetical zinc-blende ZnO films on GaAs(001) substrates with ZnS buffer layers", Applied Physics Letters. 76(5): 550-2, 2000.

[81] Kim, S.-K., Jeong, S.-Y. and Cho, C.-R. "Structural reconstruction of hexagonal to cubic ZnO films on Pt/Ti/SiO_2/Si substrate by annealing", Applied Physics Letters. 82(4): 562-4, 2003.

[82] Snedeker, L.P., Risbud, A.S., Masala, O. and et al. "Organic phase conversion of bulk (wurtzite) ZnO to nanophase (wurtzite and zinc blende) ZnO", Solid State Sciences. 7(12): 1500-5, 2005.

[83] Ebothe, J., El Hichou, A., Vautrot, P. and et al. "Flow rate and interface roughness of zinc oxide thin films deposited by spray pyrolysis technique", Journal of Applied Physics. 93(1): 632-40, 2003.

[84] Lehraki, N., Aida, M.S., Abed, S. and et al. "ZnO thin films deposition by spray pyrolysis: Influence of precursor solution properties", Current Applied Physics. 12(5): 1283-7, 2012.

[85] Arca, E., Fleischer, K. and Shvets, I.V. "Influence of the precursors and chemical composition of the solution on the properties of ZnO thin films grown by spray pyrolysis", The Journal of Physical Chemistry C. 113(50): 21074-81, 2009.

[86] Bahadur, H., Srivastava, A.K., Sharma, R.K. and et al. "Morphologies of sol–gel derived thin films of ZnO using different precursor materials and their nanostructures", Nanoscale Research Letters. 2(10): 469-75, 2007.

[87] Liu, Z., Jin, Z., Li, W. and et al. "Preparation of ZnO porous thin films by sol–gel method using PEG template", Materials Letters. 59(28): 3620-5, 2005.

REFERENCES (CONTINUED)

[88] Srinivasan, G. and Kumar, J. "Optical and structural characterisation of zinc oxide thin films prepared by sol-gel process", Crystal Research and Technology. 41(9): 893-6, 2006.

[89] Raoufi, D. and Raoufi, T. "The effect of heat treatment on the physical properties of sol–gel derived ZnO thin films", Applied Surface Science. 255(11): 5812-7, 2009.

[90] Tsay, C.-Y., Fan, K.-S., Chen, S.-H. and et al. "Preparation and characterization of ZnO transparent semiconductor thin films by sol–gel method", Journal of Alloys and Compounds. 495(1): 126-30, 2010.

[91] Lin, L.-Y. and Kim, D.-E. "Effect of annealing temperature on the tribological behavior of ZnO films prepared by sol–gel method", Thin Solid Films. 517(5): 1690-700, 2009.

[92] Ben Ayadi, Z., El Mir, L., Djessas, K. and et al. "Effect of the annealing temperature on transparency and conductivity of ZnO:Al thin films", Thin Solid Films. 517(23): 6305-9, 2009.

[93] Elilarassi, R. and Chandrasekaran, G. "Microstructural and photoluminescence properties of Co-doped ZnO films fabricated using a simple solution growth method", Materials Science in Semiconductor Processing. 14(2): 179-83, 2011.

[94] Mamat, M.H., Amizam, S., Rafaie, H.A. and et al. "Effect of Annealing Temperature on the Surface Morphology and Electrical Properties of Aluminum Doped Zinc Oxide Thin Films Prepared by Sol-Gel Spin-Coating Method", AIP Conference Proceedings. 1017(1): 139-43, 2008.

[95] Dutta, M., Mridha, S. and Basak, D. "Effect of sol concentration on the properties of ZnO thin films prepared by sol–gel technique", Applied Surface Science. 254(9): 2743-7, 2008.

[96] Suzuki, T., Horibuchi, K. and Ohishi, Y. "Structural and optical properties of $ZnO–Al_2O_3–SiO_2$ system glass–ceramics containing Ni^{2+}-doped nanocrystals", Journal of Non-Crystalline Solids. 351(27–29): 2304-9, 2005.

REFERENCES (CONTINUED)

[97] Sato, K. and Katayama-Yoshida, H. "Stabilization of Ferromagnetic States by Electron Doping in Fe-, Co- or Ni-Doped ZnO", Japanese Journal of Applied Physics. 40: 334-6, 2001.

[98] Li, B.B., Xiu, X.Q., Zhang, R. and et al., editors. Structure and magnetic properties of Co-doped ZnO powder prepared by sol-gel method. Semiconducting and Insulating Materials, 2004 SIMC-XIII-2004 13th International Conference on; 2005 20-25 Sept. 2004.

[99] He, R., Hocking, R.K. and Tsuzuki, T. "Co-doped ZnO nanopowders: Location of cobalt and reduction in photocatalytic activity", Materials Chemistry and Physics. 132(2–3): 1035-40, 2012.

[100] Nair, M.G., Nirmala, M., Rekha, K. and et al. "Structural, optical, photo catalytic and antibacterial activity of ZnO and Co doped ZnO nanoparticles", Materials Letters. 65(12): 1797-800, 2011.

[101] Wang, T., Liu, Y., Fang, Q. and et al. "Morphology and optical properties of Co doped ZnO textured thin films", Journal of Alloys and Compounds. 509(37): 9116-22, 2011.

[102] Vempati, S., Shetty, A., Dawson, P. and et al. "Solution-based synthesis of cobalt-doped ZnO thin films", Thin Solid Films. 524(0): 137-43, 2012.

[103] He, X., Yang, H., Chen, Z. and et al. "Effect of Co-doping content on hydrothermal derived ZnO array films", Physica B: Condensed Matter. 407(15): 2895-9, 2012.

[104] Singh, G., Shrivastava, S.B., Ganesan, V. and et al. "Effect of Co doping on structural, morphological, electrical and optical properties of nanocrystalline zinc oxide films ", Journal of Chemical Engineering and Materials Science. 14(1): 1-6, 2013.

[105] Su, X., Wang, L., Chen, J. and et al. "Ferromagnetism in transparent thin film of Co-doped ZnO": 78471N-N, 2010.

[106] Yousif, A.A., Haidar, A.J. and Habubi, N.F. "Study of the structure properties of Co-doped ZnO thin films grown by pulsed laser deposition", International Journal of Nanoelectronics and Materials. 5: 47-55, 2012.

REFERENCES (CONTINUED)

[107] Yakuphanoglu, F. "Controlling of electrical and interface state density properties of ZnO:Co/p-silicon diode structures by compositional fraction of cobalt dopant", Microelectronics Reliability. 51(12): 2195-9, 2011.

[108] Legrini, O., Oliveros, E. and Braun, A.M. "Photochemical processes for water treatment", Chemical Reviews. 93(2): 671-98, 1993.

[109] Kaneva, N., Stambolova, I., Blaskov, V. and et al. "A comparative study on the photocatalytic efficiency of ZnO thin films prepared by spray pyrolysis and sol–gel method", Surface and Coatings Technology. 207(0): 5-10, 2012.

[110] Lu, Y., Lin, Y., Wang, D. and et al. "A high performance cobalt-doped ZnO visible light photocatalyst and its photogenerated charge transfer properties", Nano Research. 4(11): 1144-52, 2011.

[111] Berberidou, C., Poulios, I., Xekoukoulotakis, N.P. and et al. "Sonolytic, photocatalytic and sonophotocatalytic degradation of malachite green in aqueous solutions", Applied Catalysis B: Environmental. 74(1–2): 63-72, 2007.

[112] Pierre, A.C., editor. Introduction to sol-gel processing. London: Kluwer academic publishers; 1998.

[113] Reisfeld, R. and JJørgensen, C.K., editors. Chemistry, Spectroscopy and Applications of Sol-Gel Glasses. Berlin: Springer-Verlag; 1992.

[114] Mehrotra, R.C. Present status and future potential of the Sol-Gel process. In: Reisfeld, R. and JJørgensen, C.K., editors. Chemistry, Spectroscopy and Applications of Sol-Gel Glasses: Springer Berlin Heidelberg; 1992. p. 1-36.

[115] Attia, S.M., Wang, J., Wu, G. and et al. "Review on the sol-gel derived coating: process, techniques and optical applications", Journal of materials science and technology. 18: 211-8, 2002.

[116] Brinker, C.J., Hurd, A.J., Schunk, P.R. and et al. "Review of sol-gel thin film formation", Journal of Non-Crystalline Solids. 147–148(0): 424-36, 1992.

REFERENCES (CONTINUED)

[117] Maleki, M., Reyssat, M., Restagno, F. and et al. "Landau–Levich menisci", Journal of Colloid and Interface Science. 354(1): 359-63, 2011.

[118] Rauf, M.A. and Ashraf, S.S. "Fundamental principles and application of heterogeneous photocatalytic degradation of dyes in solution", Chemical Engineering Journal. 151(1–3): 10-8, 2009.

[119] Sahel, K., Perol, N., Chermette, H. and et al. "Photocatalytic decolorization of Remazol Black 5 (RB5) and Procion Red MX-5B—Isotherm of adsorption, kinetic of decolorization and mineralization", Applied Catalysis B: Environmental. 77(1–2): 100-9, 2007.

[120] Rauf, M.A., Bukallah, S.B., Hamadi, A. and et al. "The effect of operational parameters on the photoinduced decoloration of dyes using a hybrid catalyst V_2O_5/TiO_2", Chemical Engineering Journal. 129(1–3): 167-72, 2007.

[121] Liu, Z., Li, J., Ya, J. and et al. "Mechanism and characteristics of porous ZnO films by sol–gel method with PEG template", Materials Letters. 62(8–9): 1190-3, 2008.

[122] Aslan, M.H., Oral, A.Y., MenŞur, E. and et al. "Preparation of c-axis-oriented zinc-oxide thin films and the study of their microstructure and optical properties", Solar Energy Materials and Solar Cells. 82(4): 543-52, 2004.

[123] Nanda, S. and Gupta, P.S. "Structural and Optical Properties of Sol-gel Prepared ZnO Thin Film", Applied Physics Research. 2: 19-27, 2010.

[124] Suryanarayana, C. and Grant Norton, M. X-ray Diffraction: A Practical Approach. New York: Plenum Press; 1998.

[125] Li, C., Li, X.C., Yan, P.X. and et al. "Research on the properties of ZnO thin films deposited by using filtered cathodic arc plasma technique on glass substrate under different flow rate of O_2", Applied Surface Science. 253(8): 4000-5, 2007.

REFERENCES (CONTINUED)

[126] Rushing, L.G. and Hansen Jr, E.B. "Confirmation of malachite green, gentian violet and their leuco analogs in catfish and trout tissue by high-performance liquid chromatography utilizing electrochemistry with ultraviolet-visible diode array detection and fluorescence detection", Journal of Chromatography B: Biomedical Applications. 700(1-2): 223-31, 1997.

[127] Plakas, S.M., El Said, K.R., Stehly, G.R. and et al. "Uptake, tissue distribution, and metabolism of malachite green in the channel catfish (Ictalurus punctatus)", Canadian Journal of Fisheries and Aquatic Sciences. 53(6): 1427-33, 1996.

[128] Absalan, H. and Esmaieli Ghodsi, F. "Comparative study of ZnO thin films prepared by different sol-gel route", Iranian Journal of Physics Research. 11(4): 423-8, 2012.

[129] Rusdi, R., Rahman, A.A., Mohamed, N.S. and et al. "Preparation and band gap energies of ZnO nanotubes, nanorods and spherical nanostructures", Powder Technology. 210(1): 18-22, 2011.

[130] Asiltürk, M., Sayılkan, F. and Arpaç, E. "Effect of Fe^{3+} ion doping to TiO_2 on the photocatalytic degradation of Malachite Green dye under UV and Vis-irradiation", Journal of Photochemistry and Photobiology A: Chemistry. 203(1): 64-71, 2009.

[131] Lupan, O., Chow, L., Ono, L.K. and et al. "Synthesis and Characterization of Ag- or Sb-Doped ZnO Nanorods by a Facile Hydrothermal Route", The Journal of Physical Chemistry C. 114(29): 12401-8, 2010.

[132] Qiu, Y., Chen, W., Yang, S. and et al. "Hierarchical Hollow Spheres of ZnO and $Zn_{1-x}Co_xO$: Directed Assembly and Room-Temperature Ferromagnetism", Crystal Growth & Design. 10(1): 177-83, 2009.

[133] Kshirsagar, S.D., Inamdar, D., Gopalakrishnan, I.K. and et al. "Formation of room-temperature ferromagnetic $Zn_{1-x}Co_xO$ nanocrystals", Solid State Communications. 143(10): 457-60, 2007.

[134] Xiao, Q., Zhang, J., Xiao, C. and et al. "Photocatalytic decolorization of methylene blue over $Zn_{1-x}Co_xO$ under visible light irradiation", Materials Science and Engineering: B. 142(2–3): 121-5, 2007.

REFERENCES (CONTINUED)

[135] Yang, H. and Nie, S. "Preparation and characterization of Co-doped ZnO nanomaterials", Materials Chemistry and Physics. 114(1): 279-82, 2009.

[136] Hammad, T., Salem, J. and Harrison, R.G. "Structure, optical properties and synthesis of Co-doped ZnO superstructures", Applied Nanoscience. 1-7, 2012.

[137] Li, P., Wang, S., Li, J. and et al. "Structural and optical properties of Co-doped ZnO nanocrystallites prepared by a one-step solution route", Journal of Luminescence. 132(1): 220-5, 2012.

[138] Shafique, M., Shah, S., Nafees, M. and et al. "Effect of doping concentration on absorbance, structural, and magnetic properties of cobalt-doped ZnO nano-crystallites", International Nano Letters. 2(1): 1-7, 2012.

[139] Udayakumar, S., Renuka, V., Kavitha, K. and et al. "Structural, optical and thermal studies of cobalt doped hexagonal ZnO by simple chemical precipitation method ", Journal of Chemical and Pharmaceutical Research. 4(2): 1271-80, 2012.

[140] Elilarassi, R. and Chandrasekaran, G. "Influence of Co-doping on the structural, optical and magnetic properties of ZnO nanoparticles synthesized using auto-combustion method", Journal of Materials Science: Materials in Electronics. 24(1): 96-105, 2013.

[141] Shannon, R.D. and Prewitt, C.T. "Effective ionic radii in oxides and fluorides", Acta Crystallographica Section B. 25(5): 925-46, 1969.

[142] Wang, L., Meng, L., Teixeira, V. and et al. "Structure and optical properties of ZnO:V thin films with different doping concentrations", Thin Solid Films. 517(13): 3721-5, 2009.

[143] Peltonen, J., Järn, M., Areva, S. and et al. "Topographical parameters for specifying a three-dimensional surface", Langmuir. 20(22): 9428-31, 2004.

[144] Das, K., Ray, S., Chaudhuri, S. and et al. "Structural and luminescence properties of sol-gel derived Cu doped ZnO films", Indian Journal of Pure and applied Physics. 47: 377-82, 2009.

[145] Ozerov, I., Chabre, F. and Marine, W. "Incorporation of cobalt into ZnO nanoclusters", Materials Science and Engineering: C. 25(5–8): 614-7, 2005.

REFERENCES (CONTINUED)

[146] Liu, Z., Xu, X., Fang, J. and et al. "Microemulsion synthesis, characterization of bismuth oxyiodine/titanium dioxide hybrid nanoparticles with outstanding photocatalytic performance under visible light irradiation", Applied Surface Science. 258(8): 3771-8, 2012.

[147] Wu, J.J. and Liu, S.C. "Low-Temperature Growth of Well-Aligned ZnO Nanorods by Chemical Vapor Deposition", Advanced Materials. 14(3): 215-8, 2002.

[148] Ullah, R. and Dutta, J. "Photocatalytic degradation of organic dyes with manganese-doped ZnO nanoparticles", Journal of Hazardous Materials. 156(1–3): 194-200, 2008.

[149] Liu, H., Cheng, S., Wu, M. and et al. "Photoelectrocatalytic Degradation of Sulfosalicylic Acid and Its Electrochemical Impedance Spectroscopy Investigation", The Journal of Physical Chemistry A. 104(30): 7016-20, 2000.

[150] Liqiang, J., Xiaojun, S., Baifu, X. and et al. "The preparation and characterization of La doped TiO_2 nanoparticles and their photocatalytic activity", Journal of Solid State Chemistry. 177(10): 3375-82, 2004.

VITAE

NAME	Mr. Praphan Kenthao
BIRTH DATE	23 June 1986
BIRTH PLACE	Ubon Ratchathani Province, Thailand
EDUCATION	B. Sc. (Chemistry), Department of Chemistry, Faculty of Science, Ubon Ratchathani Univerisity, Ubon Ratchathani, Thailand, 2004-2008. M. Sc. (Chemistry), Department of Chemistry, Faculty of Science, Ubon Ratchathani Univerisity, Ubon Ratchathani, Thailand, 2009-2012.
SCHOLARSHIPS	Research Price from Center of Excellence for Innovation in Chemistry, Office of the Higher Education Commission, Ministry of Education: Postgraduate Education and Research Program in Chemistry (PERCH-CIC), 2009-2011. Research Price from Faculty of Science, Ubon Ratchathani University, Ubon Ratchathani, Thailand, 2009-2012.
PUBLICATION	Praphan Kenthao and Suwat Pabchanda. "Effect Of Cobalt Doping On Photocatalytic Activity Of Zinc Oxide Thin Film Under UV Light Illumination". Proceeding of 6th Ubon Ratchathani Research Conference (UBRC 6th), 25 – 27 July 2012, pages 203 - 211.

PRESENTATIONS

6th Ubon Ratchathani Research Conference (UBRC 6th) in the title of "Effect Of Cobalt Doping On Photocatalytic Activity Of Zinc Oxide Thin Film Under UV Light Illumination", Sunee Grand & Convention Center Hotel, Ubon Ratchathani, Thailand, 2012, (Oral presentation).

7th PERCH Congress in the title of "Preparation and Characterization of Iron Doped Tin Oxide Thin Films by Dip-coating Technique". Jomtien Palm Beach Hotel & Resort, Pattaya, Chonburi, Thailand, 2011, (Poster presentation).